Université de Liège
Faculté des Sciences
Interactions Fondamentales en Physique et en Astrophysique

Atomes noirs : propriétés et conséquences observationnelles

Wallemacq Quentin

Mémoire présenté en vue de l'obtention
du grade de Master en Sciences Spatiales

Année académique 2010-2011

Remerciements

Je tiens particulièrement à remercier Jean-René Cudell, promoteur de ce mémoire, pour sa très grande disponibilité tout au long de cette année, ses nombreux conseils au cours de nos discussions, ses relectures et ses corrections fines et efficaces. L'encadrement dont j'ai bénéficié a de manière certaine rendu plus agréable la réalisation de ce travail.

Je remercie Maxim Yu. Khlopov, à l'origine des idées développées dans ce mémoire, pour sa disponibilité lors de notre collaboration à distance.

Merci à Perrine, pour sa présence et son soutien à toutes épreuves.

Mes remerciements vont également à Vincent, pour son interêt envers ce mémoire et nos discussions de physique passionnées. Merci pour les bons moments passés en cinq années d'études, et pour les souvenirs que nous en garderons.

Merci à mes parents, sans qui rien de tout cela ne serait.

A ma famille, mes amis, sources d'équilibre indispensables.

Contents

Chapter 1

Introduction

Measurements of rotation curves of galaxies, the virial paradox in heavy clusters and the effects of gravitational lensing are today indirect pieces of evidence for the existence of a non-luminous matter that dominates luminous matter in terms of cosmological density. The share of this dark matter is estimated at 25% of the total cosmological density and the arguments of modern cosmology plead for a non-baryonic matter. The difference between baryonic density and total density is indeed apparent in the analysis of the abundances of light elements in primordial nucleosynthesis and in the measurements of the fluctuations in the cosmic microwave background (CMB). The need for a non-baryonic matter is also felt when trying to explain the major structures of the universe from fluctuations of the baryonic density observed in the CMB.

Historically, this missing matter was postulated by Fritz Zwicky in 1933 who observed a large velocity dispersion of the members of the Coma galaxy cluster. The total mass deduced from the dynamics of the cluster was indeed several hundred times larger than the mass deduced from its luminosity. According to Zwicky, the observed cohesion of the cluster could only be due to the presence of a large amount of matter that emitted no light (hence the appellation "dark matter"). At the time, Zwicky's suggestion did not generate much interest in the scientific community and one had to wait for the discovery of the flatness of the rotation curves of galaxies in the 1970's to recognize dark matter as a real puzzle. Since the 1980's, most physicists and astrophysicists are convinced that dark matter exists around galaxies and clusters, and try to explain its nature.

To understand the rotation curves of galaxies, early theories postulated the presence in the halo of our galaxy of heavy normal (baryonic) objects such as black holes, neutron stars or white dwarfs that may have escaped observation until now. These faint objects were called MACHO's (MAssive Compact Halo Objects) and gave rise to several research projects in the early 1990's. Among them, the MACHO and EROS projects undertook to observe the Magellanic clouds. The strategy was based on the phenomenon of microlensing : if one of

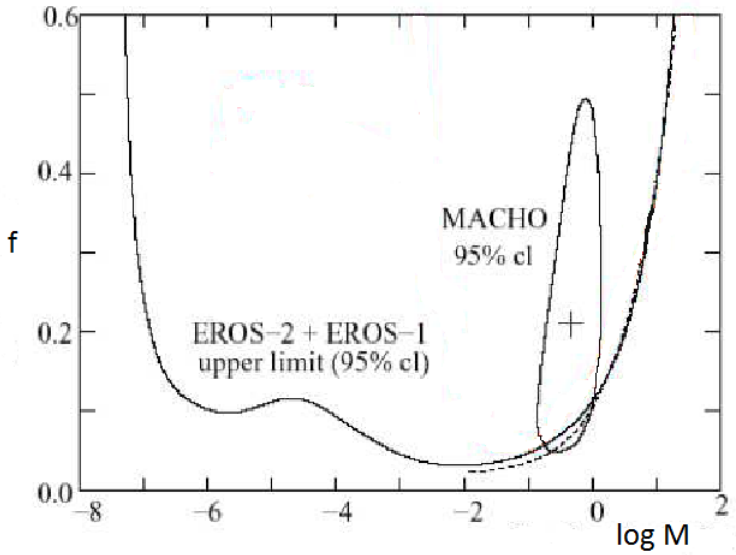

Figure 1.1: EROS upper limit on the mass fraction of a spherical Galactic halo realized by compact baryonic objects as a function of their mass, based on zero observed LMC (Large Magellanic Cloud) and SMC (Small Magellanic Cloud) events. f is the halo mass fraction (in %) and M is the mass of the deflector (in solar masses $M_\odot$). *Figure extracted from [2].*

these objects passed in front of a background star, one would have been able to detect an amplification varying with time and hence betraying its presence. The observation of a great number of events would have given an indication on the density of MACHO's (which would be proportional to this number) and on their characteristic mass, which can be shown to be proportional to the square of the characteristic time of the event [1].

The results of the MACHO collaboration were not conclusive : firstly, the observed events allowed to deduce that only 20% of dark matter could be explained by the MACHO's (0% or 100% would have been more natural). Secondly the most probable mass was estimated to be $0.5\,M_\odot$. This eliminated the possibility of normal stars that would have been visible and that of stellar remnants that would have implied a metallicity higher than observed. This leaves us with the possibility of primordial black holes of stellar masses, which is still not completely ruled out. Thirdly, in three particular cases, it was shown that the lenses were probably stars of the Magellanic clouds. This casted doubt on the other observations whose nature could not be determined with certainty.

The EROS collaboration tried to observe events with smaller characteristic times, and hence lenses of smaller masses. No such events were observed, leading only to uppers limits on the MACHO content of the halo, as seen in Figure 1.1.

The role of baryonic dark matter constituted by mini black holes seems therefore to be very restricted nowadays. Furthermore, X-ray studies of galaxy clusters reveal vast amounts of gas present between the galaxies in such clusters, accounting for a non-negligible part of the baryonic dark matter. In summary, baryonic dark matter certainly constitutes a small

part, estimated to be less than 15%, of the total density of dark matter [3].

In response to the observations above, astronomers have begun to turn to non-baryonic forms of dark matter, composed of elementary particles. Thus, in the middle of the 1990's, one considered neutrinos as contributors to non-baryonic dark matter, with the advantage that they were at least known to exist. With a relic neutrino number density evaluated at $N_\nu = 113\, cm^{-3}$ per neutrino flavor, the sum of the masses of the three flavors had to have the value $\sum m_\nu c^2 = 47$ eV to explain the observed dark matter density [3]. It is believed that the mass of the electron-neutrino lies below 2.5 eV/c^2, the masses of the other two (muon and tau neutrinos) being rather uncertain, but evidence from neutrino oscillations indicated very small mass differences, suggesting very low masses for these too. A sum of neutrino masses of 47 eV/c^2 seems therefore too high, although this possibility has not yet been completely rejected. But another more serious problem appeared to be the fact that neutrinos were a kind of "hot" dark matter, i.e. relativistic at the time of decoupling and also when the structures in the universe were forming. Indeed, it was realized that dark matter should have been non-relativistic at the time of decoupling from plasma and radiation, so that one talks today about Cold Dark Matter (CDM), to condense and accelerate the collapse mechanism of baryonic matter after its decoupling from radiation. A kind of hot dark matter would in fact stream away rapidly and tend to iron out any primordial density fluctuations.

In the present context of cold dark matter, a very popular hypothesis is that it is made of Weakly Interacting Massive Particles (WIMPs), moving with non-relativistic velocities at the time of decoupling, well before the beginning of the matter-dominated era. These new massive particles must be stable and, because they have not yet been directly observed, should not interact electromagnetically. Models must then be proposed to explain their origin and properties. Among others, we encounter massive sterile neutrinos or particles from supersymmetric theories (SUSY), such as the neutralino.

There are two possibilities to detect WIMPs : direct or indirect detection. The first one corresponds to an interaction of the particle in a certain type of detector and the second one relies on the observation of the annihilation products of WIMPs. Such annihilations could happen in the halo of the galaxy as well as in the core of the sun. In the case of the sun, this emission of secondary products would mimic an extra flux of high energy neutrinos from the direction of our star, which is in fact not observed, excluding this possibility in the particular case of the sun.

One way to detect directly particles that interact very little is to measure the nuclear recoil that they produce by hitting the nuclei constituting the detector. One can show that the maximum laboratory kinetic energy E_r of the recoiling nucleus is given by [3] :

$$E_r(max) = \frac{2\mu^2 v^2}{M_N}$$

where $\mu = \frac{M_N M}{M_N + M}$ is the reduced mass, M is the mass of the WIMP, M_N is the mass of the recoiling nucleus of mass number A, and v is the WIMP velocity. This corresponds to the situation in which the momentum vector of the nucleus in the center of mass system is reversed in the collision, so that it is scattered in the forward direction. $E_r$varies from $\frac{v^2 M_N}{2}$ when $M = M_N$ to $2v^2 M_N$ when $M \gg M_N$, so with $v \sim 10^{-3} c$ (galactic escape velocity) and $M_N \sim A$ GeV/c^2, we expect E_r to be of the order of $E_r \sim M_N v^2 \sim A \times 1/c^2 \times 10^{-6} c^2 = A$ keV. Hence, sensitive detectors are needed to detect such small recoil energies.

Several methods have been used to record that kind of signal. Among them, one encounters the detection of the scintillation light from scintillating materials such as NaI or liquid Xe. Several experiments are underway, such as the underground XENON100 experiment installed in Italy. XENON100 is a liquid xenon detector [4, 5] that, because of the rock that protects it from the muons coming from cosmic rays, its ultra-pure active material and its excellent position reconstruction of the events, is an almost background-free instrument to detect the faint signal that dark matter constituted by WIMPs could deposit in the medium in the form of a nuclear recoil. The last configuration of XENON100 uses 161 kg of material, 99 kg being used to oppose radioactivity and cosmic rays and 62 kg as active target. It is in fact a two-phase liquid xenon detector equipped with photomultiplier tubes amplifying the two signals $S1$ and $S2$ produced by an event : a particle generates primary scintillation light ($S1$) and ionizations electrons in the liquid phase. The electrons drift upward because of an electric field and are detected via secondary scintillation light ($S2$) in the gas phase. The origin of the $S2$ signal gives the position of the event in the xy-plane and the drift time corresponding to the time interval between $S1$ and $S2$ gives the last coordinate z, locating the event in three dimensions with a very good resolution. Additionally, the ratio $S2/S1$ allows event discrimination between nuclear recoils due to WIMPs (low $S2/S1$ ratio) from backgrounds due to gamma or beta decays (electron recoils with much higher $S2/S1$ ratio). The experiment has a low-energy threshold of about 5 keVr (nuclear recoil energy).

Using the discrimination parameter $\log_{10}(S2/S1)$, three events have survived all the subtraction tests performed on the data acquired on 100.9 live days between January and June 2010 [6] and fall into the WIMP search region, where (1.8 ± 0.6) events from background were expected. Given the background expectation, the observation of three events does not constitute evidence for dark matter because the probability to observe three or more events was 28%. Therefore, only upper limits on the elastic WIMP-nucleon cross section σ versus the mass of the hypothetical particles could be determined and are shown in Figure 1.2.

The thick blue line (XENON100 2011) corresponds to the 90% confidence level (CL) limit and has a minimum $\sigma = 7.0 \cdot 10^{-45}$ cm^2 at a WIMP mass of $m_\chi = 50$ GeV/c^2. We see that it excludes part of the parameter space of supersymmetric theories (in grey) and that it contradicts in particular the interpretation of the DAMA (red) and CoGent (green) results

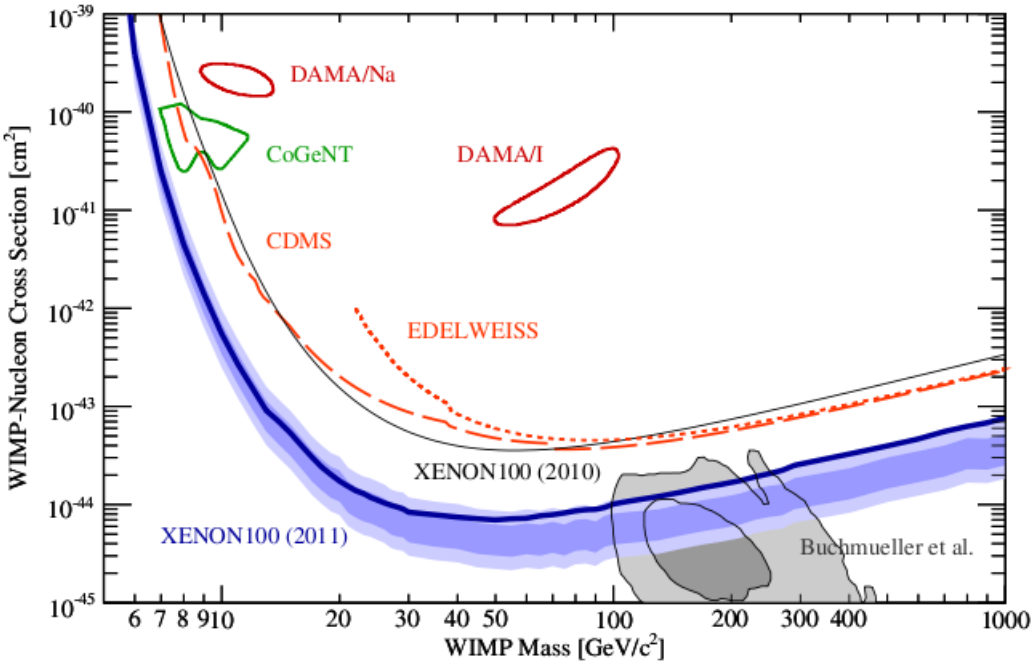

Figure 1.2: Spin-independent elastic cross section σ as function of WIMP mass m_χ. The thick blue line shows the latest XENON100 upper limit at 90% confidence level. The upper limit from previous XENON100 (2010) is shown by the thin black line. The two 90% CL areas favored by DAMA [7] (corresponding to scattering on each of the components of the detector : Na and I) are in red, while the 90% CL area from CoGent is in green (see [8]). The limits from CDMS II (2010) (Cryogenic Dark Matter Search) and EDELWEISS II (2010) correspond to the dotted and dashed orange lines respectively. These latter two are not discussed in this thesis but show the same trend as XENON100, with parameters a little less constrained. For more details about the CDMS and EDELWEISS experiments, see [9, 10]. *Figure extracted from* [6].

as being due to light mass WIMPs.

The DAMA underground experiments, which will be discussed further in Chapter 2, have indeed detected a signal in the range $(2-4)$ keV presenting an annual modulation that could be due to the motion of the Earth around the sun in a dark matter halo. One way to resolve the contradiction with XENON100 as well as with other experiments that could only set upper limits on the cross section would be for example to find another explanation in terms of dark matter, i.e. find another candidate than WIMPs, and try to explain the positive results of experiments as DAMA observing a signal without contradicting the others. This is obviously only one possibility to try to remove the contradictions that seem to divide the current research in the field of dark matter and all the options should continue to be considered.

It should be noted that the CoGent experiment, including a 440-gram crystal of germanium, as it is seen in Figure 1.2, had already detected (in early 2010) a signal with ionization

energies in the range of approximately 0.4 to 1.0 keV [8] through the ionization caused by nuclear recoils within the crystal and had deduced the green region in the hypothesis of light WIMPs with masses around 10 GeV. But no evidence for annual modulation had been reported. However, very recently, it has been observed that the signal changes with the seasons in the same way as the DAMA results does. If this is confirmed, this will be the first evidence for annual modulation somewhere else than in the DAMA detectors.

Under the previous approach consisting in finding another candidate than WIMPs, one of the alternatives to these popular particles as the constituents of dark matter consists in new heavy stable charged particles bound in neutral "dark atoms". Cosmological arguments indicate that these charged particles should be of charge -2 only and there exist several theories in which such particles, generically called O^{--}, are indeed predicted. In all these models, O^{--} behaves either as a lepton or as a specific heavy quark cluster with strongly suppressed hadronic interactions. Therefore the strong interactions of these dark atoms with matter are determined by the nuclear interactions of He only. This will be an important point hereafter. Cosmological scenarios predict that, just after its formation in primordial nucleosynthesis, He^{++} screens the O^{--} charged particles in composite $(O^{--}He^{++})$ "atoms", which are called O-helium (abbreviated as OHe) [11, 12, 13].

The hypothesis of OHe can be tested by the confrontation with experimental data from DAMA/NaI or DAMA/LIBRA [14, 15]. The annual modulation detected by these experiments can be understood in the framework of a dark matter dominated by OHe. The emission of a signal may result from the interactions of OHe with matter in the detector. A bound state OHe-nucleus in the range $(2-4)$ keV could exist and lead thermal OHe to emit a photon at the same energy when approaching the nucleus (radiative capture), providing the observed signal. In the case of CoGent, the emitted photon would ionize the medium, producing the observed signal at about 1 keV. The annual modulation is easy to explain by assuming the existence of a halo of OHe surrounding the galaxy. Indeed, the equilibrium concentration of OHe in underground detectors can be estimated by equaling the incoming flux at the terrestrial surface and the infalling flux towards the center of the earth. Any change in the initial flux at the surface leads to a change in concentration in the detector and therefore to a modulation in intensity. The incoming flux directly depends on the sum of the velocities of the earth around the sun and the sun around the center of the galaxy: when they are aligned, the flux reaches its maximum but when they are opposed, it is at its minimum, hence the observed one-year period.

The challenge is thus to find a 3 keV bound state of OHe with one of the components of DAMA. This task has been envisaged by Maxim. Yu. Khlopov et. al. [11, 12, 13]. Having established an analytic form for the potential, they simplified it by a square well potential to solve it exactly and search for a bound state at 3 keV in one of the regions.

Hints about the existence of this bound state began to favour to sodium of the detector, and they succeeded, by adjusting the parameters, to reproduce this level. The potential they used at large distances includes electrostatic and nuclear interactions, corresponding respectively to the coulomb potential of O^{--} screened by He^{++} and to σ meson exchange between He and the nucleus, giving rise to a Yukawa-like potential, both decreasing as $\exp(-r)/r$. No bound states have been found for the other constituent of the DAMA detector, iodine, and for xenon from XENON experiments, this last result allowing to remove the contraction between the two experiments.

The observations of DAMA raise a lot of questions and the track of the OHe should be followed with great interest given the encouraging theoretical results. However, a closer analysis of the potential of interaction OHe-nucleus has to be carried out, using its true shape in the Schrödinger radial equation. Here we propose to use an approximate analytical solution as provided by the WKB (Wentzel-Kramers-Brillouin) method. The main objectives of this Master thesis are thus at first to understand the WKB method before applying it to the interaction potential, in the framework of a three-dimensional problem, to provide an improved resolution and verify or disprove the existence of a bound state at 3 keV for sodium.

This Master thesis will be organized as follows : in Chapter 2, we will present the DAMA experiment and its positive results. Then we will summarise the properties of OHe as the candidate for these observations. The potential of interaction O^{--} - nucleus will be drawn from physical arguments first and then derived mathematically. This will fix the problem and it will be time to consider and describe the WKB method as a source of approximate analytical solution. This last point will be the subject of Chapter 3. Chapter 4 will be dedicated to the resolution of the WKB equations, extended to all the known nuclei. We will first use the non-modified WKB method, which is a pure copy at three dimensions of the one-dimensional case in which the method is usually presented. Then a modified WKB method will be tried, probably better suited to the case in three dimensions. The third section of chapter 4 will treat the resolution of the simplified square well potential with the exact solution in order to compare it to the approximate WKB solution. This will be a way to estimate the accuracy of the WKB method in our problem. In all cases, the numerical results will be presented. In chapter 5, we will calculate the transmission coefficients that are obtained in the non-modified and modified cases and that correspond to tunneling leading to the formation of heavy isotopes of known elements and to possible products of nuclear and electromagnetic reactions between OHe and the surrounding material. Of course, we will have to consider these results together with the rate of tunneling in order to determine a mean lifetime of a bound state OHe - nucleus before it enters the nuclear interaction region. This thesis ends with a conclusion summarizing the results and discussing the possible

improvements to the model.

Chapter 2

DAMA and the OHe hypothesis

2.1 The DAMA experiment

This Master thesis centers on the DAMA (DArk Matter) experiment, and will try to explain its positive results in terms of OHe. So we present here a brief description of the experiment and typical results that were obtained, following references [14, 15].

In fact, there exist two DAMA experiments, both located at the Gran Sasso National Laboratory in Italy and searching for direct evidences of DM (Dark Matter) particles. The former, DAMA/NaI has collected results during the period 1996-2002. Its successor is the DAMA/LIBRA (Large sodium Iodine Bulk for RAre processes) experiment, which uses very similar technology but has a larger target mass of 250 kg, and is still running today. The highly pure $\simeq$ 250 kg NaI (doped with thallium) DAMA/LIBRA set-up is running using the annual modulation signature of dark matter in the hypothesis of a dark matter halo that surrounds the galaxy. The exploitation of the annually modulated DM signature with highly radiopure NaI(Tl) as target material can permit to know if there are actually Dark Matter (DM) particles in the galactic halo, by direct detection and regardless of the nature of the candidate and of the astrophysical aspects. The set-up consists of NaI(Tl) scintillators used as target detectors. Nuclei recoiling after a collision cause emissions of photons that are detected using photomultiplier tubes. In our case, the emission will be instead due to radiative capture of OHe by a nucleus, detectable in the same way as a recoil. DAMA is sensitive up to the MeV scale, even though the optimization is made for the lowest energy region, that is for several keV, in which a signal is actually detected.

Let us recall that the DM modulation signature uses the effect of the Earth revolution around the Sun on the number of events induced by DM particles in a suitable low background set-up placed deep underground. As a consequence of its annual revolution, the Earth is crossed by larger and smaller fluxes of DM particles at different times of the year, as its rotational velocity adds up to the one of the Sun with respect to the Galaxy (around

June 2nd), or on the contrary is subtracted to it (around December 2nd, i.e. six months later). Therefore, the counting rate of events in the k–th energy interval can be written as :

$$S_k = S_{0,k} + S_{m,k}\cos(\omega(t - t_0)) \tag{2.1}$$

where $S_{o,k}$ is the constant part of the signal, $S_{m,k}$ is the modulation amplitude, $\omega = \frac{2\pi}{T}$ with period T and t_0 is the phase ($\simeq$ June 2^{nd}).

An annually modulated signal is very distinctive since a seasonal effect induced by DM particles must satisfy many restrictive constraints. Among others, the rate must contain a component modulated according to a cosine function, with a one-year period, with a phase roughly around June 2^{nd}, in a well-defined low-energy range, where DM particles can induce signals. DAMA/LIBRA and the former DAMA/NaI are the only experiments effectively exploiting all the aspects the DM annual modulation signature and all the restrictive constraints associated with it. This may be the reason of the lack of observations in some other experiments.

Table 2.1 and Figure 2.1 present some results obtained over several years by DAMA/NaI and DAMA/LIBRA. The curves in Figure 2.1 are quite convincing and leave little doubt on an annual modulation in the signal in the range $(2-4)$ keV. With the cumulative exposure, the modulation amplitude of the events in the $(2-6)$ keV energy interval measured in the NaI(Tl) detector is (0.0116 ± 0.0013) cpd/kg/keV (counts per day per kg per keV). The measured phase is (146 ± 7) days and the measured period is (0.999 ± 0.002) yr, well in agreement with the values expected for an annual modulation signature. These results motivate the study of OHe and the search for a bound state with one of the components of the detector in the energy range $(2-4)$ keV.

Figure 2.2 shows the cumulative low-energy distribution of the single-hit scintillation events measured by the DAMA/LIBRA detectors in an exposure of 0.53 ton×yr. The observed signal is visible between 2 and 4 keV, while the higher signal below 2 keV corresponds to experimental noise and shows that the energy threshold is equal to 2 keV.

To support the observations, a theoretical model is needed, which proposes a serious candidate that could explain the observational results. This is just what we are trying to do with the OHe in this Master thesis. Before entering into the details of developments specific to this work, let us give an overview of what is already known about OHe.

2.2 Presentation of OHe

In this section, we mainly follow some of the aspects considered in [11, 12, 13]. OHe is an example of a new type of objects that are called “dark atoms”. Whereas most dark matter models propose candidates that are neutral particles, we consider here new stable charged

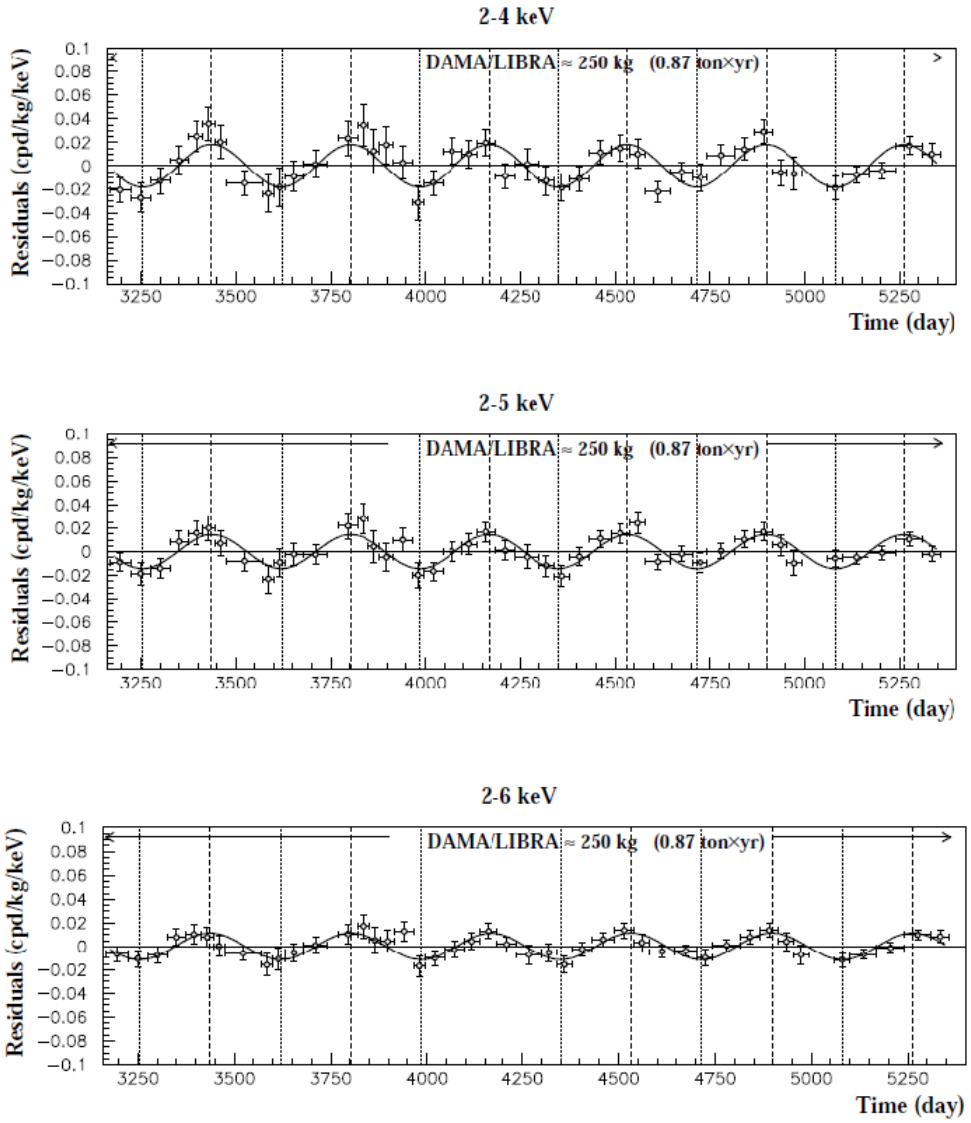

Figure 2.1: Experimental residual rate of the single-hit scintillation events, measured by DAMA/LIBRA runs in the $(2-4)$, $(2-5)$ and $(2-6)$ keV energy intervals as a function of time. The zero of the time scale is January 1st of the first year of data taking of the former DAMA/NaI experiment. The experimental points present the errors as vertical bars and the associated time bin width as horizontal bars. The superimposed curves are the cosine functions $A\cos(\omega(t-t_0))$ with a period $T = \frac{2\pi}{\omega} = 1$ yr, with a phase $t_0 = 152.5$ day (June 2nd) and with amplitudes A equal to the central values obtained by best fit over the whole data including also the exposure previously collected by the former DAMA/NaI experiment: cumulative exposure is 1.17 ton $\times$ yr. The dashed vertical lines correspond to the times of the maxima expected for the DM signal (June 2nd), while the dotted vertical lines correspond to the minima. *Figure extracted from [15].*

	Period	mass (kg)	exposure (kg × day)	$(\alpha - \beta^2)$
DAMA/LIBRA-1,2,3,4	Sept. 9, 2003 - July 17, 2007	232.8	192824	0.537
DAMA/LIBRA-5	July 17, 2007 - Aug. 29, 2008	232.8	66105	0.468
DAMA/LIBRA-6	Nov. 12, 2008 - Sept. 1, 2009	242.5	58768	0.519
DAMA/LIBRA-1 to -6	Sept. 9, 2003 - Sept. 1, 2009		317697 $\simeq$ 0.87 ton × yr	0.519
DAMA/NaI + DAMA/LIBRA-1 to -6			1.17 ton × yr	

Table 2.1: Exposures of the DAMA/LIBRA annual cycles and the cumulative exposure of runs 1,2,3,4,5,6, when including the former DAMA/NaI. Here $\alpha = \langle \cos(\omega(t - t_0)) \rangle^2$ is the mean value of the squared cosine and $\beta = \langle \cos(\omega(t - t_0)) \rangle$ is the mean value of the cosine (the averages are taken over the live time of the data taking and $t_0 = 152.5$ day, i.e. June 2^{nd}); thus $(\alpha - \beta^2)$ indicates the variance of the cosine. *Data extracted from [15].*

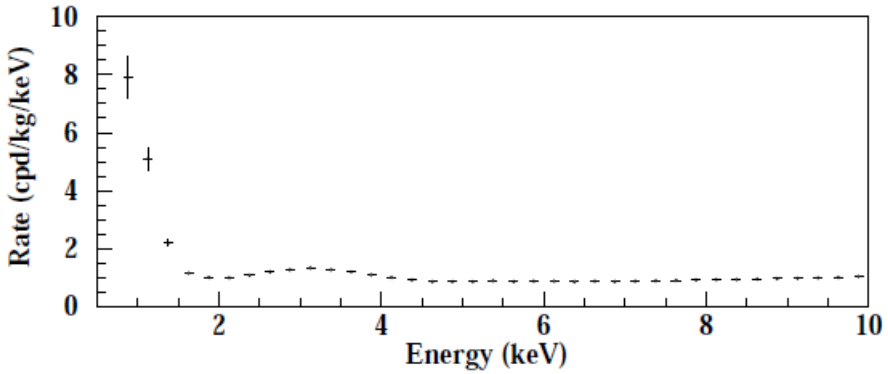

Figure 2.2: Cumulative low-energy distribution of the single-hit scintillation events as measured by the DAMA/LIBRA detectors in an exposure of 0.53 ton×yr. This shows that the energy threshold of the experiment is 2 keV. *Figure extracted from [14].*

particles bound to primordial helium in neutral dark atoms and we can already talk about unconventional dark matter in the sense that it is a kind of composite dark matter.

As we already mentioned in the Introduction, these particles should be of charge -2. Indeed, the main problem with charged particles as the solution for dark matter is to suppress the abundance of positively charged particles bound to ordinary electrons, the result being anomalous isotopes of hydrogen or helium. This problem is insurmountable if the particles are of charge -1. In 2005, Glashow proposed a model in which stable tera-U-quarks of charge $+2/3$ formed clusters UUU bound with tera-electrons E of charge -1 in neutral $(UUU)\,EE$ tera-helium that behaved like WIMPs. The problem is that as soon as primordial helium is formed in Big Bang nucleosynthesis, it captures all the free E in positively charged $(HeE)^{+}$ ions, preventing any further suppression of positively charged antiparticles. The acceptable solution is then obtained by considering particles of charge -2 only. It is also necessary that such stable particles are predicted by some models. This last point is verified since several exotic theories of elementary particles predict the existence of heavy stable particles of charge -2. We also may think about stable antibaryons $\bar{U}\bar{U}\bar{U}$ where U is a quark of fourth generation and charge $+2/3$.

In all the models, these -2 charge particles, generically called O^{--}, behave either as leptons or as specific heavy quark clusters, leading to strongly suppressed hadronic interactions. Indeed, O^{--} is expected to be very massive, of the order of 1 TeV. Not being constituted of quarks u or d (the constituents of baryonic matter in normal conditions), it does not interact through pion exchange (strong nuclear interaction). The only possible strong interaction is then reduced to pure gluon exchange between O^{--} and quarks u and d of conventional matter. The amplitude of the simplest interaction, corresponding to the exchange of only one gluon, is proportional to the strong coupling constant α_S. But this constant depends on the mass scale at which we are working, here the mass of O^{--}, and the standard model tells us that α_S is small in that case. This makes the hadronic interactions of O^{--} with matter strongly suppressed .

After it is formed in Big Bang nucleosynthesis, ${}^4He^{++}$ screens the O^{--} in composite $({}^4He^{++}O^{--})$, called O-helium (OHe) atoms [1]. Given the suppressed interaction of O^{--}, these dark atoms will interact mostly via the nuclear interactions of OHe.

The Big Bang theory states that all the primordial helium was formed after the first few minutes of the universe. When it has cooled enough, all free O^{--} are trapped by ${}^4He$, electromagnetically bound in O-helium atoms with an ionization potential given by the binding energy of an hydrogen-like atom :

$$I_0 = \frac{1}{2} Z_O^2 Z_{He}^2 \alpha^2 m_{He} \simeq 1.6\ MeV$$

[1] For more details about the cosmological aspects of OHe, see [11, 13].

where α is the fine structure constant, $Z_{He} = 2$ and $Z_O = 2$ are the absolute value of the electric charges of He^{++} and O^{--}.

From here, if not specified otherwise, it should be noted that we work with natural units supplemented by the Heaviside-Lorentz units :

$$\begin{cases} \hbar = c = k = 1 \\ \epsilon_0 = \mu_0 = 1 \end{cases}$$

where $\hbar = \frac{h}{2\pi}$ is the reduced Planck constant, c the speed of light, k the Boltzmann constant, ϵ_0 the dielectric permittivity of vacuum and μ_0 the magnetic permeability of vacuum.

The Bohr radius of OHe is obtained by simply replacing m_e by m_{He} and e^2 by $Z_O Z_{He} e^2$ in its expression : $r_0 = \frac{4\pi^2}{\pi m_e e^2} \rightarrow \frac{4\pi^2}{\pi m_{He} Z_O Z_{He} e^2} = \frac{4\pi}{e^2} \frac{1}{Z_O Z_{He} m_{He}} = \frac{1}{Z_O Z_{He} \alpha m_{He}}$ with $\alpha = \frac{e^2}{4\pi}$. In a first approximation, we assimilate the Bohr radius to the size of an O-helium atom :

$$r_0 \simeq 2.10^{-13}\, cm = 2\, fm$$

Hence we consider OHe as a semi-classical atom, with He^{++} orbiting around O^{--} on its Bohr orbit. This vision will be heavily used to establish the potential of interaction of OHe with matter in the next section.

2.2.1 OHe interaction with matter

Being decoupled from baryonic matter, the OHe gas does not follow the formation of baryonic astrophysical objects such as stars, planets or galaxies but forms dark matter halos surrounding the galaxies. The galaxy as a whole is transparent for OHe in spite of its interactions, making only individual compact objects (stars, planets) opaque for it. So, a consequence is the presence of OHe in terrestrial matter, which stores all its in-falling flux from the halo. After they hit the surface, the OHe particles fall down and are slowed down due to elastic nuclear collisions. So much that they are thermalized and give rise to so low energy transfer by recoil effects that this kind of direct detection is not appropriate for this form of dark matter. However, other observable effects due to OHe in underground detectors can take place.

To evaluate them, we first have to know the concentration of OHe in terrestrial matter, to which the rate of events is proportional. This can be estimated by the equilibrium between the in-falling and down-drifting fluxes. It can be shown that the down-drifting velocity of the particles towards the center of the earth is given by

$$V \simeq 80 S_3 A_{med}^{1/2}\, cm/s$$

where $A_{med} \simeq 30$ is the average atomic weight in terrestrial surface matter and $S_3 = M_{OHe}/(1\, TeV)$ with M_{OHe} the mass of OHe. The in-falling OHe flux from the halo is

given by

$$F = \frac{n_0}{4} |\overrightarrow{V}_h + \overrightarrow{V}_E|$$

where $V_h = 220$ km/s is the velocity of the solar system, $V_E = 29.5$ km/s is the velocity of the Earth around the Sun and $n_0 = 3.10^{-4} S_3^{-1} cm^{-3}$ is the local density of OHe in the dark matter halo. The $\frac{1}{4} = \frac{1}{2} \times \frac{1}{2}$ factor takes into account the "day-night cycle" due to the rotation of the Earth and the average of the flux on all latitudes and longitudes. Velocity dispersion and distribution of particles in the in-falling flux have not been taken into account for simplicity.

The equilibrium concentration n_{0E} deep beneath the surface is therefore obtained by equaling the two fluxes

$$n_{0E} V = F$$

The norm $|\overrightarrow{V}_h + \overrightarrow{V}_E|$ can be evaluated as follows

$$\begin{aligned} \left(\overrightarrow{V}_h + \overrightarrow{V}_E\right)^2 &= \overrightarrow{V}_h^2 + \overrightarrow{V}_E^2 + 2V_h V_E \cos(\omega(t - t_0)) \\ \Rightarrow |\vec{V}_h + \overrightarrow{V}_E| &\simeq V_h \left(1 + \frac{V_E}{V_h} \cos(\omega(t - t_0))\right) \end{aligned}$$

so that

$$\begin{aligned} n_{0E} &= n_{0E}^{(1)} + n_{0E}^{(2)} \cos(\omega(t - t_0)) \\ &= \frac{n_0}{320 S_3 A_{med}^{1/2}} V_h + \frac{n_0}{320 S_3 A_{med}^{1/2}} V_E \cos(\omega(t - t_0)) \end{aligned} \tag{2.2}$$

with obvious definitions of $n_0^{(1)}$ and $n_0^{(2)}$[2], which correspond respectively to the constant part and to the amplitude of modulation of the equilibrium concentration, and where ω has the same definition as for the counting rate (2.1) with a one-year period and with the same phase t_0.

In fact, the phase t_0 is not exactly the same as the time when the flux F reaches its maximum (when $\vec{V}_h$ and $\vec{V}_E$ are parallel) because of the drift time of the particles from the surface to the underground detector : the change of the incoming flux caused by the motion of the earth along its orbit leads at a depth $L \sim 10^5$ cm to the corresponding change in the equilibrium concentration of OHe on the timescale $t_{dr} \simeq \frac{L}{V} \simeq 2.510^2 S_3^{-1} = 2500$ s for $M_{OHe} = 1$ TeV.

The effects of OHe in the detector lead to the release of a signal with an intensity proportional to the concentration n_{0E}, depending on the details of the interactions of OHe with nuclei. Hereafter we derive the interaction potential, which will be repeatedly used in the following pages of this work.

[2]Note that this formula differs from that of [11] by a factor 2 in the amplitude of the oscillation.

As already announced, the explanation of the results of DAMA experiments is based on the assumption that OHe can form a few-keV bound state with at least one of the constituents of the detector (sodium, iodine and thallium). We are thus interested by the reaction :

$$A + ({}^4He^{++}O^{--}) \rightarrow [A({}^4He^{++}O^{--})] + \gamma$$

with nuclei of mass number A.

The main task is now to derive, from physical arguments, the potential of interaction OHe - nucleus, which will be later used in the Schrödinger equation. If this potential has spherical symmetry, we know that the spatial wave function can be separated in radial and angular parts : $\psi_{nlm}(r,\theta,\varphi) = \frac{u_{nl}(r)}{r} Y_l^m(\theta,\varphi)$ where Y_l^m are the spherical harmonics, with the condition $u_{nl}(0) = 0$ so that the wave function is regular at the origin. The radial part $u(r)$ is a solution of the radial Schrödinger equation taken in the center of mass of the system and representing the relative motion of the reduced mass μ:

$$\frac{d^2u}{dr^2} + 2\mu[E - V(r)] - \frac{l(l+1)}{r^2} = 0 \tag{2.3}$$

where E is the energy in the center of mass system, l is the relative angular momentum and the reduced mass is :

$$\mu = \frac{M_{OHe} M_A}{M_{OHe} + M_A} \tag{2.4}$$

where M_A is the mass of the nucleus. Since the mass of O^{--}, M_O, is expected to be very high, $M_{OHe} \simeq M_O \gg M_A$, the center of mass of the system approximately coincides with the position of O^{--} and $\mu \simeq M_A$.

An important remark is that strictly speaking, the problem at hand is a three-body problem ($O^{--} - He^{+} - nucleus$, each with an extension). Given the difficulty of dealing with this kind of problem, this is simplified to a two-body problem, OHe and nucleus, where the nucleus is seen as a point-like entity. To build the potential, we will need to consider OHe as an extended entity, that may be polarized for example. We will go from a representation of OHe as a simplified version of the atom (Bohr atom), where He is on a Bohr orbit of radius r_0 around O^{--}, to another one based on the ground state of a hydrogen-like atom. It is clear that a complete comprehension of the interactions of OHe with matter will only follow from a three-body analysis.

The approach [ ] assumes the following picture : at a distance larger than its size, OHe is neutral, being only the source of a Coulomb field of O^{--} screened by He^{++}

$$U_{III} = \frac{Z_O Z\alpha . F_O(r)}{r}$$

where $Z_O = -2$ is the charge of O^{--}, Z is the charge of the nucleus and $F_O(r) = (1 + \frac{r}{r_0}) \exp(-2r/r_0)$ is the screening factor of the Coulomb field of O^{--}, r_0 being the size (Bohr radius) of OHe. This results in an attraction between OHe and the nucleus at large distances.

Let us derive this expression for U_{III}. The main problem is to determine the electrostatic potential $U(r)$ generated at a point P at a distance r from the origin by a spherical distribution of charges [16], i.e. He of charge $2e$ in an s-state around O^{--}. The wave function in the ground state is given by $\psi(r') = \frac{2}{\sqrt{4\pi}} (r_0)^{-3/2} \exp(-r'/r_0)$ [17], so that the charge density $\rho(r') = 2e|\psi|^2$ is equal to

$$\rho(r') = \frac{2e}{\pi} \frac{1}{r_0^3} \exp(-2r'/r_0)$$

where $\overrightarrow{r'}$ locates the sources. To perform this calculation, it is appropriate to divide the charge distribution into concentric spherical shells of radius r' and thickness dr' and separate the cases where P is inside or outside the shells. Recall that the electrostatic potential is the same as though the shell were concentrated at the origin if P is outside and is constant whatever the position of P inside the shell. The infinitesimal elements to integrate from $r' = 0$ to $r' = \infty$ are therefore

$$dU(r) = \begin{cases} \frac{4\pi r'^2 \frac{2e}{\pi r_0^3} \exp(-2r'/r_0) dr'}{4\pi r}, & r \geq r' \\ \frac{4\pi r'^2 \frac{2e}{\pi r_0^3} \exp(-2r'/r_0) dr'}{4\pi r'}, & r \leq r' \end{cases}$$

and the electrostatic potential

$$U(r) = \frac{2e}{\pi r_0^3} \left(\frac{1}{r} \int_0^r r'^2 \exp(-2r'/r_0) dr' + \int_r^\infty r' \exp(-2r'/r_0) \right)$$

After integration by parts of these two integrals, we get easily

$$U(r) = \frac{-2e}{4\pi r_0} \left(1 + \frac{r_0}{r}\right) \exp(-2r/r_0) + \frac{2e}{4\pi r}$$

So far we have not taken into account the presence of O^{--} at the center of the charge distribution, generating a Coulomb potential $\frac{-2e}{4\pi r}$ that gives a total electrostatic potential at point P

$$\widetilde{U}(r) = \frac{-2e}{4\pi r_0} \left(1 + \frac{r_0}{r}\right) \exp(-2r/r_0)$$

Considering now the interaction potential OHe-nucleus and introducing the fine structure constant, we finally get

$$U_{III}(r) = \frac{-2Z\alpha}{r_0} \left(1 + \frac{r_0}{r}\right) \exp(-2r/r_0) \tag{2.5}$$

which is the desired screened Coulomb potential.

The difference with the studies that have already been made in [11, 12, 13] about this potential appears here : whereas in other works a Yukawa-like nuclear potential resulting from particles exchange between He and nucleus is added, we consider here only the purely electrostatic case at large distance.

When OHe approaches the nucleus, strong nuclear attraction between He and the nucleus causes the polarization of OHe and the mutual screened Coulomb attraction is changed by dipolar repulsion. Let us consider the negatively charged O^{--} at the origin and the positively charged He^{++} on its Bohr orbit, at a distance r_0 along the z axis. The nucleus is at distance r from O^{--}, r' from He^{++} and at an angle θ from the z axis. The electrostatic interaction potential at position $\overrightarrow{r}$ of the nucleus is given by :

$$U(r) = \frac{-2Z\alpha}{r} + \frac{2Z\alpha}{r'}$$

We have :

$$\begin{aligned} \overrightarrow{r'}^2 &= (\overrightarrow{r} - \overrightarrow{r_0'})^2 \\ &= \overrightarrow{r}^2 + \overrightarrow{r}_0^2 - 2\overrightarrow{r}\overrightarrow{r_0'}\cos\theta \\ &= r^2\left(1 + \frac{r_0^2}{r^2} - 2\frac{r_0}{r}\cos\theta\right) \end{aligned}$$

so that

$$\begin{aligned} \frac{1}{r'} &= \frac{1}{r\sqrt{1 + \frac{r_0^2}{r^2} - 2\frac{r_0}{r}\cos\theta}} \\ &\simeq \frac{1}{r}\left(1 + \frac{r_0}{r}\cos\theta\right) \end{aligned}$$

at the first order in $\frac{r_0}{r}$. Therefore, we find the well known dipolar approximation : $U(r) = \frac{2Z\alpha r_0}{r^2}\cos\theta$. We note that in our case, the nucleus, causing the polarization, is necessarily on the z axis, so that $\cos\theta = 1$. We finally have in the second region[3] :

$$U_{II}(r) = \frac{2Z\alpha r_0}{r^2} \tag{2.6}$$

where the factor 2 in the right hand side stands for the absolute value of the charge of the dipole ($= |Z_0|$). This simple remark allows us to keep a spherical symmetry for the problem, otherwise the solutions in the form of a radial part and spherical harmonics would no longer be valid, nor the time-independent radial equation recalled above.

When helium is completely merged with the nucleus, the interaction is dominated by the nuclear interaction of He with the nucleus, which can in a very good approximation be treated as a very deep rectangular well. The minimum value of this well will not be fixed

[3]Note that the assumption $\left(\frac{r_0}{r}\right)^2 \ll 1$ seems here not well verified because the polarization takes place when the nucleus and OHe are close from each other. It would be more appropriate to consider the exact expression for $\frac{1}{r'}$, always asking $\cos\theta = 1$: $\frac{1}{r'} = \frac{1}{r\sqrt{1+\frac{r_0^2}{r^2}-2\frac{r_0}{r}}} = \frac{1}{r\sqrt{\left(1-\frac{r_0}{r}\right)^2}} = \frac{1}{r-r_0}$, giving $U_{II}(r) = \frac{2Z\alpha r_0}{r(r-r_0)}$.
The direct effect of this correction is to raise the potential barrier that is this dipolar interaction region. The singularity in $r = r_0$ is only apparent because, as we shall see, the dipolar interaction is no longer valid at so small distances and has to be replaced by nuclear interaction.

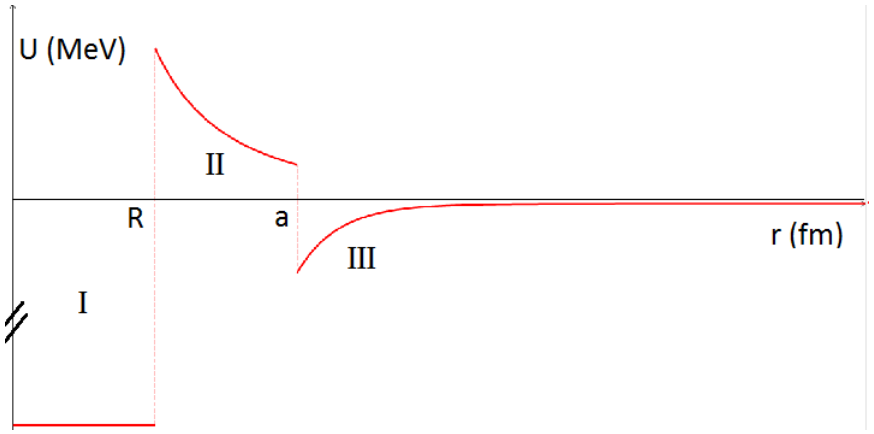

Figure 2.3: Shape of the potential of interaction OHe-nucleus

now but will be discussed later. Nevertheless, we can already say that it will be a value of the order of several tens of MeVs or perhaps a hundred MeVs, i.e. a typical magnitude for a nuclear potential well. We have therefore, in the region of the shortest distances

$$U_I = -V_0 \tag{2.7}$$

We are now ready to draw the shape of the potential. Figure 2.3 shows the type of curve with which we will have to deal. Typically, U_{II} takes values of the order of several MeVs and U_{III} is of the order of several keVs. Therefore, Figure 2.3 does not respect the proportions for clarity. The potential well in region III, in which we will search for a 3 keV bound state, is indeed very shallow compared to the other two regions. To delimitate the size of the different regions, we use the following simple arguments : region I corresponds to nuclear interaction between He and the nucleus, when helium is completely merged with the nucleus. Therefore, we consider that it extends from $r = 0$ to $r = R$ where R is the radius of the nucleus. Polarization takes place when helium and the nucleus are almost in contact, due to nuclear interaction. Thus, region II begins at $r = R$ and ends at $r = a \simeq r_0 + r_{He} + R$ where r_{He} is the radius of a helium nucleus. This is of course a very rough approximation, that will need to be refined later, but that is sufficient to understand the shape of the curve.

To be able to predict a rate of events, we must know the rate of radiative capture of OHe by the nucleus to the energy level E in a medium at temperature T. It can be shown that it is equal to [ ]

$$\sigma v = \frac{f\pi\alpha}{m_p^2}\frac{3}{\sqrt{2}}\left(\frac{Z}{A}\right)^2\frac{T}{\sqrt{Am_pE}}\ GeV^{-2} \tag{2.8}$$

when expressed in natural units. σ is the cross section of radiative capture and v is the relative velocity between OHe and the nucleus. The factor $f = \frac{m_n - m_p}{m_p} \simeq 1.4 \cdot 10^{-3}$ corresponds to the relative mass difference between neutron and proton, m_n and m_p being the masses of neutron and proton respectively.

The rate of events in a detector, measured in counts per day per kg (cpd/kg), separates into a constant part ξ and a modulated part of amplitude ς because of the annual modulation

$$\begin{aligned}\frac{dN}{dt} &= \sigma v(cm^3 s^{-1}) \times n_{0E}(cm^{-3}) \times n_{atoms}^{1\,kg\,of\,detector} \times t(=1\,day\,in\,seconds) \\ &= \sigma v\, n_{0E}^{(1)}\, n_{atoms}^{1\,kg\,of\,detector}\, t + \sigma v\, n_{0E}^{(12)}\, n_{atoms}^{1\,kg\,of\,detector}\, t\, \cos(\omega(t-t_0)) \\ &= \xi + \zeta \cos(\omega(t-t_0)) \end{aligned} \tag{2.9}$$

where $n_{atoms}^{1\,kg\,of\,detector} = \frac{1\,kg\,of\,detector \times N_A}{(A_I + A_{Na})} = \frac{QN_A}{(A_I+A_{Na})}$ is the number of atoms in 1 kg of matter of detector (made of NaI for the DAMA detector), with N_A Avogadro's number, and t the number of seconds in one day. With the previous expressions for σv and $n_{0E}^{(1)}$, the constant part ξ of the signal in the case of the detector of DAMA is given by

$$\begin{aligned}\xi &= \frac{3\pi\alpha n_0 N_A V_h t Q}{320\sqrt{2} A_{med}^{1/2}\,(A_I + A_{Na})} \frac{f}{S_3 m_p^2} \left(\frac{Z}{A}\right)^2 \frac{T}{\sqrt{A m_p E}} \\ &= 64.13 \cdot 10^{10} \frac{f}{S_3^2} \left(\frac{Z}{A}\right)^2 \frac{T}{\sqrt{A m_p E}} \end{aligned} \tag{2.10}$$

while the amplitude ς of the annual modulation of the signal can be expressed in the same way as

$$\begin{aligned}\varsigma &= \frac{3\pi\alpha n_0 N_A V_E t Q}{320\sqrt{2} A_{med}^{1/2}\,(A_I + A_{Na})} \frac{f}{S_3 m_p^2} \left(\frac{Z}{A}\right)^2 \frac{T}{\sqrt{A m_p E}} \\ &= 8.6 \cdot 10^{10} \frac{f}{S_3^2} \left(\frac{Z}{A}\right)^2 \frac{T}{\sqrt{A m_p E}} \end{aligned} \tag{2.11}$$

To get the right cpd/kg units and multiplicative factors, we used $n_0 = 3 \cdot 10^{-4} S_3^{-1}\, cm^{-3}$, $N_A = 6.022{\cdot}10^{23}\, mol^{-1}$, $V_E = 29.5{\cdot}10^5\, cm/s$, $t = 86400\, s$, $Q = 1000\, g$, $A_I{+}A_{Na} = 150\, g/mol$, $640 A_{med}^{1/2} S_3 \simeq 3505 S_3\, cm/s$, $m_p = 0.938\, GeV$, $\hbar c = 0.197{\cdot}10^{-13}\, cm{\cdot}GeV$ and $c = 3{\cdot}10^{10}\, cm/s$. The remaining temperature T has to be expressed in GeV via the conversion $1\, eV \leftrightarrow 11600\, K$ as well as m_p and E. Expression (2.11) will be useful to directly compare our results to the observations.

Using (2.11), we realize that the results of DAMA/NaI and DAMA/LIBRA experiments can approximately be reproduced in particular for a binding energy $E_{Na} = 3$ keV (taken in absolute value) for the OHe-Na system.

We have now to analyse the potential of interaction on Figure 2.3, to which can be added a centrifugal potential when the angular momentum is non-vanishing. Although it looks simple, no analytic solution exists for the potential of region III. To search for a low energy bound state in region III and to be able to begin the calculations, we thus need a method that can give us an approximate analytic solution. It is the role of the WKB method that we present in the following Chapter.

Chapter 3

The WKB approximation

The WKB (Wentzel-Kramers-Brillouin) approximation is a method of approximate resolution of the Schrödinger equation, applicable when the Schrödinger equation can be replaced by its classical limit, except in certain regions of space around singular points, called "turning points" (points where $E = V(\overrightarrow{r})$). This method is closely related to the classical limit of the Schrödinger equation and finds an interpretation in this context. So, before introducing the method itself, we consider the classical limit of quantum mechanics. In the first three sections of this Chapter, we follow some of the calculations that are made in [18]. The last one is from [16]. Note that in this particular chapter, we reinsert the reduced Planck constant ($\hbar \neq 1$) for reasons that will become clear shortly.

3.1 The classical limit of the Schrödinger equation

In the limit where $\hbar \to 0$, the laws of quantum mechanics must reduce to those of classical mechanics. This requirement has played a fundamental role in the elaboration of the theory. Classical mechanics must thus provide a good description of phenomena under circumstances where the quantum of action $\hbar$ may be considered as infinitely small, in the same way that we recover the geometrical optics when the wavelength λ goes to zero in wave optics. This idea is used in the WKB approximation where the wave function is developed in powers of $\hbar$, before we only keep the terms of first order in $\hbar$.

To better understand the WKB approach, let us therefore examine the classical approximation. Let us consider a particle in a potential $V(\overrightarrow{r})$ and separate the modulus and the phase of its wave function :

$$\psi(\overrightarrow{r}, t) = A(\overrightarrow{r}, t) \exp(\frac{i}{\hbar} S(\overrightarrow{r}, t)) \tag{3.1}$$

where A and S are real functions of t and $\overrightarrow{r}$. We can substitute expression (3.1) in the

Schrödinger equation dependent on time :

$$i\hbar\partial_t\psi(\overrightarrow{r},t)=\left[-\frac{\hbar^2}{2m}\triangle+V(\overrightarrow{r})\right]\psi(\overrightarrow{r},t) \tag{3.2}$$

and separate the real and the imaginary parts multiplying the phase factors to get respectively :

$$\partial_t S+\frac{\left(\overrightarrow{\nabla}S\right)^2}{2m}+V=\frac{\hbar^2}{2m}\frac{\triangle A}{A} \tag{3.3}$$

$$m\partial_t A+\left(\overrightarrow{\nabla}A.\overrightarrow{\nabla}S\right)+\frac{A}{2}\triangle S=0 \tag{3.4}$$

after developing $\triangle\psi$ as

$$\triangle A\exp(\frac{i}{\hbar}S)+\frac{2i}{\hbar}\left(\overrightarrow{\nabla}A.\overrightarrow{\nabla}S\right)\exp(\frac{i}{\hbar}S)+\frac{i}{\hbar}A\triangle S\exp(\frac{i}{\hbar}S)-\frac{1}{\hbar^2}A\left(\overrightarrow{\nabla}S\right)^2\exp(\frac{i}{\hbar}S)$$

The equations (3.3) and (3.4) are equivalent to equation (3.2). Equation (3.4) corresponds to the continuity equation. Indeed, the density of probability and the current density, respectively given by $P=|\psi|^2$ and $\overrightarrow{J}=\frac{\hbar}{2mi}\left(\psi^*\overrightarrow{\nabla}\psi-\psi\overrightarrow{\nabla}\psi^*\right)$, are in terms of A and S given by

$$P=A^2 \tag{3.5}$$

$$\overrightarrow{J}=A^2\frac{\overrightarrow{\nabla}S}{m} \tag{3.6}$$

By multiplying (3.4) by $2A$, we get $2mA\partial_t A+2A\left(\overrightarrow{\nabla}A.\overrightarrow{\nabla}S\right)+A^2\triangle S=m\partial_t A^2+\overrightarrow{\nabla}.\left(A^2\overrightarrow{\nabla}S\right)=0$, i.e.

$$\partial_t A^2+\overrightarrow{\nabla}.\left(A^2\frac{\overrightarrow{\nabla}S}{m}\right)=0 \tag{3.7}$$

which is nothing else than the continuity equation given expressions (3.5) and (3.6).

The classical approximation consists here in neglecting the term of order $\hbar^2$ in equation (3.3) (limit $\hbar\to 0$), which gives

$$\partial_t S+\frac{\left(\overrightarrow{\nabla}S\right)^2}{2m}+V=0 \tag{3.8}$$

If it really corresponds to the classical limit, the velocity $\overrightarrow{v}$ of the classical particles should be given by

$$\overrightarrow{v}=\frac{\overrightarrow{J}}{P}=\frac{\overrightarrow{\nabla}S}{m} \tag{3.9}$$

where P and $\overrightarrow{J}$ are seen as the density and the current density of a classical fluid. Therefore, the continuity equation being already verified, it remains to show that the velocity field (3.9) verifies the evolution law of a classical fluid. Equation (3.8) can be rewritten as $\partial_t S+\frac{mv^2}{2}+V=0$ and taking the gradient one gets $\partial_t\overrightarrow{\nabla}S+m\overrightarrow{v}.\overrightarrow{\nabla}v+\overrightarrow{\nabla}V=\left(\partial_t+\left(\overrightarrow{v}.\overrightarrow{\nabla}\right)\right)m\overrightarrow{v}+$

$\overrightarrow{\nabla} V = 0$. In other words, the particles obey the equation of motion of a classical fluid subjected to a potential V :

$$m\frac{d\overrightarrow{v}}{dt} = -\overrightarrow{\nabla} V$$

This last equation proves the desired result.

The optical analogy that we mentioned at the beginning of this section takes now all its meaning : since the velocities of the classical particles are proportional to $\overrightarrow{\nabla} S$, these, and hence the trajectories, are orthogonal to the surfaces $S = Cst$. But remember that S corresponds to the phase of the wave function, so that the surfaces $S = Cst$ are the wave front. In the classical limit, the trajectories are orthogonal to the surfaces of matter waves which are solutions of the Schrödinger equation, as in geometrical optics the rays are orthogonal to the surfaces of light waves which are solutions of the Maxwell equations.

3.2 WKB solutions in one dimension

As just mentioned, the method consists in replacing the Schrödinger equation by its classical limit through the introduction of a development in powers of $\hbar$ and in neglecting the terms of order greater than or equal to $\hbar^2$, after having done the same substitution as for the previous classical limit. But we want to make this replacement even in the regions where the classical interpretation has no sense (regions in which $E < V$). We have to change slightly the definitions of A and S to include these regions

$$\psi(\overrightarrow{r}) = \exp(\frac{i}{\hbar} W(\overrightarrow{r})) \tag{3.10}$$

$$W(\overrightarrow{r}) = S(\overrightarrow{r}) + \frac{\hbar}{i} T(\overrightarrow{r}) \tag{3.11}$$

$$A(\overrightarrow{r}) = \exp(T(\overrightarrow{r})) \tag{3.12}$$

where A and S can now be complex.

Here we derive the WKB solutions that are approximations of the stationary solutions of the Schrödinger equation independent of time. As the radial equation, recalled in section (2.2.1) relative to interactions of OHe with matter, is of the form of the equation in one dimension, we will be able to use the solutions established in one dimension in the three-dimensional case, when the potential has a spherical symmetry.

In one dimension, we have

$$y'' + \frac{2m}{\hbar^2}\left[E - V(x)\right] y = 0 \tag{3.13}$$

where the prime denotes the derivative with respect to x. The substitutions (3.10), (3.11), (3.12) give here

$$y = \exp(\frac{i}{\hbar}w), \qquad w = S + \frac{\hbar}{i}\ln A,$$

i.e. $y = A\exp(\frac{i}{\hbar}S)$. We can easily see that equation (3.13) becomes

$$S'^2 - 2m\,(E - V) = \hbar^2\frac{A''}{A} \tag{3.14}$$

$$AS'' + 2A'S' = 0 \tag{3.15}$$

for the real and imaginary parts respectively. These equations are to be compared with equations (3.3) and (3.4). Equation (3.15) can easily be integrated : $\frac{A'}{A} = -\frac{1}{2}\frac{S''}{S'} \Rightarrow \int\frac{dA}{A} = -\frac{1}{2}\int\frac{S''}{S'}dx = -\frac{1}{2}\int\frac{df}{f}$ where $f = S' \Rightarrow \ln A = \ln(S')^{-1/2} + C$, i.e.

$$A = C\left(S^{'}\right)^{-1/2} \tag{3.16}$$

which can be substituted in equation (3.14) to give :

$$S'^2 - 2m\,(E - V) = \hbar^2\,(S')^{1/2}\left[C\left(\frac{1}{2}\right)\left(\frac{3}{2}\right)(S')^{-5/2}\,(S'')^2 - Cs\left(\frac{1}{2}\right)(S')^{-3/2}\,S'''\right]$$

so that

$$S'^2 = 2m\,(E - V) + \hbar^2\left[\frac{3}{4}\left(\frac{S''}{S}\right)^2 - \frac{1}{2}\frac{S'''}{S'}\right] \tag{3.17}$$

The WKB approximation consists in introducing the development in powers of $\hbar^2$:

$$S = S_0 + \hbar^2 S_1 + ..., \tag{3.18}$$

to substitute in equation (3.17) for S and in keeping only the terms of order zero :

$$S'^2 \simeq S_0'^2 = 2m\,(E - V(x)) \tag{3.19}$$

Two cases are to be considered, corresponding to the classical and non classical regions

1. $E > V(x)$ (classical region)

We define the wavelength

$$\bar{\lambda} = \frac{\hbar}{\sqrt{2m\,(E - V(x))}} \tag{3.20}$$

which has length units. We can rewrite $\bar{\lambda} = \frac{\hbar}{p}$ where p is the local momentum of the classical particle. Indeed, $E = K + V$ with $K = \frac{mv^2}{2}$ the kinetic energy, so that $p^2 = m^2v^2 = 2m\,(E - V)$ and $p(x) = \sqrt{2m(E - V(x))}$. We have

$$S_0'^2 = \frac{\hbar^2}{\bar{\lambda}^2} \Rightarrow S_0' = \pm\frac{\hbar}{\bar{\lambda}} \simeq S'$$

$$S(x) = \int^x S' dx \simeq \int^x \frac{\hbar}{\bar{\lambda}} dx$$

$$\Rightarrow w(x) \simeq \pm \int^x \frac{\hbar}{\bar{\lambda}} dx + \frac{\hbar}{i} \ln C - \frac{1}{2} \frac{\hbar}{i} \ln S'$$

by definition of w. Therefore, we find that $y \simeq e^{\pm i \int^x \frac{dx}{\bar{\lambda}}} \times e^{\ln Cst} \times e^{-\frac{1}{2} \ln S'} = \frac{Cst}{\sqrt{k(x)}} e^{\pm i \int^x k(x) dx}$, so the most general solution has the form

$$y(x) \simeq \frac{1}{\sqrt{k(x)}} \left(A \exp(+i \int^x k(x) dx) + B \exp(-i \int^x k(x) dx) \right) \tag{3.21}$$

where $k(x) = \frac{1}{\bar{\lambda}(x)}$ and A and B are arbitrary constants. Solution (3.21) corresponds to the WKB approximation in the region $E > V(x)$.

2. $E < V(x)$ (forbidden region for classical particles)

This time we define

$$l(x) = \frac{\hbar}{\sqrt{2m\,(V(x) - E)}} \tag{3.22}$$

In the same way, we find

$$y(x) \simeq \frac{1}{\sqrt{\kappa(x)}} \left(C \exp(-\int^x \kappa(x) dx) + D \exp(+\int^x \kappa(x) dx) \right) \tag{3.23}$$

where $\kappa(x) = \frac{1}{l(x)}$ and C and D are arbitrary constants. Solution (3.23) is the WKB approximation in the region $E < V(x)$.

We immediately notice that solutions (3.21) and (3.23) diverge near the turning points $E = V(x)$ due to the factor $\frac{1}{|E-V|}$ contained in the amplitudes. So, the WKB solutions cannot be good approximations in these regions. As any approximation method, the WKB approximation has validity conditions that we derive hereafter.

3.3 Validity conditions

The most natural way to find a validity criterion is to calculate the second term $\hbar^2 S_1$ of the development (3.18) and see if the correction $e^{i\hbar S_1}$ to the wave function can be neglected or not. It will be the case if $\hbar S_1$ is negligible ($\hbar S_1 \ll 1$).

We have to substitute the development (3.18) into the equation (3.17) for S and keep the terms of order 0 and 1 in $\hbar^2$. We obtain an equation for S_1 by equaling the terms in $\hbar^2$. The details of the calculations can be found in Appendix A. The differential equation for S_1 is found to be

$$2S_0'S_1' = \frac{3}{4}\left(\frac{S_0''}{S_0'}\right)^2 - \frac{1}{2}\frac{S_0'''}{S_0'} \tag{3.24}$$

If $E > V$, we saw that $S_0' = \pm\frac{\hbar}{\bar{\lambda}}$. By inserting this last expression in (3.24), we obtain

$$\hbar S_1' = \pm\left(\frac{1}{4}\bar{\lambda}'' - \frac{1}{8}\frac{\bar{\lambda}'^2}{\bar{\lambda}}\right) \tag{3.25}$$

and therefore, after integration

$$\hbar S_1 = \pm\left(\frac{1}{4}\bar{\lambda}' - \frac{1}{8}\int^x \frac{\bar{\lambda}'^2}{\bar{\lambda}}dx\right) \tag{3.26}$$

The results are found to be the same, with $\bar{\lambda}(x)$ replaced by $l(x)$, when $E < V$. In view of equation (3.26), the condition $\hbar S_1 \ll 1$ is satisfied if

$$\bar{\lambda}'(x) \ll 1 \; when \; E > V(x)$$

$$l'(x) \ll 1 \; when \; E < V(x)$$

These two conditions can be simplified into one by using the definitions (3.20) and (3.22)

$$\frac{|m\hbar V'|}{|2m\,(E-V)\,|^{3/2}} \ll 1 \tag{3.27}$$

which we will consider as the criterion of validity of the WKB approximation. If it is not satisfied, the second term of the development (3.18) cannot be neglected and the approximation is not good. We see that near the turning points, and as already announced, the criterion is certainly not satisfied. This comes from the fact that, mathematically, the WKB approximation corresponds to the replacement of the Schrödinger equation by another equation which has a singular point at x such that $E = V(x)$. To obtain the complete solution, we must therefore solve the Schrödinger equation in a suitable region around the turning point and connect it with the WKB solutions on both sides, where they are good approximations. But in practice, it is not necessary to know the solution around a turning point. The most important issue is to be able to connect the WKB solutions on both sides, i.e. to connect the solution (3.21) in a region $E > V(x)$ far from the turning point to the solution (3.23) in a remote region $E < V(x)$ on the other side of it. Because they will be of paramount importance for the calculations that we will perform, we propose to complete this Chapter on the WKB method by presenting these connection formulas.

3.4 Connection formulas

Here we don't demonstrate the connection formulas but just explain the method to obtain them. The usual way to make the connection between the oscillatory solution (3.21) and

the exponential solution (3.23) is to separate out a small region around the turning point, in which we solve the Schrödinger equation exactly. We approximate the potential in this region by a linear function, and connect the exact solution to the asymptotic forms (3.21) and (3.23) to make a function that, together with its first derivative, is continuous. This procedure is general and has not to be done for each new problem. The result is a set of formulas that relate the constants A, B, C and D of (3.21) and (3.23), independently of what happens in the intermediate region. Two cases are to be considered :

Barrier to the right ($E < V$ to the right of the turning point) :

$$\begin{cases} C = \frac{1}{2}\left(\theta^* A + \theta B\right) \\ D = \theta A + \theta^* B \end{cases} \tag{3.28}$$

Barrier to the left ($E > V$ to the right of the turning point) :

$$\begin{cases} C = \theta^* A + \theta B \\ D = \frac{1}{2}\left(\theta A + \theta^* B\right) \end{cases} \tag{3.29}$$

where $\theta = e^{i\pi/4}$. These formulas will allow us to connect without any difficulty the two types of WKB solutions on both sides of a continuous transition from a classical (non classical) to a non classical (classical) region. Of course, in the case of a discontinuity of the potential, we will require as usual the continuity of the wave function and its first derivative.

Chapter 4

Resolution of the Schrödinger equation

In this chapter we analyse the potential presented in the Chapter 1 using the WKB approximation in order to find an energy level around 3 keV corresponding to a bound state in the third region. This is done in two ways : using the non-modified WKB approximation and a modified version thereof. The first method is a mere copy of the one-dimensional case given the similarity between the radial equation (2.3) and the Schrödinger equation in one dimension (3.13) if we consider the effective potential $V_{eff}(r) = V(r) + \frac{l(l+1)}{2\mu r^2}$, and the second one will be detailed in the corresponding section. Then we consider a simplified version of our problem, which is a square well-potential. The goal being to determine a minimum energy state in a given region, we will search for the minimum energy solution in that region corresponding to an angular momentum equal to zero, so that we can set $l = 0$ in the effective potential. Higher levels for $l = 0$ are also considered. In each case, we present the numerical results.

4.1 Non-modified WKB approximation

4.1.1 Construction of the solutions

In the case $l = 0$, the spherical harmonic $Y_l^m(\theta, \varphi)$ becomes $Y_0^0 = \frac{1}{\sqrt{4\pi}}$. Therefore, the wave function $\psi_{n,l,m}(r, \theta, \varphi) = \frac{u_{n,l}(r)}{r} Y_l^m(\theta, \varphi)$ takes the form $\psi_{n,0,0}(r) = \frac{1}{\sqrt{4\pi}} \frac{u_{n,0}(r)}{r}$, with $u_{n,0}$ a solution of the radial equation

$$\frac{d^2 u_{n,0}}{dr^2} + 2\mu[E_{n,0} - V(r)] = 0 \tag{4.1}$$

Here we impose the condition $0 > E_{n,0} > min(U_{III}(r))$ and to simplify the notations we write $E_{n,0} \equiv E$ as well as $u_{n,0}(r) \equiv u(r)$. Equation (4.1) for $u(r)$ has the same form as the equation in one dimension, therefore we will apply the WKB solutions derived in subsection

3.2 to $u(r)$. Taking into account the classical and non-classical regions, one gets :

$$\begin{aligned} u_I(r) &= u(0 < r < R) \\ &= A\sin(Kr + \delta) \end{aligned} \tag{4.2}$$

in region I, where $K = \sqrt{2\mu(E + V_0)}$. This is of course the exact solution.

$$\begin{aligned} u_{II}(r) &= u(R < r < a) \\ &= \frac{C}{\sqrt{\kappa_{II}(r)}} \exp(-\int_R^r \kappa_{II}(r)dr) + \frac{D}{\sqrt{\kappa_{II}(r)}} \exp(+\int_R^r \kappa_{II}(r)dr) \end{aligned} \tag{4.3}$$

in region II, where $\kappa_{II}(r) = \sqrt{2\mu(U_{II}(r) - E)}$, $U_{II}(r) = \frac{2Z\alpha r_0}{r^2}$. Region III has to be separated in two regions (III $\rightarrow$ III and IV) on both sides of the turning point d such that $U(d) = E$:

$$\begin{aligned} u_{III}(r) &= u(a < r < d) \\ &= \frac{A'}{\sqrt{k_{III}(r)}} \exp(+i\int_a^r k_{III}(r)dr) + \frac{B'}{\sqrt{k_{III}(r)}} \exp(-i\int_a^r k_{III}(r)dr) \end{aligned} \tag{4.4}$$

in region III, where $k_{III}(r) = \sqrt{2\mu(E - U_{III}(r))}$, $U_{III}(r) = \frac{-2Z\alpha}{r_0}\left(1 + \frac{r_0}{r}\right)\exp(-2r/r_0)$ and

$$\begin{aligned} u_{IV}(r) &= u(r > d) \\ &= \frac{C'}{\sqrt{\kappa_{IV}(r)}} \exp(-\int_d^r \kappa_{IV}(r)dr) + \frac{D'}{\sqrt{\kappa_{IV}(r)}} \exp(+\int_d^r \kappa_{IV}(r)dr) \end{aligned} \tag{4.5}$$

in region IV, where $\kappa_{IV}(r) = \sqrt{2\mu(U_{IV}(r) - E)}$, $U_{IV}(r) = U_{III}(r)$.

4.1.2 Connections - quantization of the energy

The constants A, δ, C, D, A', B', C' and D' are constrained by the requirement that the solution must be zero at the origin , by the conditions of continuity of the wave function and its first derivative at the points of discontinuity of the potential, and by the connection formulas (3.28) on both sides of the turning point :

$$u_I(0) = 0 \tag{4.6}$$

$$u_I(R) = u_{II}(R) \tag{4.7}$$

$$u'_I(R) = u'_{II}(R) \tag{4.8}$$

$$u_{II}(a) = u_{III}(a) \tag{4.9}$$

$$u'_{II}(a) = u'_{III}(a) \tag{4.10}$$

$$C' = \frac{1}{2}\left(\theta^* A' e^{i\rho} + \theta B' e^{-i\rho}\right) \tag{4.11}$$

$$D' = \theta A' e^{i\rho} + \theta^* B' e^{-i\rho} \tag{4.12}$$

where the u' denotes the derivative of u with respect to r. Conditions (4.7) to (4.12) ensure in fact that the probability current, in which the wave function and its gradient appear, is continuous, as well as the density of probability. Expressions (4.11) and (4.12) are obtained by slightly changing the expression of $u_{III}(r)$ such that it refers to the turning point $r = d$, as $u_{IV}(r)$, since it is in that situation that the connection formulas (3.28) and (3.29) have been derived. So we simply make the decomposition $\int_a^r k_{III}(r)dr = \int_a^d k_{III}(r)dr + \int_d^r k_{III}(r)dr$ and rewrite

$$u_{III}(r) = \frac{A'}{\sqrt{k_{III}(r)}}\, e^{i\rho} \exp(+i\int_d^r k_{III}(r)dr) + \frac{B'}{\sqrt{k_{III}(r)}}\, e^{-i\rho} \exp(-i\int_d^r k_{III}(r)dr)$$

where ρ is defined as

$$\rho = \int_a^d k_{III}(r)dr \tag{4.13}$$

With the new constants $A'e^{i\rho}$ and $B'e^{-i\rho}$ we can use the WKB connection formulas. To the seven previous conditions, we add the constraint :

$$D' = 0 \tag{4.14}$$

which guarantees that the exponential solution in region IV will not diverge when $r \to \infty$. Equations (4.6) to (4.12) together with (4.14) will enable us to determine a condition on the energy, which will be checked for only specific values of E. This expression will be our quantization condition, and its first solution will correspond to the desired value of the binding energy. In what follows, details of pure algebra are not all included. Some calculations are shown in Appendix B.

Condition (4.6) directly implies $\delta = 0$. Condition (4.7) is written as

$$A\sin(KR) = \frac{C+D}{\sqrt{\kappa_{II}(R)}}$$

and (4.8) gives

$$\begin{aligned} AK\cos(KR) &= -C\left(\sqrt{\kappa_{II}(R)} + \frac{1}{2}\left(\kappa_{II}(R)\right)^{-3/2}\kappa'_{II}(R)\right) \\ &+ D\left(\sqrt{\kappa_{II}(R)} - \frac{1}{2}\left(\kappa_{II}(R)\right)^{-3/2}\kappa'_{II}(R)\right) \end{aligned}$$

remembering that $\frac{d}{dr}\int_R^r \kappa_{II}(r)dr = \kappa_{II}(r)$. The inversion of these two equations allows us to write C and D in terms of A

$$\begin{aligned} C &= -\frac{A}{2}\left(\frac{K}{\sqrt{\kappa_{II}(R)}}\cos(KR) - \sqrt{\kappa_{II}(R)}\sin(KR) + \frac{1}{2}\sin(KR)\left(\kappa_{II}(R)\right)^{-3/2}\kappa'_{II}(R)\right) \\ D &= \frac{A}{2}\left(\frac{K}{\sqrt{\kappa_{II}(R)}}\cos(KR) + \sqrt{\kappa_{II}(R)}\sin(KR) + \frac{1}{2}\sin(KR)\left(\kappa_{II}(R)\right)^{-3/2}\kappa'_{II}(R)\right) \end{aligned}$$

which we rewrite, for simplicity

$$C = -\frac{A}{2}X \tag{4.15}$$

$$D = \frac{A}{2}Y \tag{4.16}$$

with the real numbers X and Y given by

$$X = \frac{K}{\sqrt{\kappa_{II}(R)}}\cos(KR) - \sqrt{\kappa_{II}(R)}\sin(KR) + \frac{1}{2}\sin(KR)\left(\kappa_{II}(R)\right)^{-3/2}\kappa'_{II}(R) \tag{4.17}$$

$$Y = \frac{K}{\sqrt{\kappa_{II}(R)}}\cos(KR) + \sqrt{\kappa_{II}(R)}\sin(KR) + \frac{1}{2}\sin(KR)\left(\kappa_{II}(R)\right)^{-3/2}\kappa'_{II}(R) \tag{4.18}$$

To treat equations (4.9) and (4.10), we first decompose the integral involved in $u_{II}(r)$ in the same way as previously : $\int_R^r \kappa_{II}(r)dr = \int_R^a \kappa_{II}(r)dr + \int_a^r \kappa_{II}(r)dr$ giving

$$u_{II}(r) = \frac{C}{\sqrt{\kappa_{II}(r)}}\, e^{-\sigma_{II}} \exp(-\int_a^r \kappa_{II}(r)dr) + \frac{D}{\sqrt{\kappa_{II}(r)}}\, e^{\sigma_{II}} \exp(+\int_a^r \kappa_{II}(r)dr)$$

where we defined

$$\sigma_{II} = \int_R^a \kappa_{II}(r)dr \tag{4.19}$$

Equation (4.9) is written

$$\frac{C}{\sqrt{\kappa_{II}(a)}}\, e^{-\sigma_{II}} + \frac{D}{\sqrt{\kappa_{II}(a)}}\, e^{\sigma_{II}} = \frac{A'}{\sqrt{k_{III}(a)}} + \frac{B'}{\sqrt{k_{III}(a)}}$$

and (4.10) gives

$$-C\left(\sqrt{\kappa_{II}(a)} + \frac{1}{2}\left(\kappa_{II}(a)\right)^{-3/2}\kappa'_{II}(a)\right)e^{-\sigma_{II}} + D\left(\sqrt{\kappa_{II}(a)} - \frac{1}{2}\left(\kappa_{II}(a)\right)^{-3/2}\kappa'_{II}(a)\right)e^{\sigma_{II}}$$
$$= A'\left(-\frac{1}{2}\left(k_{III}(a)\right)^{-3/2}k'_{III}(a) + i\sqrt{k_{III}(a)}\right) - B'\left(\frac{1}{2}\left(k_{III}(a)\right)^{-3/2}k'_{III}(a) + i\sqrt{k_{III}(a)}\right)$$

We immediately notice the presence of exponentials with a positive argument and of exponentials with the same argument of opposite sign in the two previous expressions. Dropping the exponentials $e^{-\sigma_{II}}$ would greatly simplify the calculations but we are not sure for now whether it is justified. Indeed, the terms in parentheses could invalidate this simplification and lead to bad results. We must wait for an evaluation of these terms as well as of the argument of the exponentials and keep all the terms in the following calculations. The resolution of these two equations is straightforward but gives rather complicated expressions for

A' and B':

$$\begin{aligned} A' &= \frac{1}{2}iC\left(\sqrt{\frac{\kappa_{II}(a)}{k_{III}(a)}} + \frac{1}{2}\left(\kappa_{II}(a)\right)^{-3/2}\frac{\kappa'_{II}(a)}{\sqrt{k_{III}(a)}} - \frac{1}{2}\left(k_{III}(a)\right)^{-3/2}\left(\kappa_{II}(a)\right)^{-1/2}k'_{III}(a)\right. \\ &- \left. i\sqrt{k_{III}(a)}\left(\kappa_{II}(a)\right)^{-1/2}\right)e^{-\sigma_{II}} - \frac{1}{2}iD\left(\sqrt{\frac{\kappa_{II}(a)}{k_{III}(a)}} - \frac{1}{2}\left(\kappa_{II}(a)\right)^{-3/2}\frac{\kappa'_{II}(a)}{\sqrt{k_{III}(a)}}\right. \\ &+ \left.\frac{1}{2}\left(k_{III}(a)\right)^{-3/2}\left(\kappa_{II}(a)\right)^{-1/2}k'_{III}(a) + i\sqrt{k_{III}(a)}\left(\kappa_{II}(a)\right)^{-1/2}\right)e^{\sigma_{II}} \qquad (4.20) \\ B' &= \sqrt{\frac{k_{III}(a)}{\kappa_{II}(a)}}\,C\,e^{-\sigma_{II}} + \sqrt{\frac{k_{III}(a)}{\kappa_{II}(a)}}\,D\,e^{\sigma_{II}} - A' \qquad (4.21) \end{aligned}$$

We are now ready to use equation (4.12) to express D' directly in terms of A, using (4.15), (4.16), (4.20) and (4.21). Condition (4.14) allows us to simplify the only remaining A, leading us, after the calculations of Appendix B, to

$$\begin{aligned} &\sin(\rho+\frac{\pi}{4})\left(\sqrt{\frac{\kappa_{II}(a)}{k_{III}(a)}} + \frac{1}{2}\left(\kappa_{II}(a)\right)^{-3/2}\frac{\kappa'_{II}(a)}{\sqrt{k_{III}(a)}} - \frac{1}{2}\left(k_{III}(a)\right)^{-3/2}\right. \\ &\qquad\left.\times\left(\kappa_{II}(a)\right)^{-1/2}k'_{III}(a)\right)e^{-\sigma_{II}}\frac{X}{2} - \cos(\rho+\frac{\pi}{4})e^{-\sigma_{II}}\sqrt{\frac{k_{III}(a)}{\kappa_{II}(a)}}\frac{X}{2} \\ &+\sin(\rho+\frac{\pi}{4})\left(\sqrt{\frac{\kappa_{II}(a)}{k_{III}(a)}} - \frac{1}{2}\left(\kappa_{II}(a)\right)^{-3/2}\frac{\kappa'_{II}(a)}{\sqrt{k_{III}(a)}} + \frac{1}{2}\left(k_{III}(a)\right)^{-3/2}\right. \qquad (4.22) \\ &\qquad\left.\times\left(\kappa_{II}(a)\right)^{-1/2}k'_{III}(a)\right)e^{\sigma_{II}}\frac{Y}{2} + \cos(\rho+\frac{\pi}{4})e^{\sigma_{II}}\sqrt{\frac{k_{III}(a)}{\kappa_{II}(a)}}\frac{Y}{2} = 0 \end{aligned}$$

$$\begin{aligned} &-\sin(\rho+\frac{\pi}{4})\sqrt{\frac{k_{III}(a)}{\kappa_{II}(a)}}e^{-\sigma_{II}}\frac{X}{2} + \sin(\rho+\frac{\pi}{4})e^{-\sigma_{II}}\sqrt{\frac{k_{III}(a)}{\kappa_{II}(a)}}\frac{X}{2} \\ &+\sin(\rho+\frac{\pi}{4})\sqrt{\frac{k_{III}(a)}{\kappa_{II}(a)}}e^{\sigma_{II}}\frac{Y}{2} - \sin(\rho+\frac{\pi}{4})e^{\sigma_{II}}\sqrt{\frac{k_{III}(a)}{\kappa_{II}(a)}}\frac{Y}{2} = 0 \\ &\Leftrightarrow 0 = 0 \end{aligned}$$

for the real and imaginary parts respectively, so that we are left with only one condition.

Equation (4.22) is a transcendental equation for the energy E, because it is involved in the definitions of K, κ_{II}, k_{III} and in the integrals ρ and σ_{II}. There exist only specific values of E that satisfy this equation. To find the binding energy of the system OHe-nucleus, the strategy will be to write a program that tests values of E from $min(U_{III}(r))$ to 0 and returns the first value which satisfies equation (4.22).

4.1.3 Numerical analysis

4.1.3.1 Description of the program

The program is written in Fortran 90, double precision. Its function is to test values of E from $min(U_{III}(r))$ to 0 and evaluate the expression (4.22). The stopping condition of the loop is the first change of sign of (4.22), which we recognize by keeping the last two evaluations and multiplying them. If the result is negative, we return the estimation of the binding energy by taking the intersection of the straight line passing through the last two values of (4.22) with the axis of abscissa E. The integrals ρ and σ_{II} are evaluated by an algorithm that divides the area under the curve into small trapezoids.

The constants of the problem are put into a module and their values are indicated in Table 4.1. The mass of OHe has been taken equal to 1 TeV [11] but all the following results weakly depend on the values of $M_O > 1$ TeV. The nuclear parameters are calculated through the Bethe-Weizsacker formula for the binding energy of a nucleus [19]

$$B = -a_1 A + a_2 A^{2/3} + a_3 \frac{Z^2}{A^{1/3}} + a_4 \frac{(A-2Z)^2}{A} \pm a_5 A^{-3/4} \tag{4.23}$$

In the last term, the positive sign is chosen for odd-odd nuclei (odd number of neutrons and odd number of protons), implying that such nuclei are relatively unstable. On the other hand, for even-even nuclei, the sign is taken as negative, implying greater stability. And for odd-even or even-odd, this last term is chosen to be zero, corresponding to an intermediate situation. Formula (4.23) is used by the program to calculate the mass of the nucleus

$$M_N = Z\, M_p + (A - Z)\; M_n + B \tag{4.24}$$

and then the reduced mass (2.4). The radius of helium, as well as all the radii that we will need later, are calculated by the empirical formula [19]

$$R \simeq 1.2\, A^{1/3}\, fm \tag{4.25}$$

Finally, the nuclear range corresponds to the range of the strong nuclear interaction between nucleons and its choice will be explained when analyzing the results.

To treat a great number of nuclei, a second loop is nested and runs over nuclei according to a defined rule. For example, $A = 2Z$ or the valley of stability derived by requiring that the binding energy (4.23) is at its maximum for a given A, i.e. $\frac{\partial B}{\partial Z} = 0$, giving the rule

$$Z = \frac{1}{2} \frac{A}{1 + A^{2/3} \frac{a_3}{a_4}} \tag{4.26}$$

Of course in that second case we must ensure that Z rounded to the nearest integer. Once the nucleus (A, Z) is determined, the program identifies the parity of the number of nucleons

Description	symbol	value (Units)
Fine structure constant	α	0.00729735253
Mass of neutron	M_n	939.565 (MeV)
Mass of proton	M_p	938.272 (MeV)
Mass of OHe ($\simeq$ mass of O^{--}) [11]	M_O	10^6 (MeV)
Nuclear parameters [19]	a_1	15.6 (MeV)
	a_2	16.8 (MeV)
	a_3	0.72 (MeV)
	a_4	23.3 (MeV)
	a_5	34 (MeV)
"Size" of OHe [11]	r_0	2 (fm)
	$\hbar c$	197 (fm MeV)
Radius of helium	r_{He}	1.90488128859 (fm)
Nuclear range	s	1.2 (fm)

Table 4.1: Values of the constants

(even-even, even-odd or odd-odd) to calculate the nuclear binding energy and then its mass and the reduced mass of the system.

The parameter R in the first region of the potential (2.3) is taken as the radius of the nucleus given by formula (4.25) and V_0 is fixed to several tens of MeVs. The only remaining parameter is the distance at which the polarization of OHe by the nucleus takes place. We said in the end of subsection (2.2.1) that it could be roughly estimated to $a \simeq r_0 + r_{He} + R$. We will now refine this a bit. Let us first pay attention at the order of magnitude of the distances involved in the problem : $R \simeq 1.2\, A^{1/3} \simeq 3.7$ fm and $a \simeq 7.6$ fm for a nucleus of mass number $A = 30$. Both nuclei (nucleus and helium) are considered as spheres filled with nucleons interacting by strong nuclear interaction of range $s \simeq 1$ fm. Therefore, this range cannot be neglected here and has to be taken into account. Polarization will take place when two nucleons will be within $\simeq 1$ fm from each other, so we can write

$$a \simeq r_0 + r_{He} + R + s \tag{4.27}$$

as a better approximation. We will see that this improves the results with a reasonable value of the range of the strong nuclear interaction.

Equation (4.27) is the last task of the program before beginning the second loop that tests the values of E satisfying (4.22). If it finds a solution, it writes it in a results file, otherwise (if the energy reaches zero without satisfying the stopping condition) it writes 0 in the same file. Then the following nucleus is treated and so on.

4.1.3.2 Results

By first running the program with a value of $V_0 = 60$ MeV to fix ideas and for mass numbers going from 1 to 250 and Z adjusted according to (4.26), we find by plotting the binding

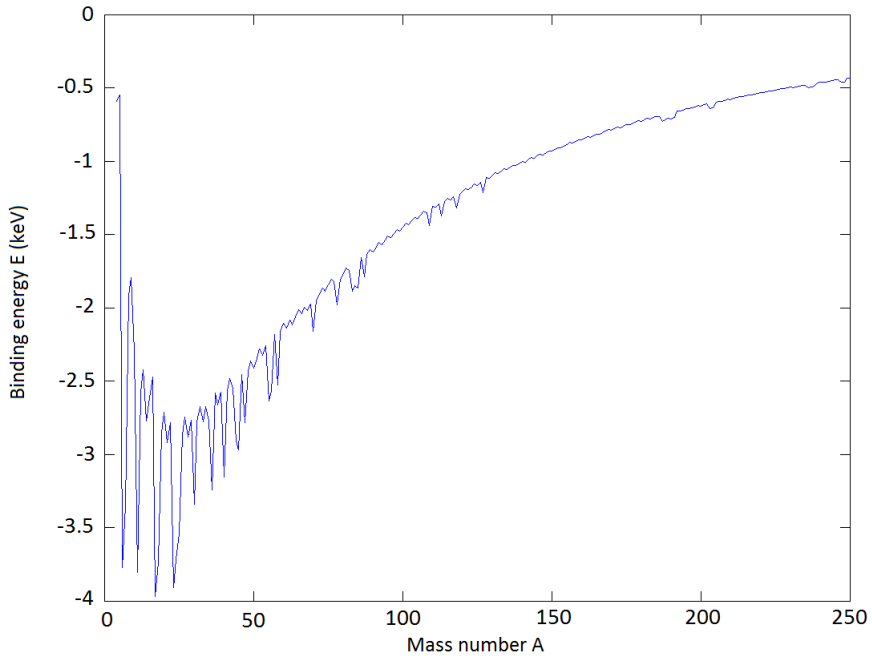

Figure 4.1: Binding energy (keV) for values of A from 1 to 250

energy E as a function of the mass number A the graph in Figure 4.1.

We see immediately that there are oscillations that look like numerical errors more than a physical effect. This may be due to the fact that we manipulate large numbers in expression (4.22) because of the terms proportional to $e^{\sigma_{II}}$. Indeed, by looking more closely at the values taken by σ_{II}, X and Y for the different nuclei, we note that X and Y are always of the same order and that $\sigma_{II} \simeq 2-4$ for A between 4 and 10, $\sigma_{II} \simeq 10$ for $A = 35$ and continues to increase for heavier nuclei to reach about 35 for $A = 250$. Therefore, in all cases we can simplify the complete expression (4.22) by neglecting each term proportional to $e^{\sigma_{II}}$ with respect to its associated term in $e^{\sigma_{II}}$ to get

$$\begin{aligned} \sin(\rho+\frac{\pi}{4})\Bigg(\sqrt{\kappa_{II}(a)} - \frac{1}{2}\left(\kappa_{II}(a)\right)^{-3/2}\kappa'_{II}(a) + \frac{1}{2}\left(k_{III}(a)\right)^{-1} \\ \times \left(\kappa_{II}(a)\right)^{-1/2} k'_{III}(a)\Bigg) + \cos(\rho+\frac{\pi}{4})e^{\sigma_{II}}\frac{k_{III}(a)}{\sqrt{\kappa_{II}(a)}} \quad = \quad 0 \end{aligned} \tag{4.28}$$

as a simplified quantization condition.

By implementing this new expression in the program we obtain the graph shown in Figure 4.2, which no longer has the previous behaviour of Figure 4.1. The remaining oscillations are simply due to the selection rule of stable nuclei explained in subsection 4.1.3.1 that makes Z remain at the same value for several A and then jump abruptly to the next integer value. For example the rule $A = 2Z$ gives a smooth curve.

We note that there seems not to exist bound states for nuclei with $A = 1, 2, 3$, to which correspond the values $Z = 0, 1, 1$, or, in other words, for the neutron, ${}^2H$ and ${}^3H$. We do not

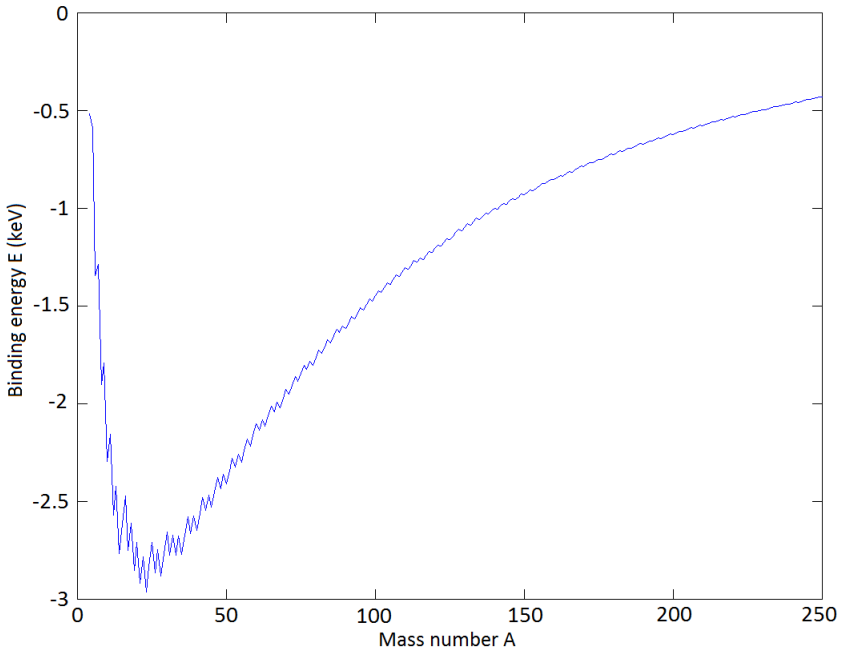

Figure 4.2: Binding energy (keV) for values of A from 1 to 250 obtained with the simplified quantization condition (4.28).

either find any level for hydrogen ^1H. The case of the neutron is not surprising because there is no Coulomb screened potential region (because of its neutrality) and hence no potential well in region III but the three other cases are real predictions.

All the other nuclei selected by formula (4.26) present a bound state. In particular, the only stable isotope of sodium, ^{23}Na, has a bound state at -2.96 keV, which is just the lowest value on the curve (4.2). We see therefore that adding of a nuclear range of 1.2 fm to the parameter a of the model with a simple argument is sufficient to explain the DAMA results with one of its components. Moreover, this value of the range of the strong nuclear interaction is within the interval of generally accepted values.

The successful prediction for sodium is to be associated with the prediction for the other component of the detector, iodine, whose only stable isotope is ^{127}I. For this, we find a bound sate at -1.22 keV. This gives rise to a scintillation signal at 1.22 keV that is not in contradiction with the DAMA results because, as we have seen in the section 2.1 dedicated to the experiment, this is under the energy threshold of 2 keV. This signal could therefore contribute to the events lying under 2 keV in Figure 2.2.

For information, Table 4.2 shows the binding energies of some interesting stable nuclei included or not in Figure 4.2.

In a general manner, we realize that there are bound states for all nuclei (except for the lightest ones), intermediate as well as heavy ones. But we know from experiments that

Nucleus	Binding energy (keV)	Nucleus	Binding energy (keV)
^{3}He	-0.35	^{71}Ga	-2.02
^{4}He	-0.52	^{70}Ge	-2.14
^{12}C	-2.57	^{72}Ge	-2.04
^{16}O	-2.91	^{73}Ge	-1.99
^{19}F	-2.85	^{74}Ge	-1.95
^{27}Al	-3.00	^{76}Ge	-1.86
^{28}Si	-3.13	^{127}I	-1.22
^{35}Cl	-2.96	^{132}Xe	-1.15
^{37}Cl	-2.76	^{203}Tl	-0.68
^{40}Ar	-2.65	^{205}Tl	-0.66
^{69}Ga	-2.11	^{238}U	-0.52

Table 4.2: Binding energies for several interesting stable nuclei

there should not exist any signals for heavy nuclei, in particular for xenon in the XENON100 experiment mentioned in Chapter 1. However, Table 4.2 shows that the binding energy for the most abundant isotope of xenon, ^{132}Xe, is equal to -1.15 keV. We could therefore look at the constant part of the signal that we would observe in a medium made of xenon, at the operating temperature of the experiment, i.e. $T = -100\,^{\circ}\mathrm{C}$=173.15 K [4]. With (2.10), we find $\xi_{^{132}Xe} = 0.215$ cpd/kg at about 1.15 keV for the most abundant isotope. Note that the binding energies with the other stable isotopes of xenon differ little from the value for the isotope 132 and remain in all cases under the threshold. Once again, this signal lies under the energy threshold of the XENON experiments, which is higher than for the DAMA detectors, as mentioned in the Introduction. This avoids any contradiction with the negative results of this experiment without necessarily a radical suppression of the bound states with the different isotopes of xenon. The values of the binding energies for the isotopes of germanium in Table 4.2, giving rise to the same photon energies in absolute values by the process of radiative capture, appear to be too high to correctly reproduce the results of the CoGent experiment, which correspond to energies below 1 keV.

In the case of sodium, we are left with a model without any free parameter (except for V_0, but we will see that its value do not influence the results) that gives us the desired binding energy. However, we can force the change of the elements R, a and V_0 and see their influence on the results. We can be sure, before having done any test, that V_0 and R will not greatly influence the results because the simplified expression (4.28) does not depend at all on these parameters. If we want to verify this, we thus have to reinsert the complete expression (4.22) into the program. For sodium, we see effectively that the binding energy is very stable against a variation of V_0 form 10 to 200 MeV and of R from $0.5R$ to $2R$. The fact that the results depend very slightly on the parameters of region I is fortunate because we do not actually know very well the details of the interaction at distances shorter than the

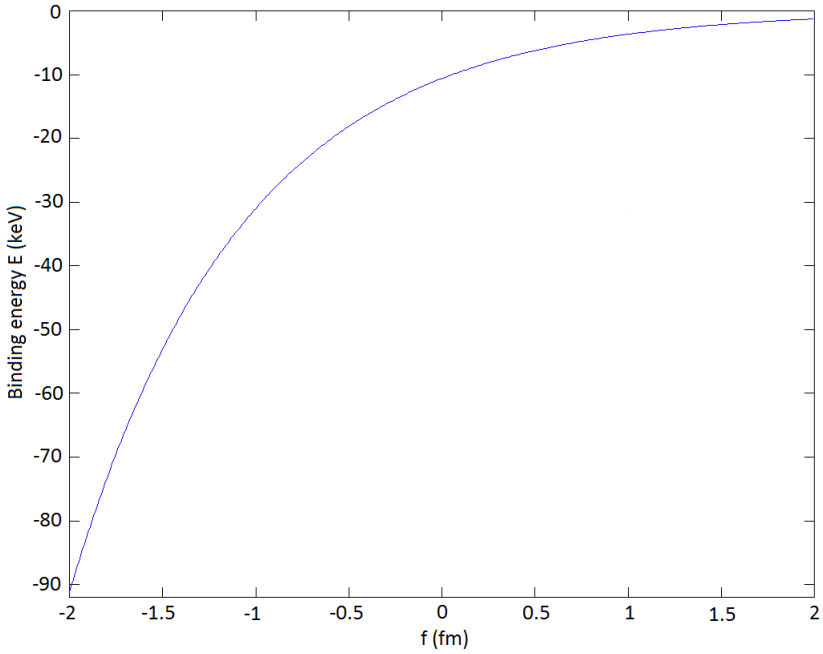

Figure 4.3: Influence of parameter a on the binding energy in the case of sodium

dipolar region (region II). Region I indeed corresponds to the nuclear interaction of an alpha particle within a nucleus, depending on the considered nucleus[1] and requires a detailed study of the scattering of alpha particles by nuclei. The ranges of variation of the parameters V_0 and R above allow us to concentrate on the third region with some confidence. The last parameter, a, influences however very much the results because it is involved in the shape of the well in which the energy level is found. Figure 4.3 shows the modification of E in response to the variation of a from both sides of the first approximate value $a \simeq r_0 + r_{He} + R$. We added to a the parameter f that takes positive values, corresponding to different values of the nuclear range, and negative ones, in the interval $[-2, 2]$ fm with a 0.01-fm spacing. This strong dependence makes the discovery of a -3-keV bound state for sodium with the right nuclear range even more astounding. For example, the non-consideration of the nuclear range ($f = 0$) would have given a solution at about -10 keV.

We can also wonder whether there are higher levels for $l = 0$. By letting the program continue after the first detected level, we realize that no other level is detected for all nuclei considered. There seems therefore to exist only one bound state in the case $l = 0$.

In fact, it is possible that the direct use of the WKB approximation that we made above is not entirely appropriate. It may be that the validity criterion (3.27) is not satisfied at any

[1] see [20, 21] for more information about the elastic scattering, as well as absorption or reactions, of alpha particles with a nucleus.

point in region III on the left of the turning point ($a < r < d$), making the approximation too poor in that domain of values of r while the connections formulas (3.28) and (3.29) have been established by requiring that the approximation is correct on both sides far from the turning point. But we can in fact not speak about an asymptotic region on the left of the turning point because the variable r takes only values in the interval $[0, +\infty[$ and thus cannot tend to $-\infty$. The problem, if indeed there is a problem, seems therefore to lie in the fact that we passed from a variable $x \in]-\infty, +\infty[$ in one dimension to a variable r that is positive definite. To get rid of these uncertainties and assess unambiguously the quality of the approximation we use hereafter a modified version of the WKB method.

4.2 Modified WKB approximation

4.2.1 Change of variable

To get as close as possible to the one-dimensional problem, one possibility is to perform a change of variable such that the new variable takes any real value while conserving the shape of the Schrödinger equation. This requires also to change the wave function. The changes of variable and function proposed by Langer [22] are

$$r = e^{x}, \tag{4.29}$$

$$u = e^{x/2}\phi \tag{4.30}$$

which ensures that when r varies from 0 to ∞, x varies from $-\infty$ to $+\infty$. We must verify that the shape of the equation remains unchanged by substituting (4.29) and (4.30) into the radial equation (2.3). We have

$$\begin{aligned}
\frac{dx}{dr} &= e^{-x} \\
\frac{d^2x}{dr^2} &= -e^{-2x} \\
\frac{du}{dx} &= \frac{1}{2}e^{x/2}\phi + e^{x/2}\frac{d\phi}{dx} \\
\frac{d^2u}{dx^2} &= \frac{1}{4}e^{x/2}\phi + e^{x/2}\frac{d\phi}{dx} + e^{x/2}\frac{d^2\phi}{dx^2} \\
\frac{d^2u}{dr^2} &= \frac{d^2u}{dx^2}\left(\frac{dx}{dr}\right)^2 + \frac{du}{dx}\frac{d^2x}{dr^2} \\
\Rightarrow \frac{d^2u}{dr^2} &= \left(\frac{1}{4}e^{x/2}\phi + e^{x/2}\frac{d\phi}{dx} + e^{x/2}\frac{d^2\phi}{dx^2}\right)e^{-2x} \\
&\quad - \left(\frac{1}{2}e^{x/2}\phi + e^{x/2}\frac{d\phi}{dx}\right)e^{-2x} \\
&= -\frac{1}{4}e^{-3x/2}\phi + e^{-3x/2}\frac{d^2\phi}{dx^2}
\end{aligned}$$

so that the radial equation becomes in terms of x and ϕ

$$\frac{d^2\phi}{dx^2} + 2\mu\left[Ee^{2x} - V(r=e^x)e^{2x}\right]\phi - \left(l+\frac{1}{2}\right)^2\phi = 0 \tag{4.31}$$

where we have restored the angular momentum for a while. We see that this equation is the same as in one dimension, but now we are left with a problem of a particle of mass μ described by ϕ in a potential

$$\tilde{V}(x) = -Ee^{2x} + V(r=e^x)e^{2x} + \frac{\left(l+\frac{1}{2}\right)^2}{2\mu}$$

with an energy

$$\tilde{E} = 0$$

We can apply the WKB solutions (3.21) and (3.23) to ψ and search the value of E (determining the shape of the new potential) that allows the particle of energy $\tilde{E} = 0$ to be bound in $\tilde{V}(x)$. We will see that it is not necessary to apply the WKB solutions to ψ because it amounts to applying the WKB method of the three-dimensional problem by replacing $l(l+1)$ by $(l+\frac{1}{2})^2$ in the centrifugal term of the effective potential $V_{eff}(r)$.

Let us first note that the turning points of $\tilde{V}$(x) correspond to the turning points of the three-dimensional effective potential in which we have replaced $l(l+1)$ by $(l+\frac{1}{2})^2$

$$\begin{aligned}
\tilde{V}(x) &= 0 \\
\Leftrightarrow -Er^2 + V(r)r^2 + \frac{\left(l+\frac{1}{2}\right)^2}{2\mu} &= 0 \\
\Leftrightarrow E - V(r) - \frac{\left(l+\frac{1}{2}\right)^2}{2\mu r^2} &= 0 \\
\Leftrightarrow E &= V_{eff}\left(r,\, l\,(l+1) \to \left(l+\frac{1}{2}\right)^2\right)
\end{aligned}$$

by using the change of variable (4.29).

To illustrate this, let us consider the case of the screened Coulomb potential. The previous calculation makes the correspondence between the three regions of the potential $\tilde{V}(x)$ in Figure 4.4a and the three regions of $U_{III,eff}\left(r,\, l\,(l+1) \to \left(l+\frac{1}{2}\right)^2\right)$ in figure 4.4b where x_1, x_2 and r_1, r_2 are the respective turning points.

The WKB solution in region II of $\tilde{V}(x)$ gives $\psi_{II}(x) = \frac{A}{\sqrt{k_{II}(x)}} e^{i\int_{x_1}^{x} k_{II}(x)dx}$, where $k_{II}(x) = \sqrt{2\mu\left(-\tilde{V}(x)\right)}$, $x \in [x_1, x_2]$. We have dropped the second term of the most general solution

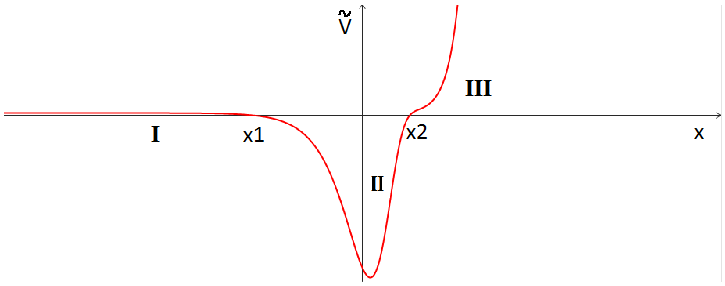

(a) Shape of the fictive potential $\tilde{V}(x)$ evaluated with U_{III} given in (2.5). $x_1$and x_2 are the turning points of the fictive problem.

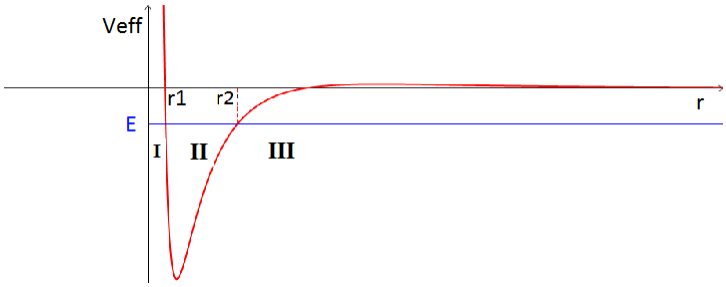

(b) Shape of the effective potential $U_{III,eff}$ in which we have replaced $l\,(l+1)$ by $\left(l+\frac{1}{2}\right)^2$ in the case $l=0$. r_1 and r_2 are the turning points.

Figure 4.4

because it is treated in the same way. According to (4.30), we have for $u_{II}(r)$, $r \in [r_1, r_2]$

$$\begin{aligned} u_{II}(r) &= \sqrt{r}\frac{A}{\left(2\mu\left(Er^2+\frac{2Z\alpha}{r_0}\left(1+\frac{r_0}{r}\right)\exp(-2r/r_0)r^2-\frac{\left(l+\frac{1}{2}\right)^2}{2\mu}\right)\right)^{1/4}}e^{i\int_{x_1}^{x}k_{II}(x)dx} \\ &= \frac{A}{\left(2\mu\left(E+\frac{2Z\alpha}{r_0}\left(1+\frac{r_0}{r}\right)\exp(-2r/r_0)-\frac{\left(l+\frac{1}{2}\right)^2}{2\mu r^2}\right)\right)}e^{i\int_{x_1}^{x}k_{II}(x)dx} \\ &= \frac{A}{\sqrt{k_{II}\left(r,\, l\,(l+1)\to\left(l+\frac{1}{2}\right)^2\right)}}e^{i\int_{x_1}^{x}k_{II}(x)dx} \end{aligned}$$

the argument of the exponential becomes

$$\begin{aligned} \int_{x_1}^{x}k_{II}(x)dx &= \int_{r_1}^{r}rk_{II}\left(r,\, l\,(l+1)\to\left(l+\frac{1}{2}\right)^2\right)\frac{1}{r}\,dr \\ &= \int_{r_1}^{r}k_{II}\left(r,\, l\,(l+1)\to\left(l+\frac{1}{2}\right)^2\right) \end{aligned}$$

so that

$$u_{II}(r) = \frac{A}{\sqrt{k_{II}\left(r,\, l\,(l+1)\to\left(l+\frac{1}{2}\right)^2\right)}}e^{i\int_{r_1}^{r}k_{II}\left(r,\, l(l+1)\to\left(l+\frac{1}{2}\right)^2\right)}$$

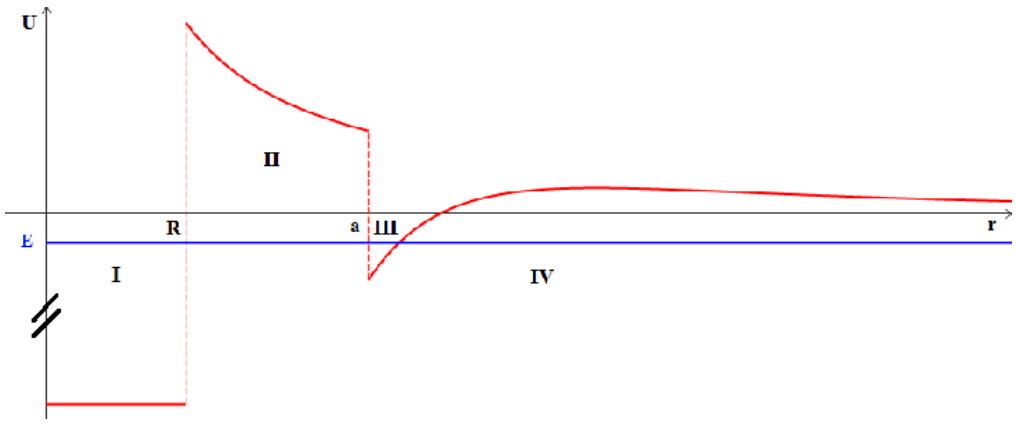

Figure 4.5: Shape of the modified potential of interaction in the case $l = 0$.

The previous calculation is valid for all regions and shows that it is sufficient to replace $l(l+1)$ by $\left(l+\frac{1}{2}\right)^2$ in the effective potential of the three-dimensional problem and then work with the WKB solutions as they were established in one dimension.

If we perform this replacement in all the regions where a WKB solution is needed, i.e. in regions II and III (the last one being separated in two regions on both sides of the turning point) of the potential on Figure 2.3, with the consequence that even in the case $l = 0$, a term $\frac{1}{8\mu r^2}$ will remain in the potential. The direct effect of this term is to raise the potential of interaction, and we can already suspect that the energy levels will therefore also be increased. The complete modified potential is shown in Figure 4.5 (proportions not respected). Let us recall that region I admits an exact solution, for which we do not have to make any change.

4.2.2 Results

To take into account the changes made in the potential, we have to modify the program slightly and add the centrifugal term in the definitions of the functions κ_{II}, k_{III}, κ_{IV} and their derivative. This poses no problem because the calculations related to the WKB solutions do not involve the exact expression of the potential. Region I on the other hand remains unchanged, as we used the exact solution there, and it is the only thing that distinguishes this case from the non-vanishing angular momentum situation that we will consider later.

The first thing we note by running the program for nuclei given by (4.26) and A going from 1 to 250, with our standard values $V_0 = 60$ MeV, $R = 1.2A^{1/3}$ and $s = 1.2$ fm for the nuclear range, is that there are more light nuclei without any bound state. So much so that even sodium seems not to have a bound state with OHe anymore. The lightest nucleus that has a bound state with formula (4.26) is the isotope ^{26}Mg of magnesium. This is not a general rule and it is possible that some slightly lighter nuclei possess a bound state but they are just not taken into account by the formula, which runs approximately over stable nuclei but do not consider all the stable isotopes of a given element. This should be made

by hand, by entering specific values of A and Z into the program. This time again, there is no more than one bound state per nucleus. The fact that light nuclei are suppressed is easily understood by looking at the graph in Figure (4.5). Indeed, for the lightest nuclei, the centrifugal term $\frac{1}{8\mu r^2}$ is larger than for heavier ones, so that the potential well in region III ends up disappearing, and, thereby, the bound states that we are seeking.

Then we might wonder whether it is sodium that has a bound state with OHe and not iodine or thallium. We find binding energies at -0.85, -0.47 and -0.45 keV respectively for ^{127}I, ^{203}Tl and ^{205}Tl. These results are not in very good agreement with the DAMA observations of section 2.1 because they do not lie in the right energy range. This situation is obviously not acceptable and we must modify the only parameter influencing the results, namely the parameter a, and therefore the nuclear range. The three curves on Figure 4.6 show the variation of the binding energy of sodium, iodine and thallium with respect to the nuclear range. We allowed it to go from 0 to 1.5 fm with a 0.01-fm spacing and the red parts of the curves correspond to binding energies approximately in the desired range $(2-4)$ keV. We see that thallium admits in extremis a binding energy for a nuclear range equal to 0 and that the interval $(2-4)$ keV is realized fully or partially for a nuclear range between 0.3 and 0.62 fm for sodium and between 0 and 0.53 fm for iodine.

These results alone do not allow us to conclude about the origin of the observed signal : sodium, iodine, or both may have a binding energy in the interval $(2-4)$ keV with a reduced nuclear range comparable to the generally accepted values.

However, we saw, in the end of subsection 2.2.1 about the interaction of OHe with matter, that the results of DAMA, i.e. $\varsigma = (0.0116 \pm 0.0013)$ cpd/kg/keV in the energy interval $(2-6)$ keV for the amplitude of the annual modulation of the signal, could be approximately explained by $E_{Na} = -3$ keV. For iodine, we find with formula (2.11) that this amplitude is reproduced if $E_I \simeq -1.1$ keV, which is under the threshold of the experiment and out of the interval of detection of the interesting signal, making this second constraint not verified. It seems therefore that iodine cannot explain the results alone and that is the reason why we can, in this case again, turn to sodium and adopt the value that gives a -3 keV bound state for this nucleus, that is to say, $s \simeq 0.44$ fm. With this last value, thallium is under the threshold and iodine is at $E_I = -2.2$ keV, i.e. in the interval of detection. But it is clear that this value lies very close to the energy threshold of the DAMA experiment at 2 keV, and, given the uncertainties relative to the model, it is possible that the value for iodine lies in reality under the threshold while sodium remains in the right interval. If it is not the case, formula (2.11) used at room temperature $T = 300$ K shows for iodine $\varsigma_I = 0.0334$ cpd/kg, which appears as an unobserved supplement with respect to the contribution of sodium.

By running the program for all nuclei (built from formula (4.26) again) with the value

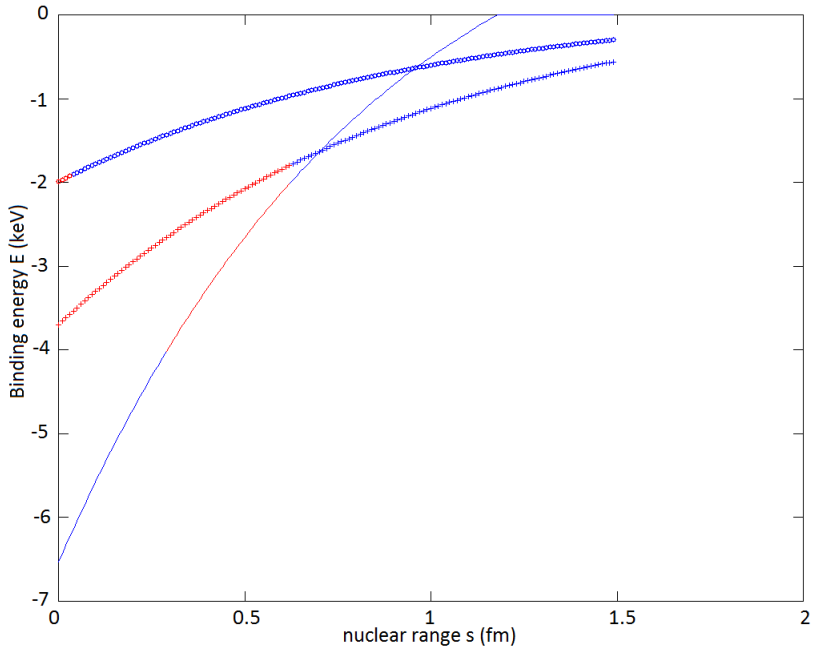

Figure 4.6: Binding energy (keV) of sodium (continuous line), iodine ("+" symbols) and thallium ("o" symbols) as a function of the strong nuclear interaction range (fm). The red parts of the curves correspond to binding energies in the range $(2-4)$ keV.

of the nuclear range now adopted, we obtain a graph for the binding energies (Figure 4.7) similar to that of the non-modified WKB approximation (Figure 4.2), with the difference that more light nuclei are now suppressed, the lightest admitting a bound state with OHe being ^{16}N.

Note that, in the particular case of ^{132}Xe, the binding energy is found to be $E_{^{132}Xe} = -2.1$ keV, with similar values for the other isotopes, which is under the threshold of the corresponding XENON100 experiment, avoiding any contradiction with its negative results. For germanium, we find for example $E_{^{74}Ge} = -3.42$ keV, with values going from -3.77 to -3.26 keV for the different stable isotopes. These values seem even more difficult to relate to the results of CoGent than in the case of the non-modified WKB method and attention should be paid to the future publications of observational results.

Finally, no higher level is found at zero angular momentum for all the considered nuclei.

4.3 Square well potential approximation

4.3.1 Simplification of the potential

It could be interesting to consider a simplified version of the potential of interaction, that would admit exact solutions, in order to compare the corresponding results with the previous

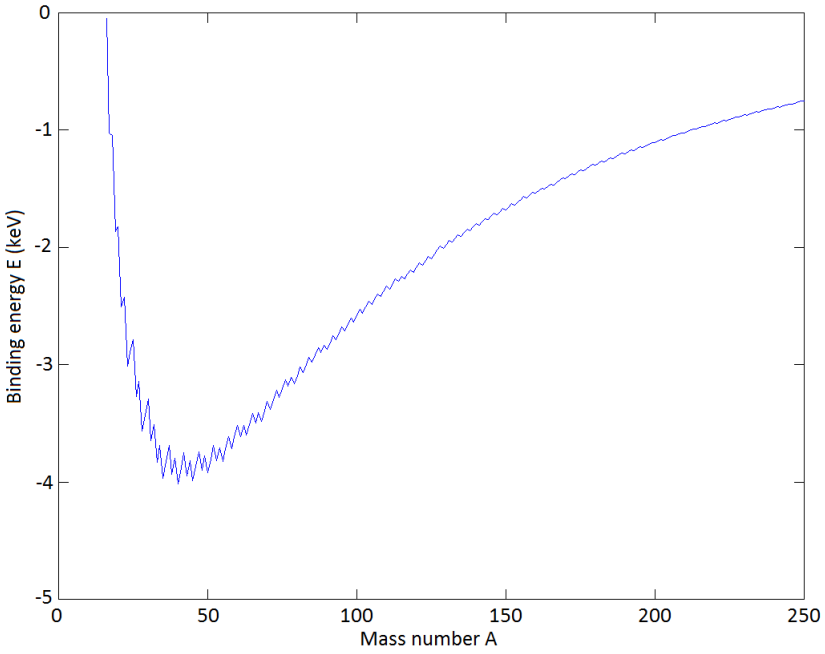

Figure 4.7: Binding energy (keV) for values of A from 1 to 250 obtained by the modified WKB approximation with a nuclear range equal to 0.44 fm.

ones. This task has already been done by M. Yu. Khlopov et al. [11, 12, 13] and the proposed method to simplify the potential is as follows : region I of the potential on Figure (2.3) already admits an exact solution, so that it does not have to be changed, and we have in region I

$$U(0 < r < R) = -U_1 = -V_0$$

Region II is replaced by its average value over the interval $[R, a]$, which gives

$$U(R < r < a) = U_2 = \frac{\int_R^a \frac{2Z\alpha r_0}{r^2} dr}{(a - R)} = \frac{2Z\alpha r_0}{aR}$$

Region III is replaced by a rectangular well equal to the minimum value of U_{III} (expression (2.5))

$$U(a < r < b) = -U_3 = \frac{-2Z\alpha}{r_0}\left(1 + \frac{r_0}{a}\right)\exp(-2r_0/a)$$

and b is determined by requiring that the area of the rectangle is equal to the integral of U_{III} from $r = a$ to infinity : $(b - a) \times (-U_3) = \int_a^\infty U_{III}(r)dr$, so that it is, a priori, not a new parameter, but it is fixed by the choice of a. The simplified potential, superimposed on the "exact" one, is shown on Figure 4.8. The term "exact" must here not be taken to the proper sense because we know well that it comes from a model which involves itself approximations and uncertainties.

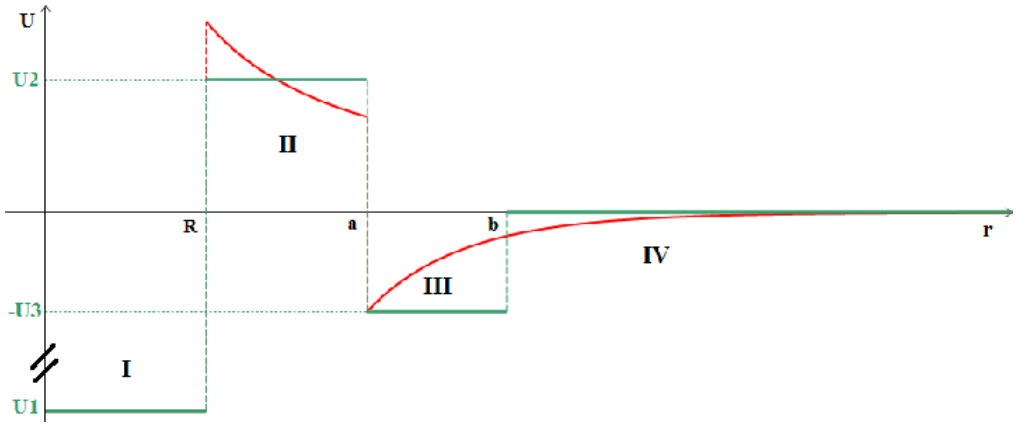

Figure 4.8: Square well potential superimposed on the "exact" potential of interaction.

4.3.2 Construction of the solutions

Two cases will be considered here, $-U_3 < E < 0$ as before and $-U_1 < E < -U_3$. The second case is intended to explore deeper levels corresponding to region I and that could be involved in releases of high energy photons if region I is reached by a tunneling effect through the dipolar barrier of region II. For $-U_3 < E < 0$, the solutions in the four regions are given by

$$\begin{aligned} u(0 \;<\; & r < R) = u_I(r) \\ = \; & A_I \exp(ik_I r) + B_I \exp(-ik_I r) \end{aligned} \tag{4.32}$$

in region I, where $k_I = \sqrt{2\mu\,(E + U_1)}$.

$$\begin{aligned} u(R \;<\; & r < a) = u_{II}(r) \\ = \; & A_{II} \exp(k_{II} r) + B_{II} \exp(-k_{II} r) \end{aligned} \tag{4.33}$$

in region II, where $k_{II} = \sqrt{2\mu\,(U_2 - E)}$.

$$\begin{aligned} u(a \;<\; & r < b) = u_{III}(r) \\ = \; & A_{III} \exp(ik_{III} r) + B_{III} \exp(-ik_{III} r) \end{aligned} \tag{4.34}$$

in region III, where $k_{III} = \sqrt{2\mu\,(E + U_3)}$.

$$\begin{aligned} u(r \;>\; & b) = u_{IV}(r) \\ = \; & A_{IV} \exp(k_{IV} r) + B_{IV} \exp(-k_{IV} r) \end{aligned} \tag{4.35}$$

in region IV, where $k_{IV} = \sqrt{-2\mu E}$.

For $-U_1 < E < -U_3$, the only difference occurs in region III where we have

$$u_{III}(r) = A_{III} \exp(k_{III} r) + B_{III} \exp(-k_{III} r) \tag{4.36}$$

where $k_{III} = \sqrt{-2\mu\,(E + U_3)}$ instead of the oscillatory solution.

4.3.3 Connections-quantization of the energy

As in the case of the WKB calculation, we have to connect the solutions of the different regions by requiring that the wave function and its first derivative are continuous at each point of discontinuity of the potential, so that the probability current as well as the density of probability are continuous. The quantization condition of the energy then comes from the requirement that the wave function cannot diverge when $r \to \infty$, which gives

$$A_{IV} = 0$$

The calculations are made in Appendix C and we show here only the final results. For $-U_3 < E < 0$ we obtain

$$\begin{aligned} S\left[\frac{k_{II}}{k_{IV}}\cos((b-a)k_{III}) + \frac{k_{II}}{k_{III}}\sin((b-a)k_{III}) + \cos((b-a)k_{III})\right. \\ \left. -\frac{k_{III}}{k_{IV}}\sin((b-a)k_{III})\right] e^{k_{II}a} + T\left[-\frac{k_{II}}{k_{IV}}\cos((b-a)k_{III})\right. \\ \left. -\frac{k_{II}}{k_{III}}\sin((b-a)k_{III} + \cos((b-a)k_{III}) - \frac{k_{III}}{k_{IV}}\sin((b-a)k_{III}\right] e^{-k_{II}a} \;=\; 0 \end{aligned} \tag{4.37}$$

where $S = [k_I \cos(k_I R) + k_{II} \sin(k_I R)]\, e^{-k_{II}R}$ and $T = [k_{II} \sin(k_I R) - k_I \cos(k_I R)]\, e^{k_{II}R}$ are real. For energies $-U_1 < E < -U_3$, we find

$$\begin{aligned} &\frac{S}{2}\left[\left(1 + \frac{k_{III}}{k_{IV}} + \frac{k_{II}}{k_{III}} + \frac{k_{II}}{k_{IV}}\right) e^{(b-a)k_{III}} + \left(1 - \frac{k_{III}}{k_{IV}} - \frac{k_{II}}{k_{III}} + \frac{k_{II}}{k_{IV}}\right) e^{-(b-a)k_{III}}\right] e^{k_{II}a} \\ &+\frac{T}{2}\left[\left(1 + \frac{k_{III}}{k_{IV}} - \frac{k_{II}}{k_{III}} - \frac{k_{II}}{k_{IV}}\right) e^{(b-a)k_{III}} + \left(1 - \frac{k_{III}}{k_{IV}} + \frac{k_{II}}{k_{III}} - \frac{k_{II}}{k_{IV}}\right) e^{-(b-a)k_{III}}\right] e^{-k_{II}a} \;=\; 0 \end{aligned} \tag{4.38}$$

with the same definitions for S and T. These last two expressions are, similarly to the WKB equation (4.22), transcendental equations, satisfied only for specific values of E.

4.3.4 Results

Because it seems by the previous WKB analysis that sodium is the best candidate to explain the DAMA results, all that follows is particularized to the case of sodium.

The most direct way to compare the results to those obtained via the WKB approximation is to take for the parameters U_1, R and a the values used until now, i.e. 60 MeV, the radius of helium nucleus given by (4.25) and $a = r_0 + r_{He} + R + s$ respectively, with $s = 1.2$ or 0.44 fm according to the case of the non-modified or modified WKB methods. By running the program a first time to test values of E from $-U_3$ to 0 with a 10-eV spacing, it appears that we do not find any level, independently of the fact that $s = 0$, 0.44 or 1.2 fm.

Therefore, we can try to vary simultaneously all the parameters of the potential, that is to say U_1, U_2, U_3, R, a and b, within a certain interval around their standard value (established

Set A		Set B	
E	-3.016 keV	E	-2.997 keV
U_1	60 MeV	U_1	60.215 MeV
U_2	2.532 MeV	U_2	2.554 MeV
U_3	1.070 MeV	U_3	1.065 MeV
R	3.413 fm	R	3.437 fm
a	7.317 fm	a	7.313 fm
b	8.294 fm	b	8.295 fm

Table 4.3: Sets of parameters of the simplified potential. Set A is obtained by varying U_3 in order to get $E_{Na} = -3$ keV and fixing the five other parameters to their standard value. Set B results from the simultaneous modification of all parameters of Set A within 1%.

in section 4.3.1 for U_2, U_3 and b). Running the program for a great number of random values within 1% and 10% around these central values, we do not find any level for any set of parameters.

Since even a perturbation of the parameters within 10% of their orignal value seems not to be sufficient, we could try to modify further the parameter U_3, by lowering the well in region III. We thus fix the five other parameters to their original values (note that we dropped here the nuclear range, so that we are left with $a = r_0 + r_{He} + R$) and try different values of U_3 from the original one ($-U_{III}(r = a) = 13.3$ keV) to ~ 2 MeV with a 1-keV spacing. It is found that the first value of U_3 that gives a bound state is $U_3 = 0.997$ MeV and the value that gives a binding energy $E_{Na} = -3$ keV is $U_3 = 1.07$ MeV.

Note that, at vanishing angular momentum l, there are no higher levels.

Set A of Table 4.3 summarizes the parameters deduced from previous discussions that we will use for the considerations below. Note that, by varying all the parameters of Set A simultaneously within 1% for example, we generate a lot of other sets that give other values of E_{Na} around -3 keV. Indeed, the relatively large number of free parameters causes a kind of degeneracy in the space of parameters and we can, on a great number of tests, look for the one that gives the closest value to -3 keV, giving rise to Set B.

The most important point to note here is thus that, in the case of this simplified potential, we have to greatly lower the depth of the well in region III, i.e. to order of 1 MeV, in order to obtain the desired binding energy for the system OHe-NaI, compared to the WKB analysis where a well of several keVs was sufficient.

We can therefore wonder which resolution method is the closest to reality : the approximate WKB resolution with the exact potential or the exact resolution with a simplified potential. First, it may be that the WKB method is not a good approximation, even in the case of the modified version. In fact, the evaluation of the validity criterion (3.27) for the wave function $\phi(x)$ used for the modified method in the region in $x-$space, corresponding to region III in Figure 2.3 on the left of the turning point, shows that it is greater than

unity. Therefore, even with the modified WKB method, the solution seems not to be a good approximation in that small region. But it is also possible that the square well potential is so far from the exact one that the levels in region III are completely modified too. The biggest difference could lie at large distances : normally, an approaching OHe is supposed to feel a gradually (negatively) increasing attractive potential (screened Coulomb potential) but in the case of the square well potential, it feels a single kick, corresponding to a potential varying abruptly form 0 to a constant value. This could prevent bound states until we greatly lower the well.

One way to provide a partial answer is to apply the WKB method to the square well potential. We could therefore compare the approximate results to the exact ones. We have two options : if the WKB method gives here again levels with a shallow well, it is probably false in the case of the "exact" potential. But if it gives approximately the same results, then we have every reason to believe that its application in the case of the "exact" potential is an improvement. By trying to apply the approximate solutions (3.21) and (3.23) to a constant potential, we realize very quickly that these solutions are simply the exact solutions of the form $A\exp(\pm ikr)$ and $B\exp(\pm\kappa r)$ because k and κ are constant. We therefore do not have to pursue further the calculations and we can conclude that the WKB method gives exactly the same results as the exact resolution. This reasoning allows us to choose the second option. Therefore, the WKB approximation improves the results from the square well potential but is itself flawed due to the non-verified validity criterion.

All the considerations made until now concerned the existence of energy levels in region III. But we could also consider region I, where deep levels may exist and give rise to high energy release, of the order of several tens of MeV or more, in the case of tunneling effect from region III to region I. Of course, many other considerations have to be taken into account, as the transmission coefficient, to measure the impact of such levels. This will be discussed later and the best thing we can do at this point is to determine them.

Given the depth of the well in region III, compared to the order of magnitude of the two other regions (of the order of MeV), we can convince ourselves that regions II and III do not have a great influence on the determination of deep levels in region I. A WKB analysis seems therefore not necessary here, and that is the reason why we did not made it before. Moreover, the parameters related to regions II and III are certainly not very important here and the choice of the set is therefore less critical.

Let us take Set A and vary U_1 form 10 to 200 MeV with a 1-MeV spacing and determine all the levels of negative energy (at $l = 0$) of the potential, using expressions (4.37) and (4.38). Levels determined by expression (4.38) should be associated to bound states of region I and these determined by (4.37) are simply the DAMA levels of region III that we considered until now. Figure 4.9 is the result of this calculation and we see that many deep levels are

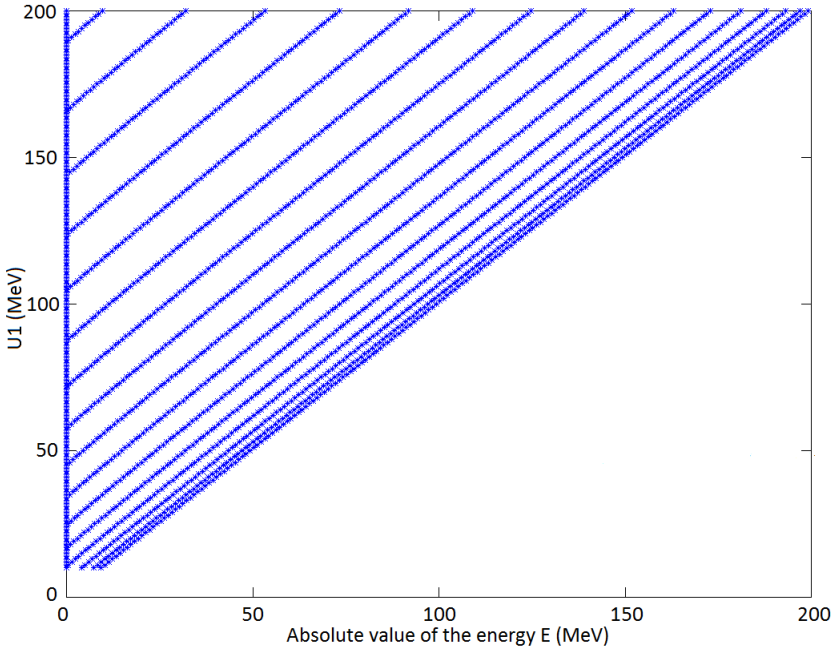

Figure 4.9: Absolute value of the levels of negative energy E (MeV) of the square well potential as a function of the depth of the well in region I U_1 (MeV).

present for a given value of U_1. For example, for $U_1 = 60$ MeV, which is the standard value used until now, around 10 levels are present in the well, to be added to the only DAMA level at ~ -3 keV. The DAMA levels are found in Figure 4.9 on the U_1 axis because they are much lower than the others and we see that their values are equal to those of Set A, the 7-th or 8-th decimal (when expressed in keV) being affected by a change of U_1 of 1 MeV. We verify therefore for a second time that region I does not have a marked influence on the levels of region III.

The values and the number of these levels should in fact not be taken strictly (except for the DAMA levels) in the sense that it is difficult to know which of them are truly free or occupied. Indeed, they do not represent the levels of the nucleons within the nucleus. They would actually correspond to the levels of alpha particles (a helium nucleus) within a nucleus made of alpha particles if we could divide it into an integer number of such particles, which is not the case for sodium since $Z = 11$ and $A = 23$. The interest is therefore reduced to give an order of magnitude of the energies implied in the transitions to region I.

Chapter 5

Tunneling through dipolar barrier

In this chapter we propose to calculate the transmission coefficients in the non-modified and modified cases considered in Chapter 4, corresponding to tunneling from region III to region I of the potential in Figure 2.3. This will allow us to estimate the mean lifetime of a bound system OHe - nucleus before it enters region I, in which case many nuclear processes are possible, such as gamma decay or neutron release by an excited compound nucleus after the fusion of the initial nucleus and the helium nucleus from the OHe system.

5.1 Transmission coefficient

In this section, we illustrate the calculation of a transmission coefficient in the case of the non-modified WKB approximation explained in Chapter 4. The calculation for the modified one gives exactly the same analytical result and is therefore not repeated. We place ourselves in the situation where OHe and the nucleus are bound, so that the energy in the center-of-mass frame E equals the binding energy of the system, and the angular momentum is equal to zero.

Let us recall that, in the case of a radial potential, such as the potential of interaction OHe-nucleus, the solution of the Schrödinger equation independent of time takes the form $\psi(r,\theta,\varphi) = \frac{u(r)}{r} Y_l^m(\theta,\varphi)$. At zero angular momentum l, we have $Y_0^0 = \frac{1}{\sqrt{4\pi}}$, so that the complete spatial wave function ψ is only a function of r : $\psi(r) = \frac{u(r)}{r}\frac{1}{\sqrt{4\pi}}$. The two regions of interest are here region I and III of Figure 2.3 for which the radial wave functions write

$$\begin{aligned} u_I(r) &= u(0 < r < R) \\ &= A\exp(iKr) + B\exp(-iKr) \end{aligned}$$

where $K = \sqrt{2\mu\,(E + V_0)}$, and

$$\begin{aligned} u_{III}(r) &= u(a < r < d) \\ &= \frac{A'}{\sqrt{k_{III}(r)}} \exp(+i \int_a^r k_{III}(r)dr) + \frac{B'}{\sqrt{k_{III}(r)}} \exp(-i \int_a^r k_{III}(r)dr) \end{aligned}$$

where $k_{III}(r) = \sqrt{2\mu(E - U_{III}(r))}$ and $r = d$ is the turning point. In the last two expression, the first and second parts correspond each time to the outgoing and incoming waves respectively. In region II, we have

$$\begin{aligned} u_{II}(r) &= u(R < r < a) \\ &= \frac{C}{\sqrt{\kappa_{II}(r)}} \exp(-\int_R^r \kappa_{II}(r)dr) + \frac{D}{\sqrt{\kappa_{II}(r)}} \exp(+\int_R^r \kappa_{II}(r)dr) \end{aligned}$$

where $\kappa_{II}(r) = \sqrt{2\mu(U_{II}(r) - E)}$, while in region IV, on the right of the turning point

$$\begin{aligned} u_{IV}(r) &= u(r > d) \\ &= \frac{C'}{\sqrt{\kappa_{IV}(r)}} \exp(-\int_d^r \kappa_{IV}(r)dr) \end{aligned}$$

where $\kappa_{IV}(r) = \sqrt{2\mu(U_{III}(r) - E)}$.

The transmission coefficient T form region III to region I is defined as the ratio of the densities of probability current in region I and III evaluated respectively in $r = R$ and $r = a$

$$T = \frac{|\overrightarrow{J}_I(R)|}{|\overrightarrow{J}_{III}(a)|} \tag{5.1}$$

where the density of probability current is defined as

$$\overrightarrow{J} = \frac{1}{2mi}\left(\psi^* \overrightarrow{\nabla}\psi - \psi \overrightarrow{\nabla}\psi^*\right) \tag{5.2}$$

The gradient operator $\overrightarrow{\nabla} = \left(\frac{\partial}{\partial x}, \frac{\partial}{\partial y}, \frac{\partial}{\partial z}\right)$ can be rewritten in spherical coordinates $\overrightarrow{\nabla} = \left(\frac{\partial}{\partial r}, \frac{1}{r}\frac{\partial}{\partial \theta}, \frac{1}{r\sin\theta}\frac{\partial}{\partial \varphi}\right)$, so that the components of $\overrightarrow{J}$ in the spherical basis are given by

$$J_r = \frac{1}{2mi}\left(\psi^* \frac{\partial}{\partial r}\psi - \psi \frac{\partial}{\partial r}\psi^*\right) \tag{5.3}$$

$$J_\theta = \frac{1}{2mi}\left(\psi^* \frac{1}{r}\frac{\partial}{\partial \theta}\psi - \psi \frac{1}{r}\frac{\partial}{\partial \theta}\psi^*\right) \tag{5.4}$$

$$J_\varphi = \frac{1}{2mi}\left(\psi^* \frac{1}{r\sin\theta}\frac{\partial}{\partial \varphi}\psi - \psi \frac{1}{r\sin\theta}\frac{\partial}{\partial \varphi}\psi^*\right) \tag{5.5}$$

In the case $l = 0$, we have $J_\theta = J_\varphi = 0$, so that $T = \frac{J_{r,I}(R)}{J_{r,III}(a)}$. We are interested in the tunneling effect through the dipolar barrier in region II of a wave coming from large r to region I, therefore, the density of probability current must be evaluated by using the

incoming waves $\psi_I(r) = \frac{B}{r}\exp(-iKr)\frac{1}{\sqrt{4\pi}} = -\frac{A}{r}\exp(-iKr)\frac{1}{\sqrt{4\pi}}$ by the condition $u_I(0) = 0$ and $\psi_{III}(r) = \frac{B'}{r\sqrt{k_{III}(r)}}\exp(-i\int_a^r k_{III}(r)dr)\frac{1}{\sqrt{4\pi}}$. Expression (5.3) applied to ψ_I and ψ_{II} gives

$$\begin{aligned} J_{r,I}(r) &= -\frac{K|A|^2}{4\pi\mu r^2} \\ J_{r,III}(r) &= -\frac{|B'|^2}{4\pi\mu r^2} \\ \Rightarrow T &= K\frac{|A|^2}{|B'|^2}\left(\frac{a}{R}\right)^2 \end{aligned} \tag{5.6}$$

We need now to express B' as a function of A. The requirement of continuity of the wave function and its first derivative at $r = R$ gives expressions (4.15) and (4.16) of subsection 4.1.2 about the connections of the solution in Chapter 4 in which we have to replace A by $2iA$ because we used here $u_I(r) = A\exp(iKr) - A\exp(-iKr) = 2iA\sin(Kr)$ instead of $u_I(r) = A\sin(Kr)$. Then, the connection at $r = a$ gives expressions (4.20) and (4.21) and we can therefore express B' in terms of A

$$B' = A\left\{\frac{1}{2}XMe^{-\sigma_{II}} - \frac{1}{2}YNe^{\sigma_{II}} + \frac{1}{2}i\left(Ye^{\sigma_{II}} - Xe^{-\sigma_{II}}\right)\sqrt{\frac{k_{III}a)}{\kappa_{II}(a)}}\right\} \tag{5.7}$$

where the real X and Y are given by equations (4.17) and (4.18) and

$$\begin{aligned} M &= -\sqrt{\frac{\kappa_{II}(a)}{k_{III}(a)}} - \frac{1}{2}\left(\kappa_{II}(a)\right)^{-3/2}\frac{\kappa'_{II}(a)}{\sqrt{k_{III}(a)}} + \frac{1}{2}\left(k_{III}(a)\right)^{-3/2}\left(\kappa_{II}(a)\right)^{-1/2}k'_{III}(a) \\ N &= \sqrt{\frac{\kappa_{II}(a)}{k_{III}(a)}} - \frac{1}{2}\left(\kappa_{II}(a)\right)^{-3/2}\frac{\kappa'_{II}(a)}{\sqrt{k_{III}(a)}} + \frac{1}{2}\left(k_{III}(a)\right)^{-3/2}\left(\kappa_{II}(a)\right)^{-1/2}k'_{III}(a) \end{aligned}$$

are real. With (5.6) and (5.7) we are now ready to write down the transmission coefficient

$$T = \frac{K}{\left(\frac{1}{2}XMe^{-\sigma_{II}} - \frac{1}{2}YNe^{\sigma_{II}}\right)^2 + \frac{1}{4}\left|\frac{k_{III}(a)}{\kappa_{II}(a)}\right|\left(Ye^{\sigma_{II}} - Xe^{-\sigma_{II}}\right)^2}\left(\frac{a}{R}\right)^2 \tag{5.8}$$

This last expression can in most cases been simplified to

$$T \simeq \frac{4K}{Y^2\left(N^2 + \left|\frac{k_{III}(a)}{\kappa_{II}(a)}\right|\right)}e^{-2\sigma_{II}}\left(\frac{a}{R}\right)^2 \tag{5.9}$$

We see therefore that the value of T will strongly depend on the integral $\sigma_{II} = \int_R^a \kappa_{II}(r)dr$, which involves the mass of the nucleus through the reduced mass μ, the width $(a - R)$ and the height of the barrier to cross in the definition of κ_{II}. The transmission coefficient T represents here the probability that the OHe atom and the nucleus, approaching each other from the turning point in region III at binding energy, cross the dipolar barrier, at each test, i.e. at each oscillation in the well of the bound state.

5.2 Mean lifetime

The value of the transmission coefficient is not sufficient to assess the impact of tunneling through the dipolar barrier. A more relevant quantity is the mean lifetime similar to that encountered for example in the processes of disintegration. Moreover, the method used here to give an order of magnitude of it is the same as that used for the alpha decay.

Let us consider a bound system OHe - nucleus. This undergoes oscillations between the barrier in $r = a$ and the turning point in $r = d$ and therefore hits the barrier at a certain frequency ν. To calculate it, we need to know the speed in the well (in fact the relative velocity), which can be obtained from the probability density and current ρ and $\overrightarrow{J}$ in a semi-classical framework

$$\overrightarrow{v} = \frac{\overrightarrow{J}}{\rho} \tag{5.10}$$

This calculation requires to know the wave function throughout the interval $[a, d]$, which is a problem for the WKB solution because we saw that it diverges at the turning point. Therefore, and since the goad is only to give an order of magnitude, we turn to the square well potential and use the exact solution. In region III, we have

$$\psi_{III}(r) = \left(\frac{A}{r}e^{ik_{III}r} + \frac{B}{r}e^{-ik_{III}r}\right)\frac{1}{\sqrt{4\pi}}$$

where $k_{III}(r) = \sqrt{2\mu\left(E - V_{min}\right)}$, V_{min} being the minimum $U_{III}(a)$ of the well in region III. Using the incoming spherical wave, we have

$$\begin{aligned} \rho_{III}(r) &= \left|\psi_{III}\right|^2 = \frac{\left|B\right|^2}{4\pi r^2} \\ J_{r,III}(r) &= -\frac{k_{III}\left|B\right|^2}{4\pi\mu r^2} \end{aligned}$$

so that

$$v = \frac{k_{III}}{\mu}$$

Assuming oscillations between $r = a$ and $r = d$ at relative velocity v, we obtain the frequency of the oscillations

$$\begin{aligned} \nu &= \frac{v}{2\left(d - a\right)} \\ &= \frac{k_{III}}{2\mu\left(d - a\right)} \end{aligned} \tag{5.11}$$

The transmission coefficient T represents the probability to cross the barrier at each test and ν is the number of tests par unit time, so that νT is the probability of tunneling per unit time. The desired mean lifetime is therefore given by

$$\tau = \frac{1}{\nu T} \tag{5.12}$$

The considerations of these first two sections are limited to tunneling of a bound system OHe - nucleus. We could interest ourselves to the case in which an incident OHe, coming from infinity at thermal energy, hits the barrier without binding to the nucleus. In this case, the transmission coefficient has to be calculated with an incident plane wave of well defined direction of propagation, which is somewhat different from the spherical waves used until now. This calculation can be performed by developing a plane wave into spherical harmonics but has not been done in the framework of this thesis. However, the counting rate of events resulting from tunneling due to collisions between external (not bound) nuclei and the OHe atoms is calculated in Appendix D given a transition probability T. It is realized on the basis of a simple model that takes into account the thermal agitation in a medium at equilibrium, causing collisions at a rate that depends on the temperature, which can then be used together with the transmission coefficient to know the counting rate.

5.3 Results

First, let us put expression (5.8) corresponding to the non-modified WKB approximation into a program and calculate the transmission coefficient for nuclei given by the usual formula (4.26). Let us recall that in this case we had for the nuclear range $s = 1.2$ fm. The energy we have to use in equation (5.8) is the binding energy of an OHe - nucleus, which we are now able to obtain for any nucleus through the analysis of Chapter 4. The results are shown on Figure 5.1. We see that T decreases of about 30 orders of magnitude from the lightest nuclei to mass numbers $A > 200$. This is easily understood because the height of the dipolar barrier increases with the radius R of the nucleus as well as with the reduced mass μ, making σ_{II} go from $\simeq 2$ to $\simeq 36$, which greatly decreases T, as is better seen in expression (5.9).

Except for heavy nuclei, it seems that the values in Figure 5.1 are very high. A transmission coefficient greater than 10^{-10} for $A < 50$ represents a very high probability of tunneling per second given the large frequencies of oscillation with which we are dealing. In particular, for our nucleus of interest, sodium, we find $T = 1.28 \cdot 10^{-4}$, while expressions (5.11) and (5.12) give $\nu = 1.67 \cdot 10^{20}$ Hz and $\tau = 4.69 \cdot 10^{-17}$ s. This last value is obviously incredibly small and implies that as soon as a bound state is formed, it is destroyed in the nuclear region by nuclear processes whose products should be visible in any case. Figure 5.2 shows the mean lifetimes corresponding to the transmission coefficients of Figure (5.1). We see that even for the heaviest nuclei, the mean lifetime is small (only a few years) and should be observable.

The calculation of the transmission coefficient in the case of the modified WKB method is the same, even in the presence of the centrifugal potential that was not present before. In region II, the height of the barrier is just a little increased and in region III, we are left with

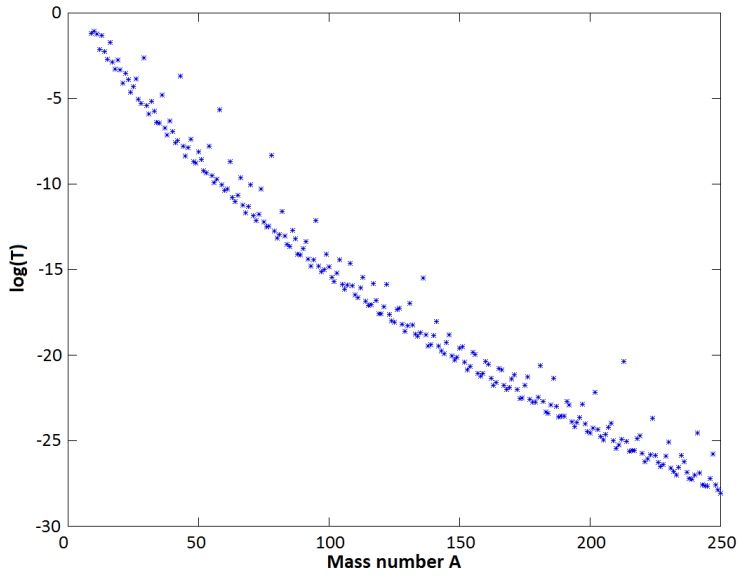

Figure 5.1: Logarithm in base 10 of the transmission coefficient for mass numbers going to 250.

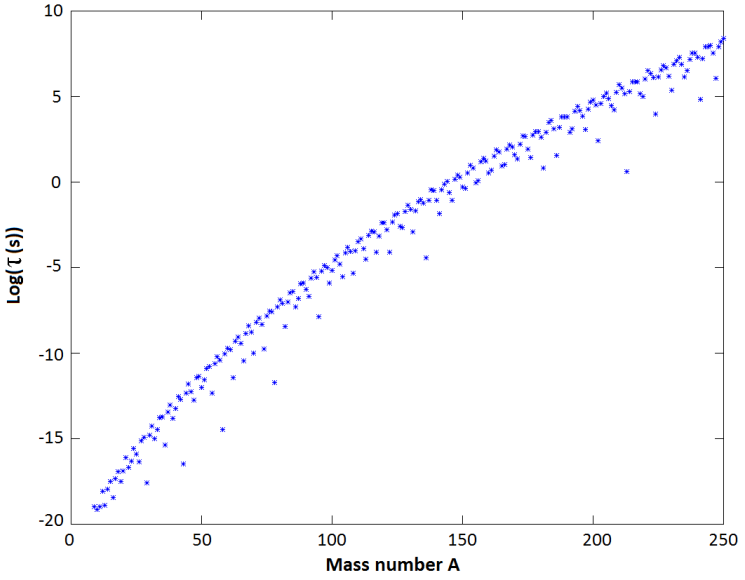

Figure 5.2: Logarithm in base 10 of the mean lifetime τ (s) for mass numbers going to 250

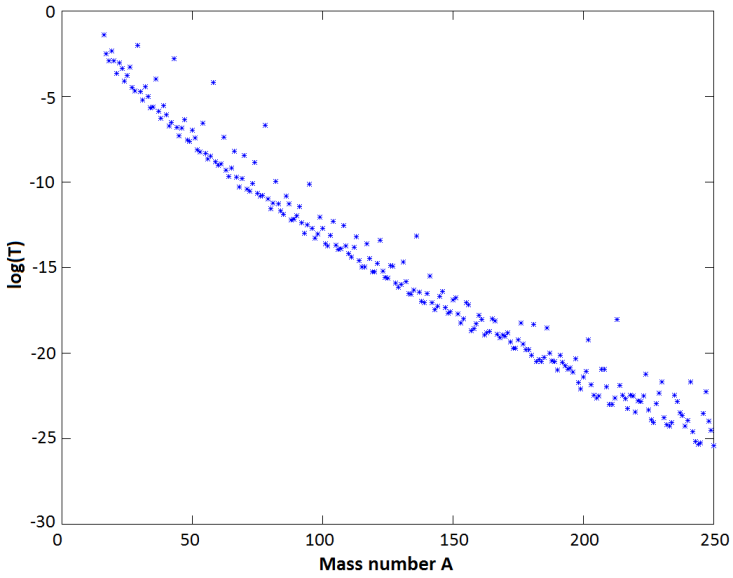

Figure 5.3: Logarithm of the modified transmission coefficient for mass numbers going to 250.

a new very extended barrier (see Figure 4.5, regions III and IV) but that has no importance in the case of a system OHe - nucleus bound in region III. We could expect that the effect of the increase of the barrier would be to suppress the transmission coefficient greatly. It is indeed decreased, but very slightly because the centrifugal potential is rather small compared to the barrier : at its maximum in $r = R$, it is only equal to $\frac{1}{8\pi\mu} \simeq 0.02$ MeV in the case of sodium. Moreover, this is offset by the decrease of the width of the barrier because of the choice $s = 0.44$ fm instead of 1.2 fm in the case of the non-modified WKB method. Thus we are left with $T = 4.43 \cdot 10^{-4}$, which is even slightly larger than previously, $\nu = 2.44 \cdot 10^{20}$ Hz and $\tau = 9.24 \cdot 10^{-18}$ s. Figure 5.3 shows the modified transmission coefficients for the usual nuclei and is very similar to Figure 5.1.

The high values of T, leading to very small values of the mean lifetime of a bound system OHe - nucleus, require some attention and discussion. We could think that the estimations of the transmission coefficients and the mean lifetime are incorrect. Assigning a velocity to a quantum system that oscillates between two well-defined spatial regions might seem wrong except in a semi-classical framework. However, we may expect that the order of magnitude is correct and in any case, an improvement would certainly not allow to win as many orders of magnitude for the value of τ to become much greater than the age of the universe, which would be the only solution to eliminate the problem of tunneling.

It seems therefore that we have to deal with these very small lifetimes, which requires considering the consequences of tunneling to the first region of the potential of interaction. As already announced, many nuclear processes, as well as electromagnetic ones, are possible,

nearly all giving rise to products whose presence cannot be unnoticed. To fix the ideas, in the case of sodium, the entry of helium (with O^{--} that has no nuclear interaction) inside the nucleus gives an aluminum nucleus in an excited state. Taking into account the nuclear binding energies of these three nuclei, we find indeed that to go from the ground state of ^{23}Na to the ground state of ^{27}Al, about 10 MeV must be released. These can be used to emit a photon at $E_\gamma = 10$ MeV, which is allowed by the conservation of the nuclear spin because $J_{Na} = 3/2$, $J_{Al} = 5/2$ and $J_\gamma = 1$, or to eject two neutrons ($J_n = 1/2$) of binding energy E_b and that would therefore leave the nucleus with a kinetic energy $10 - E_b$. The study of all the possible processes and their probabilities is of course out of the context of this thesis but we can already say that the effects should be visible. Another possibility would be that the helium nucleus, spending a very short time in the nucleus ($\sim 10^{-17}$ s), would not have time enough to be involved in a nuclear or electromagnetic reaction. It could therefore cross the dipolar barrier away and we would have a bound state at -3 keV that covers regions I, II and III of the potential of interaction, with very frequent crossings of the barrier, from front to back and vice versa. This low energy bound state, partially merged into the nucleus, would solve the problem of the products of fusion without having to increase the lifetime well beyond the age of the universe. But this possibility can in fact be ruled out immediately because, for nuclei heavier than sodium, the mean lifetime quickly becomes large enough (10^{-10} or 10^{-5} s for example are quite sufficient) to allow nuclear or electromagnetic reactions to take place, making practically all the nuclei found in our environment become unstable and radioactive in the presence of OHe. Finally, it is thought [13] that, when helium merges into the nucleus, the remaining O^{--} in the new nucleus is subject only to electrostatic interaction of harmonic oscillator type, corresponding to the electrostatic interaction of a charge (O^{--}) placed into a spherical charge distribution (nucleus of charge $Z + 2$). This gives rise to abnormal isotopes of known elements, which is an additional difficulty for the OHe hypothesis if the dipolar barrier can be crossed relatively easily.

Chapter 6

Conclusion

Currently, the most popular candidates for a dark matter constituted by particles that were non-relativistic at decoupling from plasma and radiation are the WIMPs (Weakly Interacting Massive Particles). Such neutral particles, interacting sufficiently weakly so that their existence has remained unnoticed until now, are actually predicted by supersymmetric theories (SUSY), where they are called neutralinos. Indirect and direct observations are underway, the first aiming primarily to detect the annihilation products of these particles with their antiparticles, the latter corresponding to the detection of the interaction of the dark matter particles with baryonic matter in a detector. In this case, a popular method is to observe the faint light produced by the nuclear recoil of a nucleus, caused by a massive weakly interacting particle passing through the earth and hitting the target matter of an underground scintillator.

This is the approach followed by experiments such as XENON100, DAMA/LIBRA (DArk Matter / Large sodium Iodide Bulk for RAre processes) and previous DAMA/NaI. While the first one did not observe any signal corresponding with certainty to the signature of dark matter, providing only upper limits on the elastic WIMP-nucleon cross section σ as a function of the WIMP mass m_χ, the other two have, during their successive runs, revealed a signal in the energy range $(2-4)$ keV presenting an annual modulation with a one-year period ((0.999 ± 0.002) yr) and with a modulation amplitude of (0.0116 ± 0.0013)cpd/kg/keV. When trying to explain this signal, maybe due to the motion of the earth around the sun with a one-year period in a dark matter halo, in terms of WIMPs, we realize that the region delimited in the σ versus m_χ space for WIMPs lies out the limits fixed by XENON100.

Note that another experiment, CoGent, using a germanium detector, had also detected an excess of events that could correspond to the impacts of WIMPs on the nuclei of germanium in the crystal. No annual modulation phenomenon had been identified so far and the region in the parameter space, favoring the hypothesis of light WIMPs as for DAMA, was also in contradiction with the negative results of XENON100. It is only very recently that a

modulation similar to that observed by DAMA has been reported, in the energy range below 1 keV. If this is confirmed, this will be the first evidence for such kind of signal somewhere else than at the Gran Sasso National Laboratory in Italy where is located the DAMA experiment.

The contradiction between experimental data from XENON and DAMA or CoGent has been considered by Khlopov et. al. and the approach is as follows : instead of explaining the DAMA results (or the more recent ones from CoGent) in terms of WIMPs as it is usually done, it is possible to interpret the observations using another type of dark matter, called composite dark matter, without contradicting the other negative results. This kind of dark matter consists in new heavy stable charged particles bound to baryonic matter in neutral "dark atoms". From cosmological arguments, it has been shown that these particles should be of charge -2 (denoted by O^{--}) and are bound to primordial He^{++}, giving rise to hydrogen-like atoms, called O-helium atoms ($O^{--}He^{++}$, denoted by OHe). Such particles, benefiting from theoretical support predicting their existence, are found to have strongly suppressed hadronic interactions, making their interactions with terrestrial matter dominated by the nuclear interactions of He. The mass M_O of an O^{--} is assumed to be around 1 TeV, and all the following results do not depend of a mass $M_O > 1$ TeV.

Because of these nuclear interactions coming from the helium nucleus, the OHe atoms falling onto the Earth from a dark matter halo surrounding the galaxy begin to undergo elastic nuclear collisions as they penetrate below the surface, until they thermalize and fall down towards the center of the earth. The energy transfer is therefore to low to be detected as a nuclear recoil but the OHe atoms can form a low energy bound state with nuclei, leading to the observed signal of DAMA by the process of radiative capture.

A -3 keV bound state had already been found for the system OHe - Na, together with the fact that no bound states were found for iodine from the DAMA detector and xenon, by simplifying the potential of interaction by a square well potential. While Khlopov et al. use at large distance (with respect to the size of an OHe atom) a Coulomb screened potential plus a Yukawa-like potential corresponding to σ meson exchange between helium and the nucleus, we considered here only the purely electrostatic part of the interaction at such distances. It was necessary to perform the calculation using its actual shape. This was the main objective of this master thesis and it has been done using the approximate analytical solutions provided by the WKB approximation.

This method was firstly used as a simple copy of its version in one dimension (because of the similarity between the radial equation in three dimensions and the Schrödinger equation in one dimension) and then was modified to take into account the fact that the radial variable r takes only positive values unlike the variable x in one dimension. Applying the non-modified method to a wide range of stable nuclei with a nuclear range of 1.2 fm included to parameter a, we found no bound state for the systems ${}^1n$, ${}^1H$ ${}^2H$, ${}^3H$ $-$nucleus, i.e. for light nuclei.

The most important result is that a bound state is found at -2.96 keV for sodium, i.e. one of the two components of DAMA, which allow to explain the observations in the right energy range and agree with the results of Khlopov et al., but without considering any σ exchange between helium and nucleus. This result is to be associated with a level at -1.22 keV for the other component, iodine, which gives a signal at 1.22 keV lying under the energy threshold at 2 keV of the experiment and therefore contributing to the counting rate in that region. The parameters V_0 and R of the model have no influence on the results and no higher level at $l = 0$ is found.

In a general manner, we therefore find bound states for every nuclei (except for the lightest ones). A bound state is found for xenon, at -1.15 keV in particular for the isotope 132, and similar values for the other stable isotopes. At operating temperature of XENON100 (-100 °C), this gives a constant part of the modulated signal $\xi_{^{132}Xe} = 0.215$ cpd/kg, to which should be added the contributions of the other isotopes. But this is not in contradiction with the negative results of XENON100 because it lies under the threshold of the experiment, estimated at 5 keV. For germanium, the binding energies shown in Table 4.2 are centered around -2 keV and seem too high in absolute value to reproduce the recent modulated signal observed by CoGent. But this is not a real contradiction because a level is effectively predicted while it is required to explain the observational results in terms of OHe and a refinement of the model should allow us to get closer to the required value.

Although these results are encouraging, some aspects should be analyzed further. Among them, the size effects of nuclei. Indeed, in this model, the nucleus is considered as a point feature (except for the determination of the regions of the potential). But in view of the distances involved in the problem, the nuclear radius is not negligible and its size should be taken into account. Let us illustrate this a bit more : being very massive, the OHe atom nearly corresponds to the origin of the center of mass frame. We therefore may consider that the nucleus is immersed in an external central potential, as a potential imposed to a single point particle. The bound state corresponds to the situation where the nucleus is trapped in the well of region III, but this is very small. For example, in the case of sodium, we have $a = 8.52$ fm and $d = 8.79$ fm for the turning point at -3 keV. We see that we have to deal with a nucleus of radius $R \simeq 3.5$ fm in a well of width $\simeq 0.27$ fm. This could lead to corrections or weaken and even destroy the bound state for the largest nuclei, as xenon and iodine. This analysis should therefore be reported to further works.

A modified version of the WKB method has been envisaged, where we turned, by an appropriate change of variable and function, to a problem characterized by a variable x going from $-\infty$ to $+\infty$ when r goes from 0 to $+\infty$, so that this new situation is similar in all respects to a problem in one dimension. Then we applied the WKB solutions, originally built in one dimension, to this new problem, which proved to be nothing more than applying

directly the WKB solutions to the three-dimensional problem together with the replacement of the term $l(l+1)$ by $\left(l+\frac{1}{2}\right)^2$ in the radial equation. This had the effect of adding a "centrifugal term" even at $l=0$.

In this case, we had to change the nuclear range s and take $s = 0.44$ fm, giving us a bound state for sodium at -3 keV, explaining the DAMA results. This is to be associated with a bound state for iodine at -2.2 keV, giving an unobserved supplementary modulation amplitude $\varsigma_I = 0.0334$ cpd/kg. But we cannot do without noticing that the corresponding signal at 2.2 keV is very close to the threshold and we have good reason to think that corrections could bring this value back below 2 keV. More light nuclei are in this case suppressed (do not have any bound state with OHe), the lightest one to have a bound state with OHe being ${}^{16}N$, but we are still left with levels for all heavier nuclei. Here again, no contradiction appears with the negative results form XENON100 because the binding energies (-2.1 keV for ${}^{132}Xe$ and similar values for the other isotopes) give rise to a signal by radiative capture under the energy threshold of the experiment. For the stable isotopes of germanium, however, we find binding energies going from -3.77 to -3.26 keV, which seem even more difficult to relate to the results of CoGent than in the case of the non-modified WKB method. But this time too, we cannot speak about real contradiction but rather about a lack of precision in the prediction of the binding energies. In any case, attention should be paid to the future publications of observational results of CoGent. Finally, no higher levels are found at $l=0$ for all the considered nuclei.

We are therefore left with two methods, both giving results for sodium and thereby explaining the DAMA results. It is of course necessary to choose one of them. The non-modified method has the advantage that the needed value for the nuclear range s falls in a generally accepted interval. But the modified method seems more appropriate because its only effect is to get closer to a one-dimensional problem without bringing any additional complication, and therefore the WKB solutions are necessarily better suited. That is the reason why we should turn to this version and its associated results. The less probable value of the nuclear range can be improved by requiring a bound state closer to -2 keV for sodium (which is also an acceptable value, being in the right energy range) but it is not sufficient to bring it above the unit. Uncertainties relative to the model and to the WKB method could also be partially at the origin of this low value, and again, size effects should be taken into account.

By evaluating the validity criterion of the WKB method, it has been realized that, even it the modified case, this was greater than unity only in the small region on the left of the turning point in the potential well of region III. This means that the approximation is poor in that region, while the WKB connection formulas require its validity on both sides of the turning point, at least on a reduced interval. This could be the principal source of uncertainty

(not to mention the uncertainties inherent to the model). It seems difficult to estimate the error on the binding energy with the WKB approximation but one way to improve the results would be to keep the higher order terms in the development of the solution in powers of $\hbar$ and redo all the calculations with these additional terms, which of course has not been done in the context of this thesis given the large mathematical complications that this introduces.

A third method of resolution of the Schrödinger equation has been considered, consisting in, as Khlopov et al., simplifying the potential by a square well potential. After noting that no level was found by directly replacing the true potential by its simplified version, we realized that we had to lower the well in region III to about -1 MeV to finally obtain a level at -3 keV for sodium. This was in contradiction with the WKB method that gives a level in a well of a few keV of depth. Therefore, we applied the WKB solutions to the simplified problem, and realized that it gave exactly the same results because the WKB solutions reduce to the exact solutions in the case of a constant potential. We concluded that the WKB approximation, applied to the true shape of the potential, should be an improvement.

Extending the calculations to the search of levels in region I (nuclear region) of the potential, we found the presence of deep levels that correspond to the levels of an alpha particle (helium nucleus) within a nucleus.

More interest has been given to the dipolar barrier in region II of the potential. In particular, tunneling through this barrier could lead the nucleus and the helium nucleus to merge and give an excited larger nucleus that could de-excite through many nuclear or electromagnetic processes. Because none of the products of these processes are observed, we expected the transmission coefficient T to be very low, making tunneling very inefficient. Unfortunately, it was evaluated, for sodium in particular, to $T \simeq 10^{-4}$, giving a mean lifetime τ of a bound state OHe - Na of the order of 10^{-17} s. This poses a real problem, which raises profound interrogations. If nothing is done to greatly suppress the transmission coefficient, making the mean lifetime become much large than the age of the universe, the hypothesis of OHe will no longer seem viable. Further work is therefore needed to find a way to strengthen the barrier, at its width and height. If no such mechanism can be found, attention should be payed to the size effects of a nucleus tunneling through a barrier that has roughly the same size. These effects could indeed have a significant influence on the process of tunneling.

Finally, we must note that until now, the system OHe - nucleus has been considered as a two-body system (OHe and nucleus separately) with a spherical symmetry, while it is clear that we have to deal with a three-body problem (O^{--} - He^{++} - nucleus) without any particular symmetry. So it goes without saying that the best thing to do would be to develop a program that simulates the evolution of this three-body system, taking into account the extensions of the entities. This would allow to accurately understand the behavior of the system and to definitively decide for or against the hypothesis of OHe as the constituent of

dark matter. This point would be a perfect subject for a doctoral thesis, with, in both cases, an important result at the key.

Appendix A

WKB equations

Here we show the details of calculations of section 3.3 to set the equations (3.24) and (3.25) in Chapter 3.

Recall the development of the phase S of the wave function to order 1 in $\hbar^2$:

$$S \simeq S_0 + \hbar^2 S_1$$

to be inserted in the differential equation for S :

$$S'^2 = 2m\left(E - V\right) + \hbar^2 \left[\frac{3}{4}\left(\frac{S''}{S'}\right)^2 - \frac{1}{2}\frac{S'''}{S'}\right]$$

We have :

$$\begin{aligned} S_0'^2 + 2\hbar^2 S_0' S_1' &= 2m\left(E - V\right) + \bar{h}^2 \left[\frac{3}{4}\left(\frac{S_0'' + \hbar^2 S_1''}{S_0' + \hbar^2 S_1'}\right)^2 - \frac{1}{2}\frac{S_0''' + \hbar^2 S_1'''}{S_0' + \hbar^2 S_1'}\right] \\ &= 2m\left(E - V\right) + \hbar^2 \left[\frac{3}{4}\left(S_0'' + \hbar^2 S_1''\right)^2 \left(\frac{1}{S_0'}\right)^2 \left(1 - \hbar^2 \frac{S_1'}{S_0'}\right)^2 \right. \\ &\quad \left. -\frac{1}{2}\left(S_0''' + \hbar^2 S_1'''\right)\frac{1}{S_0'}\left(1 - \hbar^2 \frac{S_1'}{S_0'}\right)\right] \end{aligned}$$

by developing $\frac{1}{1+\hbar^2 \frac{S_1'}{S_0'}}$ at first order in $\hbar^2$ as $1 - \hbar^2 \frac{S_1'}{S_0'}$.

Then,

$$\begin{aligned} S_0'^2 + 2\hbar^2 S_0' S_1' &= 2m\left(E - V\right) + \hbar^2 \left[\frac{3}{4}\frac{1}{S_0'^2}\left(S_0''^2 + 2\hbar^2 S_0'' S_1''\right)\left(1 - 2\hbar^2 \frac{S_1'}{S_0'}\right)\right. \\ &\quad \left. -\frac{1}{2}\frac{1}{S_0'}\left(S_0''' + \hbar^2 S_1'''\right)\left(1 - \hbar^2 \frac{S_1'}{S_0'}\right)\right] \end{aligned}$$

Therefore, by only keeping the terms of order 0 and 1 in $\hbar^2$,

$$S_0'^2 + 2\hbar^2 S_0' S_1' = 2m\left(E - V\right) + \frac{3}{4}\hbar^2 \frac{1}{S_0'^2} S_0''^2 - \frac{1}{2}\hbar^2 \frac{1}{S_0'} S_0'''$$

$$\Rightarrow \begin{cases} S_0'^2 = 2m\,(E-V) & at\ order\ 0 \\ 2S_0'S_1' = \frac{3}{4}\left(\frac{S_0''}{S_0'}\right)^2 - \frac{1}{2}\frac{S_0'''}{S_0'} & at\ order\ 1 \end{cases}$$

the second giving the equation (3.24).

Let us consider the case $E > V$:

We know that $S_0' = \pm\frac{\bar{\hbar}}{\bar{\lambda}}$ from the lowest-order equation, with $\bar{\lambda}$ defined in (3.20). The first-order equation gives :

$$\pm 2\frac{\hbar}{\bar{\lambda}}S_1' = \frac{3}{4}\left(\frac{\hbar\bar{\lambda}'/\bar{\lambda}^2}{\hbar/\bar{\lambda}}\right)^2 - \frac{1}{2}(\mp)(\pm)\bar{\lambda}\frac{\bar{\lambda}''\bar{\lambda} - 2\bar{\lambda}'^2}{\bar{\lambda}^3} = \frac{3}{4}\frac{\bar{\lambda}'^2}{\bar{\lambda}} + \frac{1}{2}\bar{\lambda}'' - \frac{\bar{\lambda}'^2}{\bar{\lambda}}$$

Finally, we find :

$$\hbar S_1' = \pm\left(\frac{1}{4}\bar{\lambda}'' - \frac{1}{8}\frac{\bar{\lambda}'^2}{\bar{\lambda}}\right)$$

which proves equation (3.25).

Appendix B

WKB quantization condition

Here it is shown how we set the condition (4.22) for the quantization of the energy in the case of the non-modified WKB approximation in subsection 4.1.2 of Chapter 4, which is also used for the modified method.

The condition on the constant D' of the WKB solution in region IV of the potential coming from the connection formulas of the WKB approximation is recalled hereafter

$$D' = \theta A' e^{i\rho} + \theta^* B' e^{-i\rho} \tag{B.1}$$

where $\theta = e^{i\pi/4}$ and $\rho = \int_a^d k_{III}(r)dr$, to be associated with the condition of non-divergence of the solution for $r \to \infty$

$$D' = 0 \tag{B.2}$$

By requiring the continuity of the wave function and its first derivative at the points of discontinuity of the potential, we find the following relations between the constants involved in the solutions of the different regions of the potential

$$C = -\frac{A}{2}X \tag{B.3}$$

$$D = \frac{A}{2}Y \tag{B.4}$$

$$\begin{aligned} A' = {} & \frac{1}{2}iC\left(\sqrt{\frac{\kappa_{II}(a)}{k_{III}(a)}} + \frac{1}{2}\left(\kappa_{II}(a)\right)^{-3/2}\frac{\kappa'_{II}(a)}{\sqrt{k_{III}(a)}} - \frac{1}{2}\left(k_{III}(a)\right)^{-3/2}\left(\kappa_{II}(a)\right)^{-1/2}k'_{III}(a)\right. \\ & - \left. i\sqrt{k_{III}(a)}\left(\kappa_{II}(a)\right)^{-1/2}\right)e^{-\sigma_{II}} - \frac{1}{2}iD\left(\sqrt{\frac{\kappa_{II}(a)}{k_{III}(a)}} - \frac{1}{2}\left(\kappa_{II}(a)\right)^{-3/2}\frac{\kappa'_{II}(a)}{\sqrt{k_{III}(a)}}\right. \\ & + \left.\frac{1}{2}\left(k_{III}(a)\right)^{-3/2}\left(\kappa_{II}(a)\right)^{-1/2}k'_{III}(a) + i\sqrt{k_{III}(a)}\left(\kappa_{II}(a)\right)^{-1/2}\right)e^{\sigma_{II}} \end{aligned} \tag{B.5}$$

$$B' = \sqrt{\frac{k_{III}(a)}{\kappa_{II}(a)}}\,C\,e^{-\sigma_{II}} + \sqrt{\frac{k_{III}(a)}{\kappa_{II}(a)}}\,D\,e^{\sigma_{II}} - A' \tag{B.6}$$

where

$$
\begin{aligned}
X &= \frac{K}{\sqrt{\kappa_{II}(R)}}\cos(KR) - \sqrt{\kappa_{II}(R)}\sin(KR) + \frac{1}{2}\sin(KR)\left(\kappa_{II}(R)\right)^{-3/2}\kappa'_{II}(R) \\
Y &= \frac{K}{\sqrt{\kappa_{II}(R)}}\cos(KR) + \sqrt{\kappa_{II}(R)}\sin(KR) + \frac{1}{2}\sin(KR)\left(\kappa_{II}(R)\right)^{-3/2}\kappa'_{II}(R)
\end{aligned}
$$

are real.

The use of expressions (B.1), (B.5) and (B.6) gives for D'

$$
\begin{aligned}
D' &= \theta e^{i\rho}\frac{1}{2}iC\left(\sqrt{\frac{\kappa_{II}(a)}{k_{III}(a)}} + \frac{1}{2}\left(\kappa_{II}(a)\right)^{-3/2}\frac{\kappa'_{II}(a)}{\sqrt{k_{III}(a)}} - \frac{1}{2}\left(k_{III}(a)\right)^{-3/2}\left(\kappa_{II}(a)\right)^{-1/2}\right. \\
&\quad \left.\times k'_{III}(a) - i\sqrt{k_{III}(a)}\left(\kappa_{II}(a)\right)^{-1/2}\right)e^{-\sigma_{II}} - \theta e^{i\rho}\frac{1}{2}iD\left(\sqrt{\frac{\kappa_{II}(a)}{k_{III}(a)}} - \frac{1}{2}\left(\kappa_{II}(a)\right)^{-3/2}\right. \\
&\quad \left.\times\frac{\kappa'_{II}(a)}{\sqrt{k_{III}(a)}} + \frac{1}{2}\left(k_{III}(a)\right)^{-3/2}\left(\kappa_{II}(a)\right)^{-1/2}k'_{III}(a) + i\sqrt{k_{III}(a)}\left(\kappa_{II}(a)\right)^{-1/2}\right)e^{\sigma_{II}} \\
&\quad + \theta^* e^{-i\rho}\sqrt{\frac{k_{III}(a)}{\kappa_{II}(a)}}\,C\,e^{-\sigma_{II}} + \theta^* e^{-i\rho}\sqrt{\frac{k_{III}(a)}{\kappa_{II}(a)}}\,D\,e^{\sigma_{II}} - \theta^* e^{-i\rho}A' \\
&= Coeff_C \times C + Coeff_D \times D
\end{aligned}
$$

where

$$
\begin{aligned}
Coeff_C &= \theta e^{i\rho}\frac{1}{2}i\left(\sqrt{\frac{\kappa_{II}(a)}{k_{III}(a)}} + \frac{1}{2}\left(\kappa_{II}(a)\right)^{-3/2}\frac{\kappa'_{II}(a)}{\sqrt{k_{III}(a)}} - \frac{1}{2}\left(k_{III}(a)\right)^{-3/2}\left(\kappa_{II}(a)\right)^{-1/2}\right. \\
&\quad \left.\times k'_{III}(a) - i\sqrt{k_{III}(a)}\left(\kappa_{II}(a)\right)^{-1/2}\right)e^{-\sigma_{II}} + \theta^* e^{-i\rho}\sqrt{\frac{k_{III}(a)}{\kappa_{II}(a)}}\,e^{-\sigma_{II}} \\
&\quad -\theta^* e^{-i\rho}\frac{1}{2}i\left(\sqrt{\frac{\kappa_{II}(a)}{k_{III}(a)}} + \frac{1}{2}\left(\kappa_{II}(a)\right)^{-3/2}\frac{\kappa'_{II}(a)}{\sqrt{k_{III}(a)}} - \frac{1}{2}\left(k_{III}(a)\right)^{-3/2}\right. \\
&\quad \left.\times\left(\kappa_{II}(a)\right)^{-1/2}k'_{III}(a) - i\sqrt{k_{III}(a)}\left(\kappa_{II}(a)\right)^{-1/2}\right)e^{-\sigma_{II}} \\
&= \frac{1}{2}i\left(e^{i\pi/4}e^{i\rho} - e^{-i\pi/4}e^{-i\rho}\right)\left(\sqrt{\frac{\kappa_{II}(a)}{k_{III}(a)}} + \frac{1}{2}\left(\kappa_{II}(a)\right)^{-3/2}\frac{\kappa'_{II}(a)}{\sqrt{k_{III}(a)}}\right. \\
&\quad \left.-\frac{1}{2}\left(k_{III}(a)\right)^{-3/2}\left(\kappa_{II}(a)\right)^{-1/2}k'_{III}(a) - i\sqrt{k_{III}(a)}\left(\kappa_{II}(a)\right)^{-1/2}\right)e^{-\sigma_{II}} \\
&\quad + \theta^* e^{-i\rho}\sqrt{\frac{k_{III}(a)}{\kappa_{II}(a)}}\,e^{-\sigma_{II}}
\end{aligned}
$$

and hence

$$
\begin{aligned}
Coeff_C &= -\sin(\rho + \frac{\pi}{4})\left(\sqrt{\frac{\kappa_{II}(a)}{k_{III}(a)}} + \frac{1}{2}\left(\kappa_{II}(a)\right)^{-3/2}\frac{\kappa'_{II}(a)}{\sqrt{k_{III}(a)}} - \frac{1}{2}\left(k_{III}(a)\right)^{-3/2}\right. \\
&\quad \left.\times\left(\kappa_{II}(a)\right)^{-1/2}k'_{III}(a) - i\sqrt{k_{III}(a)}\left(\kappa_{II}(a)\right)^{-1/2}\right)e^{-\sigma_{II}} + \theta^* e^{-i\rho}\sqrt{\frac{k_{III}(a)}{\kappa_{II}(a)}}\,e^{-\sigma_{II}}
\end{aligned}
\tag{B.7}
$$

and

$$
\begin{aligned}
Coeff_D &= \frac{1}{2}i\left(-e^{i\pi/4}e^{i\rho}+e^{-i\pi/4}e^{-i\rho}\right)\left(\sqrt{\frac{\kappa_{II}(a)}{k_{III}(a)}}-\frac{1}{2}\left(\kappa_{II}(a)\right)^{-3/2}\frac{\kappa'_{II}(a)}{\sqrt{k_{III}(a)}}\right.\\
&\quad\left.+\frac{1}{2}\left(k_{III}(a)\right)^{-3/2}\left(\kappa_{II}(a)\right)^{-1/2}k'_{III}(a)+i\sqrt{k_{III}(a)}\left(\kappa_{II}(a)\right)^{-1/2}\right)e^{\sigma_{II}}\\
&\quad+\theta^{*}e^{-i\rho}\sqrt{\frac{k_{III}(a)}{\kappa_{II}(a)}}\,e^{\sigma_{II}}\\
&= \sin(\rho+\frac{\pi}{4})\left(\sqrt{\frac{\kappa_{II}(a)}{k_{III}(a)}}-\frac{1}{2}\left(\kappa_{II}(a)\right)^{-3/2}\frac{\kappa'_{II}(a)}{\sqrt{k_{III}(a)}}+\frac{1}{2}\left(k_{III}(a)\right)^{-3/2}\right. \qquad \text{(B.8)}\\
&\quad\left.\times\left(\kappa_{II}(a)\right)^{-1/2}k'_{III}(a)-+i\sqrt{k_{III}(a)}\left(\kappa_{II}(a)\right)^{-1/2}\right)e^{\sigma_{II}}+\theta^{*}e^{-i\rho}\sqrt{\frac{k_{III}(a)}{\kappa_{II}(a)}}\,e^{\sigma_{II}}
\end{aligned}
$$

while the condition (B.2) and expressions (B.3) and (B.4), together with previous ones (B.7) and (B.8), give

$$
\begin{aligned}
0 &= \sin(\rho+\frac{\pi}{4})\left(\sqrt{\frac{\kappa_{II}(a)}{k_{III}(a)}}+\frac{1}{2}\left(\kappa_{II}(a)\right)^{-3/2}\frac{\kappa'_{II}(a)}{\sqrt{k_{III}(a)}}-\frac{1}{2}\left(k_{III}(a)\right)^{-3/2}\left(\kappa_{II}(a)\right)^{-1/2}\right.\\
&= \left.\times k'_{III}(a)-i\sqrt{k_{III}(a)}\left(\kappa_{II}(a)\right)^{-1/2}\right)e^{-\sigma_{II}}\frac{A}{2}X-\theta^{*}e^{-i\rho}\sqrt{\frac{k_{III}(a)}{\kappa_{II}(a)}}\,e^{-\sigma_{II}}\frac{A}{2}X\\
&\quad+\sin(\rho+\frac{\pi}{4})\left(\sqrt{\frac{\kappa_{II}(a)}{k_{III}(a)}}-\frac{1}{2}\left(\kappa_{II}(a)\right)^{-3/2}\frac{\kappa'_{II}(a)}{\sqrt{k_{III}(a)}}+\frac{1}{2}\left(k_{III}(a)\right)^{-3/2}\left(\kappa_{II}(a)\right)^{-1/2}\right.\\
&\quad\left.\times k'_{III}(a)-+i\sqrt{k_{III}(a)}\left(\kappa_{II}(a)\right)^{-1/2}\right)e^{\sigma_{II}}\frac{A}{2}Y+\theta^{*}e^{-i\rho}\sqrt{\frac{k_{III}(a)}{\kappa_{II}(a)}}\,e^{\sigma_{II}}\frac{A}{2}Y
\end{aligned}
$$

which gives, for the real part

$$
\begin{aligned}
&\sin(\rho+\frac{\pi}{4})\left(\sqrt{\frac{\kappa_{II}(a)}{k_{III}(a)}}+\frac{1}{2}\left(\kappa_{II}(a)\right)^{-3/2}\frac{\kappa'_{II}(a)}{\sqrt{k_{III}(a)}}-\frac{1}{2}\left(k_{III}(a)\right)^{-3/2}\left(\kappa_{II}(a)\right)^{-1/2}\right.\\
&\quad\left.\times k'_{III}(a)\right)e^{-\sigma_{II}}\frac{X}{2}-\cos(\rho+\frac{\pi}{4})e^{-\sigma_{II}}\sqrt{\frac{k_{III}(a)}{\kappa_{II}(a)}}\,\frac{X}{2}+\sin(\rho+\frac{\pi}{4})\left(\sqrt{\frac{\kappa_{II}(a)}{k_{III}(a)}}\right. \qquad \text{(B.9)}\\
&\quad\left.-\frac{1}{2}\left(\kappa_{II}(a)\right)^{-3/2}\frac{\kappa'_{II}(a)}{\sqrt{k_{III}(a)}}+\frac{1}{2}\left(k_{III}(a)\right)^{-3/2}\left(\kappa_{II}(a)\right)^{-1/2}k'_{III}(a)\right)e^{\sigma_{II}}\frac{Y}{2}\\
&\quad+\cos(\rho+\frac{\pi}{4})e^{\sigma_{II}}\sqrt{\frac{k_{III}(a)}{\kappa_{II}(a)}}\,\frac{Y}{2} = 0
\end{aligned}
$$

and for the imaginary part

$$\begin{aligned} -\sin(\rho+\frac{\pi}{4})\sqrt{\frac{k_{III}(a)}{\kappa_{II}(a)}}\,e^{-\sigma_{II}}\frac{X}{2}+\sin(\rho+\frac{\pi}{4})\sqrt{\frac{k_{III}(a)}{\kappa_{II}(a)}}\,e^{-\sigma_{II}}\frac{X}{2} & \\ +\sin(\rho+\frac{\pi}{4})\sqrt{\frac{k_{III}(a)}{\kappa_{II}(a)}}\,e^{\sigma_{II}}\frac{Y}{2}-\sin(\rho+\frac{\pi}{4})\sqrt{\frac{k_{III}(a)}{\kappa_{II}(a)}}\,e^{\sigma_{II}}\frac{Y}{2} &= 0 \\ \Leftrightarrow 0 &= 0 \end{aligned} \tag{B.10}$$

Expression (B.9) is the quantization condition (4.22) that we wanted.

Appendix C

Quantization conditions for the square well potential

This appendix contains the calculations relative to the energy quantization conditions in the case of the square well potential of section (4.3), in both cases $-U_3 < E < 0$ and $-U_1 < E < -U_3$. Recall that the simplified potential is shown in Figure 4.8 in section 4.3.

C.1 Case $-U_3 < E < 0$

Let us recall the solutions in the regions I, II, III and IV

$$\begin{aligned} u_I(r) &= A_I \exp(ik_I r) + B_I \exp(-ik_I r) \\ u_{II}(r) &= A_{II} \exp(k_{II} r) + B_{II} \exp(-k_{II} r) \\ u_{III}(r) &= A_{III} \exp(ik_{III} r) + B_{III} \exp(-ik_{III} r) \\ u_{IV}(r) &= A_{IV} \exp(k_{IV} r) + B_{IV} \exp(-k_{IV} r) \end{aligned}$$

where $k_I = \sqrt{2\mu\,(E+U_1)}$, $k_{II} = \sqrt{2\mu\,(U_2-E)}$, $k_{III} = \sqrt{2\mu\,(E+U_3)}$ and $k_{IV} = \sqrt{-2\mu E}$.

The finiteness of the wave function at the origin together with the continuity of the solution and its first derivative at each point of discontinuity of the potential give the following set of equations

$$\begin{aligned} A_I + B_I &= 0 \Rightarrow u_I(r) = A\sin(k_I r) & \\ A\sin(k_I R) &= A_{II} e^{k_{II} R} + B_{II} e^{-k_{II} R} & \text{(C.1)} \\ Ak_I \cos(k_I R) &= A_{II} k_{II} e^{k_{II} R} - B_{II} k_{II} e^{-k_{II} R} & \text{(C.2)} \\ A_{II} e^{k_{II} a} + B_{II} e^{-k_{II} a} &= A_{III} e^{ik_{III} a} + B_{III} e^{-ik_{III} a} & \text{(C.3)} \\ A_{II} k_{II} e^{k_{II} a} - B_{II} k_{II} e^{-k_{II} a} &= A_{III} ik_{III} e^{ik_{III} a} - B_{III} ik_{III} e^{-ik_{III} a} & \text{(C.4)} \\ A_{III} e^{ik_{III} b} + B_{III} e^{-ik_{III} b} &= A_{IV} e^{k_{IV} b} + B_{IV} e^{-k_{IV} b} & \text{(C.5)} \\ A_{III} ik_{III} e^{ik_{III} b} - B_{III} ik_{III} e^{-ik_{III} b} &= A_{IV} k_{IV} e^{k_{IV} b} - B_{IV} k_{IV} e^{-k_{IV} b} & \text{(C.6)} \end{aligned}$$

These equations can be regarded two by two in order to finally express A_{IV} in terms of A : (C.1) and (C.2) lead to

$$A_{II} = \frac{A}{2k_{II}} \left(k_I \cos(k_I R) + k_{II} \sin(k_I R)\right) e^{-k_{II} R} \tag{C.7}$$

$$B_{II} = \frac{A}{2k_{II}} \left(k_{II} \sin(k_I R) - k_I \cos(k_I R)\right) e^{k_{II} R} \tag{C.8}$$

while (C.3) and (C.4) give

$$A_{III} = \frac{1}{2i}\left[A_{II}\left(\frac{k_{II}}{k_{III}} + i\right) e^{k_{II} a} e^{-ik_{III} a} + B_{II}\left(i - \frac{k_{II}}{k_{III}}\right) e^{-k_{II} a} e^{-ik_{III} a}\right] \tag{C.9}$$

$$\begin{aligned} B_{III} &= A_{II}\left[1 - \frac{1}{2i}\left(\frac{k_{II}}{k_{III}} + i\right)\right] e^{k_{II} a} e^{ik_{III} a} \\ &\quad + B_{II}\left[1 - \frac{1}{2i}\left(i - \frac{k_{II}}{k_{III}}\right)\right] e^{-k_{II} a} e^{ik_{III} a} \end{aligned} \tag{C.10}$$

and (C.5) and (C.6) can be rewritten as

$$A_{IV} = \frac{1}{2}\left[A_{III}\left(i\frac{k_{III}}{k_{IV}} + 1\right) e^{ik_{III} b} e^{-k_{IV} b} + B_{III}\left(1 - i\frac{k_{III}}{k_{IV}}\right) e^{-ik_{III} b} e^{-k_{IV} b}\right] \tag{C.11}$$

$$\begin{aligned} B_{IV} &= A_{III}\left[1 - \frac{1}{2}\left(i\frac{k_{III}}{k_{IV}} + 1\right)\right] e^{ik_{III} b} e^{k_{IV} b} \\ &\quad + B_{III}\left[1 - \frac{1}{2}\left(1 - i\frac{k_{III}}{k_{IV}}\right)\right] e^{-ik_{III} b} e^{k_{IV} b} \end{aligned} \tag{C.12}$$

The requirement $A_{IV} = 0$, allowing the solution not to diverge at infinity, gives therefore, using (C.9), (C.10) and (C.11)

$$\begin{aligned} A_{IV} &= 0 \\ &= \frac{1}{2} A_{II} \frac{1}{2i}\left(\frac{k_{II}}{k_{III}} + i\right) e^{k_{II} a} e^{-ik_{III} a}\left(i\frac{k_{III}}{k_{IV}} + 1\right) e^{ik_{III} b} e^{-k_{IV} b} \\ &\quad + \frac{1}{2} B_{II} \frac{1}{2i}\left(i - \frac{k_{II}}{k_{III}}\right) e^{-k_{II} a} e^{-ik_{III} a}\left(i\frac{k_{III}}{k_{IV}} + 1\right) e^{ik_{III} b} e^{-k_{IV} b} \\ &\quad + \frac{1}{2} A_{II}\left[1 - \frac{1}{2i}\left(\frac{k_{II}}{k_{III}} + i\right)\right] e^{k_{II} a} e^{ik_{III} a}\left(1 - i\frac{k_{III}}{k_{IV}}\right) e^{-ik_{III} b} e^{-k_{IV} b} \\ &\quad + \frac{1}{2} B_{II}\left[1 - \frac{1}{2i}\left(i - \frac{k_{II}}{k_{III}}\right)\right] e^{-k_{II} a} e^{ik_{III} a}\left(1 - i\frac{k_{III}}{k_{IV}}\right) e^{-ik_{III} b} e^{-k_{IV} b} \end{aligned}$$

By noting

$$A_{II} = \frac{A}{2k_{II}} S \tag{C.13}$$

$$B_{II} = \frac{A}{2k_{II}} T \tag{C.14}$$

with obvious definitions of the real S and T from equations (C.7) and (C.8), we get

$$\begin{aligned} A_{IV} &= 0 \\ &= \frac{A}{4k_{II}} S \left[\frac{1}{2i} \left(i\frac{k_{II}}{k_{IV}} + \frac{k_{II}}{k_{III}} - \frac{k_{III}}{k_{IV}} + i \right) e^{-ik_{III}a} e^{ik_{III}b} + \left(1 - i\frac{k_{III}}{k_{IV}} \right. \right. \\ &\quad \left. \left. - \frac{1}{2i} \left(\frac{k_{II}}{k_{III}} - i\frac{k_{II}}{k_{IV}} + i + \frac{k_{III}}{k_{IV}} \right) \right) e^{ik_{III}a} e^{-ik_{III}b} \right] e^{k_{II}a} e^{-k_{IV}b} \\ &\quad + \frac{A}{4k_{II}} T \left[\frac{1}{2i} \left(-\frac{k_{III}}{k_{IV}} + i - i\frac{k_{II}}{k_{IV}} - \frac{k_{II}}{k_{III}} \right) e^{-ik_{III}a} e^{ik_{III}b} + \left(1 - i\frac{k_{III}}{k_{IV}} \right. \right. \\ &\quad \left. \left. - \frac{1}{2i} \left(i + \frac{k_{III}}{k_{IV}} - \frac{k_{II}}{k_{III}} + i\frac{k_{II}}{k_{IV}} \right) \right) e^{ik_{III}a} e^{-ik_{III}b} \right] e^{-k_{II}a} e^{-k_{IV}b} \end{aligned}$$

which gives, by simplifying the factors $\frac{A}{4k_{II}} e^{-k_{IV}b}$

$$\begin{aligned} 0 &= S \left[-\frac{1}{2} \left(-\frac{k_{II}}{k_{IV}} + i\frac{k_{II}}{k_{III}} - i\frac{k_{III}}{k_{IV}} + 1 \right) e^{i(b-a)k_{III}} + \left(1 - i\frac{k_{III}}{k_{IV}} \right. \right. \\ &\quad \left. \left. + \frac{1}{2} \left(i\frac{k_{II}}{k_{III}} + \frac{k_{II}}{k_{IV}} - 1 + i\frac{k_{III}}{k_{IV}} \right) \right) e^{-i(b-a)k_{III}} \right] e^{k_{II}a} \\ &\quad + T \left[-\frac{1}{2} \left(-i\frac{k_{III}}{k_{IV}} - 1 + \frac{k_{II}}{k_{IV}} - i\frac{k_{II}}{k_{III}} \right) e^{i(b-a)k_{III}} + \left(1 - i\frac{k_{III}}{k_{IV}} \right. \right. \\ &\quad \left. \left. + \frac{1}{2} \left(-1 + i\frac{k_{III}}{k_{IV}} - i\frac{k_{II}}{k_{III}} - \frac{k_{II}}{k_{IV}} \right) \right) e^{-i(b-a)k_{III}} \right] e^{-k_{II}a} \end{aligned}$$

and by separating the real and imaginary parts we get respectively

$$\begin{aligned} S \left[\frac{k_{II}}{k_{IV}} \cos((b-a)k_{III}) + \frac{k_{II}}{k_{III}} \sin((b-a)k_{III}) + \cos((b-a)k_{III}) \right. \\ \left. - \frac{k_{III}}{k_{IV}} \sin((b-a)k_{III}) \right] e^{k_{II}a} + T \left[-\frac{k_{II}}{k_{IV}} \cos((b-a)k_{III}) \right. \\ \left. - \frac{k_{II}}{k_{III}} \sin((b-a)k_{III} + \cos((b-a)k_{III}) - \frac{k_{III}}{k_{IV}} \sin((b-a)k_{III} \right] e^{-k_{II}a} = 0 \end{aligned} \tag{C.15}$$

and

$$0 = 0$$

the expression (C.15) giving the transcendental equation for the energy in the case $-U_3 < E < 0$.

C.2 Case $-U_1 < E < -U_3$

This case can be treated exactly in the same manner with the difference that the wave function in region III is now a real exponential

$$u_{III}(r) = A_{III} \exp(k_{III} r) + B_{III} \exp(-k_{III} r)$$

so that the solution is real everywhere. The connections in $r = R$ ((C.1), (C.2)) remain unchanged while the other become

$$A_{II}e^{k_{II}a} + B_{II}e^{-k_{II}a} = A_{III}e^{k_{III}a} + B_{III}e^{-k_{III}a} \tag{C.16}$$

$$A_{II}k_{II}e^{k_{II}a} - B_{II}k_{II}e^{-k_{II}a} = A_{III}k_{III}e^{k_{III}a} - B_{III}k_{III}e^{-k_{III}a} \tag{C.17}$$

$$A_{III}e^{k_{III}b} + B_{III}e^{-k_{III}b} = A_{IV}e^{k_{IV}b} + B_{IV}e^{-k_{IV}b} \tag{C.18}$$

$$A_{III}k_{III}e^{k_{III}b} - B_{III}k_{III}e^{-k_{III}b} = A_{IV}k_{IV}e^{k_{IV}b} - B_{IV}k_{IV}e^{-k_{IV}b} \tag{C.19}$$

(C.16) and (C.17) allow us to express A_{III} and B_{III} in terms of A_{II} and B_{II}

$$A_{III} = \frac{1}{2}\left[A_{II}\left(\frac{k_{II}}{k_{III}}+1\right)e^{k_{II}a}e^{-k_{III}a} + B_{II}\left(1-\frac{k_{II}}{k_{III}}\right)e^{-k_{II}a}e^{-k_{III}a}\right] \tag{C.20}$$

$$\begin{aligned} B_{III} &= A_{II}\left[1-\frac{1}{2}\left(\frac{k_{II}}{k_{III}}+1\right)\right]e^{k_{II}a}e^{k_{III}a} \\ &\quad + B_{II}\left[1-\frac{1}{2}\left(1-\frac{k_{II}}{k_{III}}\right)\right]e^{-k_{II}a}e^{k_{III}a} \end{aligned} \tag{C.21}$$

while (C.18) and (C.19) give

$$A_{IV} = \frac{1}{2}\left[A_{III}\left(\frac{k_{III}}{k_{IV}}+1\right)e^{k_{III}b}e^{-k_{IV}b} + B_{III}\left(1-\frac{k_{III}}{k_{IV}}\right)e^{-k_{III}b}e^{-k_{IV}b}\right] \tag{C.22}$$

$$\begin{aligned} B_{IV} &= A_{III}\left[1-\frac{1}{2}\left(\frac{k_{III}}{k_{IV}}+1\right)\right]e^{k_{III}b}e^{k_{IV}b} \\ &\quad + B_{III}\left[1-\frac{1}{2}\left(1-\frac{k_{III}}{k_{IV}}\right)\right]e^{-k_{III}b}e^{k_{IV}b} \end{aligned} \tag{C.23}$$

The condition $A_{IV} = 0$, together with (C.20), (C.21) and (C.22), implies

$$\begin{aligned} A_{IV} &= 0 \\ &= \frac{1}{2}A_{II}\frac{1}{2}\left(\frac{k_{II}}{k_{III}}+1\right)e^{k_{II}a}e^{-k_{III}a}\left(\frac{k_{III}}{k_{IV}}+1\right)e^{k_{III}b}e^{-k_{IV}b} \\ &\quad + \frac{1}{2}B_{II}\frac{1}{2}\left(1-\frac{k_{II}}{k_{III}}\right)e^{-k_{II}a}e^{-k_{III}a}\left(\frac{k_{III}}{k_{IV}}+1\right)e^{k_{III}b}e^{-k_{IV}b} \\ &\quad + \frac{1}{2}A_{II}\left[1-\frac{1}{2}\left(\frac{k_{II}}{k_{III}}+1\right)\right]e^{k_{II}a}e^{k_{III}a}\left(1-\frac{k_{III}}{k_{IV}}\right)e^{-k_{III}b}e^{-k_{IV}b} \\ &\quad + \frac{1}{2}B_{II}\left[1-\frac{1}{2}\left(1-\frac{k_{II}}{k_{III}}\right)\right]e^{-k_{II}a}e^{k_{III}a}\left(1-\frac{k_{III}}{k_{IV}}\right)e^{-k_{III}b}e^{-k_{IV}b} \end{aligned}$$

(C.13) and (C.14), which are always valid here, give

$$\begin{aligned} 0 &= S\left[\frac{1}{2}\left(\frac{k_{II}}{k_{IV}}+\frac{k_{II}}{k_{III}}+\frac{k_{III}}{k_{IV}}+1\right)e^{k_{III}(b-a)} + \left(1-\frac{k_{III}}{k_{IV}}\right.\right. \\ &\quad \left.\left.-\frac{1}{2}\left(\frac{k_{II}}{k_{III}}-\frac{k_{II}}{k_{IV}}+1-\frac{k_{III}}{k_{IV}}\right)\right)e^{-k_{III}(b-a)}\right]e^{k_{II}a} \\ &\quad + T\left[\frac{1}{2}\left(\frac{k_{III}}{k_{IV}}+1-\frac{k_{II}}{k_{IV}}-\frac{k_{II}}{k_{III}}\right)e^{k_{III}(b-a)} + \left(1-\frac{k_{III}}{k_{IV}}\right.\right. \\ &\quad \left.\left.-\frac{1}{2}\left(1-\frac{k_{III}}{k_{IV}}-\frac{k_{II}}{k_{III}}+\frac{k_{II}}{k_{IV}}\right)\right)e^{-k_{III}(b-a)}\right]e^{-k_{II}a} \end{aligned}$$

which finally gives

$$\frac{S}{2}\left[\left(1+\frac{k_{III}}{k_{IV}}+\frac{k_{II}}{k_{III}}+\frac{k_{II}}{k_{IV}}\right)e^{(b-a)k_{III}}+\left(1-\frac{k_{III}}{k_{IV}}-\frac{k_{II}}{k_{III}}+\frac{k_{II}}{k_{IV}}\right)e^{-(b-a)k_{III}}\right]e^{k_{II}a} \quad \text{(C.24)}$$
$$+\frac{T}{2}\left[\left(1+\frac{k_{III}}{k_{IV}}-\frac{k_{II}}{k_{III}}-\frac{k_{II}}{k_{IV}}\right)e^{(b-a)k_{III}}+\left(1-\frac{k_{III}}{k_{IV}}+\frac{k_{II}}{k_{III}}-\frac{k_{II}}{k_{IV}}\right)e^{-(b-a)k_{III}}\right]e^{-k_{II}a} = 0$$

providing the transcendental equation for the energy in the case $-U_1 < E < -U_3$.

Appendix D

Event counting rate in a medium at thermal equilibrium

In this appendix, we calculate, using a very simplified model, the counting rate of events resulting from tunneling of an external nucleus (or OHe) coming from infinity in a medium at temperature Te. We assume that the transmission coefficient T is known, even if we do not provide its expression in this situation.

Let us consider in a medium at temperature Te where the particles are subjected to thermal agitation with random movements. We first want to determine the number of collisions with nuclei per unit time that an OHe atom will undergo. OHe is seen as a sphere of radius r_0 (O^{--} at the center and He^{++} on its Bohr radius) and the nucleus as a sphere of radius R. We assume collisions of "billiard ball" type, so that an OHe atom will hit a nucleus if their center are closer to $r_0 + R$, and that the particles move in a straight line between two collisions. Therefore, all nuclei that will collide with the OHe atom have their center in a cylinder of radius $r_0 + R$ centered on OHe. The others will not collide with OHe. The situation is schematized in Figure D.1.

During a time interval dt, a particle travels a distance $l = v\,dt$, so that the cylinder has a volume $dV = \pi\left(r_0 + R\right)^2 v\,dt$. If n is the numerical density of nuclei, the number of nuclei in the collision cylinder, and hence the number of collisions during the interval dt, is given by $dN = n\,dV = n\pi\left(r_0 + R\right)^2 v\,dt$. But we are not in a situation where OHe or nuclei are at rest, and hence the velocity v to consider is in reality the average relative velocity $\langle v_{rel}\rangle$. To calculate it, let us recall some basic notions of kinetic theory of gases.

In a medium consisting of particles of mass m in equilibrium at temperature Te, the velocity distribution is given by the Maxwell-Boltzmann distribution

$$P(\overrightarrow{v})dv_x dv_y dv_z = \left(\frac{m}{2\pi Te}\right)^{3/2} \exp\left(-m\left(v_x^2 + v_y^2 + v_z^2\right)/2Te\right) dv_x dv_y dv_z \tag{D.1}$$

The average velocity can be written as $\langle v\rangle = \int\int\int vP(\overrightarrow{v})dv_x dv_y dv_z$, which can be calculated

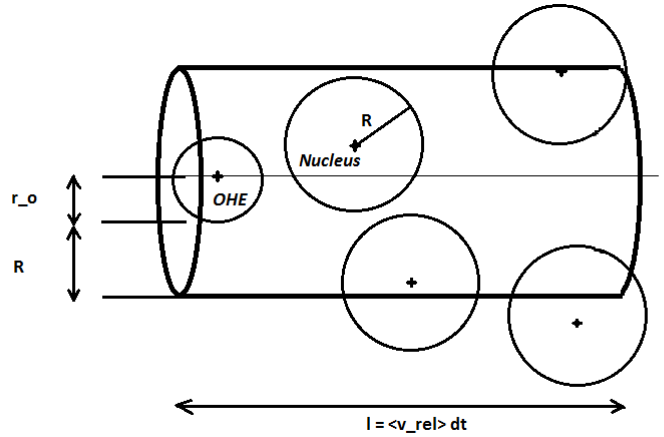

Figure D.1: Collision cylinder between OHe and nuclei subjected to thermal agitation.

by turning to spherical coordinates

$$\begin{aligned}\langle v\rangle &= \left(\frac{m}{2\pi Te}\right)^{3/2} 4\pi \int_0^\infty v^3 \exp\left(-mv^2/2T\right) dv \\ &= 2\pi \left(\frac{m}{2\pi Te}\right)^{3/2} \left(\frac{2Te}{m}\right)^2 \int_0^\infty z \exp\left(-z\right) dz\end{aligned}$$

by putting $z = \frac{mv^2}{2Te}$. The integral in last expression is the gamma function $\int_0^\infty z \exp\left(-z\right) dz = \Gamma(2) = 1\Gamma(1) = 1$ and we obtain finally

$$\langle v\rangle = \sqrt{\frac{8Te}{\pi m}}$$

In the case of a two-body problem, the mass m must be replaced by the reduced mass μ and the velocity v becomes the relative velocity v_{rel}

$$\langle v_{rel}\rangle = \sqrt{\frac{8kTe}{\pi\mu}} \tag{D.2}$$

which is the expression we missed. We are now able to write the desired collision rate of an OHe with nuclei

$$Z = \frac{dN}{dt} = n\pi \left(r_0 + R\right)^2 \sqrt{\frac{8Te}{\pi\mu}} \tag{D.3}$$

which is in fact the usual form of a interaction rate if we write $Z = n\sigma v$ where σ $(= \pi \left(r_0 + R\right)^2$ here) is the interaction cross section and v the average relative velocity.

We can estimate the order of magnitude of the counting rate χ by assuming that for each collision, we have a probability T to cross the dipolar barrier[1]. In cpd/kg units, χ is obtained

[1]Note that, to be more precise, we should consider the impact parameter of the collision and thus the angular momentum and use the corresponding transmission coefficient, which would require to determine T for the different possible values of l. Therefore T is here assumed to be the same for all values of l.

by multiplying the collision rate Z by the the transmission coefficient T, the number Q of OHe in one kg of medium of molar mass A (g/mol) and the number of seconds in one day t

$$\chi = n_{0E}\frac{\pi\left(r_0+R\right)^2 QtN_A}{A}\sqrt{\frac{8Te}{\pi\mu}}T \tag{D.4}$$

where $n_{0E}(cm^{-3})$ is the numerical density of OHe and Q, t and N_A were introduced in subsection 2.2.1 for the counting rate of low energy photons emitted by radiative capture to a level E in region III. We can put this in a more useful form by calculating the multiplying factors

$$\chi = 2\cdot 10^{33} n_{0E}(cm^{-3})\frac{\left(r_0+R\right)^2 (fm^2)}{A}\sqrt{\frac{Te(GeV)}{\mu(GeV)}}T \quad (cpd/kg) \tag{D.5}$$

In last expression, n_{0E} can be evaluated using equation (2.2) for the equilibrium concentration of OHe within the detector for example.

Bibliography

[1] P. Magain, course "Astrophysique Extragalactique" (2010)

[2] M. Moniez, "Review of results from EROS Microlensing search for Massive Compact Objects", arXiv:0901.0985 [astro-ph.GA] (2009).

[3] D. H. Perkins, Particle Astrophysics, 2nd ed. (Oxford University, 2009).

[4] E. Aprile [Xenon Collaboration], "The XENON100 dark matter experiment at LNGS: Status and sensitivity", J. Phys. Conf. Ser. **203** (2010) 012005.

[5] M. Schumann and E. Tziaferi [XENON100 Collaboration], "The XENON100 dark matter experiment", http://dx.doi.org/10.3204/DESY-PROC-2008-02/schumann marc.

[6] E. Aprile *et al.* [XENON100 Collaboration], "Dark Matter Results from 100 Live Days of XENON100 Data", arXiv:1104.2549 [astro-ph.CO] (2011).

[7] T. Schwetz, "Direct detection data and possible hints for low-mass WIMPs", arXiv:1011.5432 [hep-ph].

[8] C. Kelso and D. Hooper, "Prospects For Identifying Dark Matter With CoGeNT", JCAP **1102** (2011) 002 [arXiv:1011.3076 [hep-ph]].

[9] Z. Ahmed *et al.* [CDMS-II Collaboration], "Results from a Low-Energy Analysis of the CDMS II Germanium Data", Phys. Rev. Lett. **106** (2011) 131302 [arXiv:1011.2482 [astro-ph.CO]].

[10] E. Armengaud *et al.* [EDELWEISS Collaboration], "Final results of the EDELWEISS-II WIMP search using a 4-kg array of cryogenic germanium detectors with interleaved electrodes", arXiv:1103.4070 [astro-ph.CO].

[11] M. Y. Khlopov, A. G. Mayorov and E. Y. Soldatov, "Composite Dark Matter and Puzzles of Dark Matter Searches", Int. J. Mod. Phys. D **19** (2010) 1385 [arXiv:1003.1144 [astro-ph.CO]].

[12] M. Yu. Khlopov et al., Puzzles of Dark Matter - More Light on Dark Atoms? Contribution to Proceedings of XIII Bled Workshop "What Comes Beyond the Standard Model?" (Bled, Slovenia, July 2010). Bled Workshops in Physics (2010) V. 11, PP.186-193; e-Print:arXiv:1011.4587

[13] M. Y. Khlopov, A. G. Mayorov and E. Y. Soldatov, "Dark Atoms of the Universe: towards OHe nuclear physics", arXiv:1011.4586 [astro-ph.CO].

[14] R. Bernabei *et al.* [DAMA Collaboration], "First results from DAMA/LIBRA and the combined results with DAMA/NaI", Eur. Phys. J. C **56** (2008) 333 [arXiv:0804.2741 [astro-ph]].

[15] R. Bernabei *et al.*, "New results from DAMA/LIBRA", Eur. Phys. J. C **67** (2010) 39 [arXiv:1002.1028 [astro-ph.GA]].

[16] D. Park: Introduction to the Quantum Theory, 3rd ed. (McGraw-Hill, Inc., New York, 1992).

[17] C. Cohen-Tannoudji, B. Diu, F. Laloë, Mécanique Quantique I (Hermann, 1996)

[18] A. Messiah, Mécanique Quantique-1 (Dunod, 1969)

[19] A. Das, T. Ferbel, Introduction to Nuclear and Particle Physics, 2nd ed. (World Scientific, 2003)

[20] G. Igot, R. M. Thaler, Optical-Model Analysis of the Elastic Scattering of Alpha Particles, Phys. Rev. Vol. 106, Nbr 1 (1957)

[21] Ashok Kumar, S. Kailas, Sarla Rathi, K. Mahata, Global alpha-nucleus optical potential, Nuclear Physics A 776 (2006) 105–117

[22] R. E. Langer, "On the Connection Formulas and the Solutions of the Wave Equation", Phys. Rev. **51** (1937) 669.

[23] T. Hübsch, The Theory of Alpha Decay, homepage.mac.com/thubsch/QM2/Alpha%20Decay.pdf (Term Paper in partial fulfillment of the course requirements for Quantum Mechanics II, Howard Univ., Washington DC 20059, 1997)